INCORPORATING GLUCOSE OXIDASE ACTIVITY INTO AMYLOID FIBRILS

A thesis submitted in partial fulfilment of the requirements for the Degree of Master of Science in Biochemistry

2009

Sarah M. Pilkington
University of Canterbury

ACKNOWLEDGEMENTS

Firstly, I would like to thank my senior supervisor, Juliet. I have learnt an incredible amount from my Masters, not only techniques for my future research career (always check the pH), but also perhaps more valuable lessons, such as how not to be terse (don't cut and paste), learning how to explain science simply in talks (baby slides), and how it really is better to be the tortoise than the hare. I wholeheartedly believe I may not have learnt these lessons at all, let alone as quickly, in any other lab.

Thanks must also go to Susie, supervisor number two, who not only talked through hurdles with me, but also introduced me to spin class, where the instructor titled her 'supervisor and friend'. Thanks again for taking me to the computer place when my computer blew up. And to Grant, supervisor number three, who challenged me to think for myself and take on the role of tortoise.

Next I must thank my TEM expert and lab technician, Jackie. The TEM became a large part of my thesis and was easily the most helpful tool used. I am extremely grateful for all your time spent driving me out to Lincoln to work on the TEM, for your advice and for showing a genuine interest in my results, above and beyond your role as technician.

I would like to thank Laura, for being my co-conspirator, AFM technician and friend. Reluctantly, thanks must also go to Jared, my competitor, for sharing in the 'is it stuck?!' adventure. Good luck with GOD in the future!

Thank you to the rest of Lab 129, especially to Muscroft for knowing chemistry things and miscellaneous things and to Shiva and Sarah for sharing techniques, tips, enzymes and fibrils.

Thanks also to the experts who helped with little pieces of my project: Mark Staiger and Mike Flaws in Mechanical Engineering, Dave Collings and Manfred Ingerfeld for confocal assistance, Tony Cole and Craig Galilee in microbiology, and Matt Walters for photographs.

Finally, to Mum, Dad, Andrew and Rachael, thank you for your love, a life and a career. And to Sam, thank you for ensuring I keep all three.

CONTENTS

ABBREVIATIONS

A_{280}	absorbance at 280 nm
AU	absorbance units
AFM	atomic force microscopy
BSA	bovine serum albumin
CD	circular dichroism
Da	Dalton
DDT	dithiothreitol
DMA	dynamic mechanical analysis
DMSO	dimethyl sulfoxide
DSC	differential scanning colorimetry
DSF	differential scanning fluorimetry
EDC	ethyl-3-(3-diaminopropyl)carbodiimide hydrochloride
EDTA	ethylenediaminetetraacetic acid
FAD(H_2)	flavin adenine dinucleotide (reduced form)
GOD	glucose oxidase from *Aspergillus niger*
GA	glutaraldehyde
HRP	horseradish peroxidase
LB	Luria Bertani
NHS	*N*-hydroxysuccinimide
PVOH	poly(vinyl) alcohol
PDA	potato dextrose agar
RFU	relative fluorescence units
rpm	rotations per minute
SEM	scanning electron microscopy
SWCNT	single walled carbon nanotube
SDS-PAGE	sodium dodecyl sulfate polyacrylamide gel electrophoresis
ThT	thioflavin T
TEM	transmission electron microscopy
TFE	trifluoroethanol
UV	ultraviolet
U	units

v/v	volume per volume
w/v	weight per volume
w/w	weight per weight

ABSTRACT

Amyloid fibrils are a misfolded state formed by many proteins when subjected to denaturing conditions. Their constituent amino acids make them an excellent target for enzyme immobilisation and their strength, stability and nanometre size are attractive features for exploitation in the creation of new bionanomaterials.

The aim of this thesis was to functionalise amyloid fibrils by conjugation to glucose oxidase (GOD). GOD is a relatively stable glycoprotein that catalyses the oxidation of glucose and the release of hydrogen peroxide. The consumption of glucose can be measured to assess glucose levels, and the release of hydrogen peroxide is cytotoxic to cells and is thus an effective antibacterial agent. Three methods of attachment were used: cross-linking using glutaraldehyde, periodate oxidation of the glycoprotein shell, and cross-linking using glutaraldehyde following deglycosylation. GOD retained activity upon attachment by all three methods. These attachment methods were assessed using electrophoresis, centrifugation, sucrose gradient centrifugation and TEM. Gel electrophoresis indicated a high degree of cross-linking and TEM showed no significant change of fibril morphology upon cross-linking. Centrifugation experiments suggested a non-covalent interaction was occurring between amyloid fibrils and GOD, and a covalent attachment was occurring upon addition of glutaraldehyde. Sucrose gradient centrifugation provided increased separation of cross-linked material compared to other separation methods, and showed greater cross-linking to crystallin amyloid fibrils than insulin fibrils. Cross-linking native GOD using glutaraldehyde was chosen for further experiments, as it was found to be most effective for GOD attachment to amyloid fibrils.

The resulting functionalised enzyme scaffold was then incorporated into a model poly(vinyl alcohol) (PVOH) film, to create a new bionanomaterial. The distribution of the functionalised fibrils through the film was characterised using SEM and confocal microscopy, where film components were found to be unevenly dispersed. The antibacterial effect of the functionalised film was then tested on *E. coli* and the antifungal effect of the film was tested on *Fusarium*, *Rhizopus* and *Penicillium*. Growth of *E. coli* was inhibited around functionalised film circles, demonstrating the incorporation of GOD antibacterial activity into the PVOH film. However, no growth inhibition of fungal species was observed.

This work is of significance as it demonstrates the ability to convert a waste material, bovine lens crystallin, to high value protein nanofibres and incorporate functionality *via* GOD attachment. The incorporation of the GOD-functionalised amyloid fibrils into PVOH provides an excellent ‘proof of concept’ model for the creation of a new bionanomaterial using a functionalised amyloid fibril scaffold. Future development of this model system has the potential to lead to the production of a novel biomaterial for use in food packaging due to the antimicrobial properties of GOD.

1. CHAPTER ONE – INTRODUCTION

Amyloid fibrils are stable proteinaceous nanofibres with potential applications in bionanotechnology. Their constituent amino acids make them an excellent target for enzyme immobilisation. The ability to attach the enzyme glucose oxidase (GOD) to amyloid fibrils to create functionalised amyloid fibrils was investigated and the functionalised amyloid fibrils were then incorporated into a film system. The role of the amyloid fibrils in the film system was to act both as a scaffold for enzyme immobilisation, and to add tensile strength to the film.

1.1 Context

Can we use amyloid fibrils as a nanoscaffold for enzyme immobilisation? An amyloid fibril is a misfolded state formed by many proteins when subjected to denaturing conditions, such as low pH and high temperature (Brange *et al.* 1997a). This protein fold is remarkable due to its high stability at a wide pH range, a variety of temperatures and on exposure to proteolytic enzymes. Amyloid fibrils are also very strong, with an estimated strength similar to the strength of spider silk, which is five times that of steel (Kenney *et al.* 2002; Waterhouse and Gerrard 2004). Amyloid fibril formation by two proteins, bovine insulin and bovine lens crystallin, and immobilisation of GOD onto these amyloid fibrils was investigated in this thesis.

In biotechnology, useful properties for enzymes are high stability, use of a commercially important analyte, and high turnover number (Wilson and Turner 1992). GOD catalyses a biochemically important reaction that involves the consumption of glucose and the release of hydrogen peroxide. Hydrogen peroxide is cytotoxic to cells, making GOD an effective antimicrobial agent, and consumption of glucose by GOD is useful for measuring glucose levels (Rodriguez-Nogales 2004). GOD is also an extremely stable enzyme, as it is stable between a pH range of 2 and 8, and at temperatures up to 62 °C (Wilson and Turner 1992; Gouda *et al.* 2003). These features make the enzyme ideal for applications such as measuring glucose concentration and as an antimicrobial agent. Measurement of glucose concentration is important for determination of blood glucose levels in diabetic patients, and also in the beer and wine industry for measuring glucose levels during the fermentation process (Wong *et al.* 2008).

The functionalised amyloid fibrils were then incorporated into a film system. Poly(vinyl alcohol) (PVOH) is an ideal film system for this investigation, as it is inexpensive and readily available commercially, and provides an environment similar to that of water for the enzyme (Wong and Abdul-Aziz 2008). The ability to functionalise amyloid fibrils by conferring enzymatic activity and incorporate them in a film system provides an exciting opportunity for the creation of new bionanomaterials.

1.2 Introduction to amyloid fibrils

Amyloid fibril formation is the assembly of protein monomeric units into fibrils with a high β-sheet content (LeVine III 1999). Amyloid, originally meaning starch-like, refers to the protein deposits that were reminiscent of starch when first observed (Cohen and Calkins 1959; Hamley 2007). Amyloid fibrils are a protein fold associated with numerous disease states, such as Parkinson's and Alzheimer's diseases (Chiti and Dobson 2006). Their role in disease is thought to be due to either loss or gain of function of the protein upon forming amyloid fibrils (Luheshi *et al.* 2008). For example, the prion protein gains neurotoxicity when misfolded, which leads to the misfolding of surrounding proteins in the brain. This results in neurodegenerative disease, although the precise reasons for this are unknown (Winklhofer *et al.* 2008). Conversely, the amyloid β-protein loses its normal cellular function when misfolded and forms deposits of insoluble protein in the neurons of the brain, which also results in neurodegenerative disease (Winklhofer *et al.* 2008). It is thought that the protofibril is the toxic species in disease, rather than the mature folded amyloid fibril (Chiti and Dobson 2006; Cherny and Gazit 2008). Nature has also exploited the amyloid fibril fold in some organisms, for example in the bacterium *Escherichia coli*, amyloid fibrils are found on the surface as a part of the bacterial biofilm (Gras 2007; Jahn and Radford 2008). Class I hydrophobins in fungi and chaplains in Gram-positive streptomycetes are amyloidogenic proteins which assist branching hyphae to reduce surface tension at the water-air interface (Kwan *et al.* 2006; Cherny and Gazit 2008). Amyloid fibrils are also utilised in the egg envelopes of several fish and insects to protect the egg against chemical and physical stresses (Cherny and Gazit 2008). This shows the remarkable natural versatility of function of the amyloid fold.

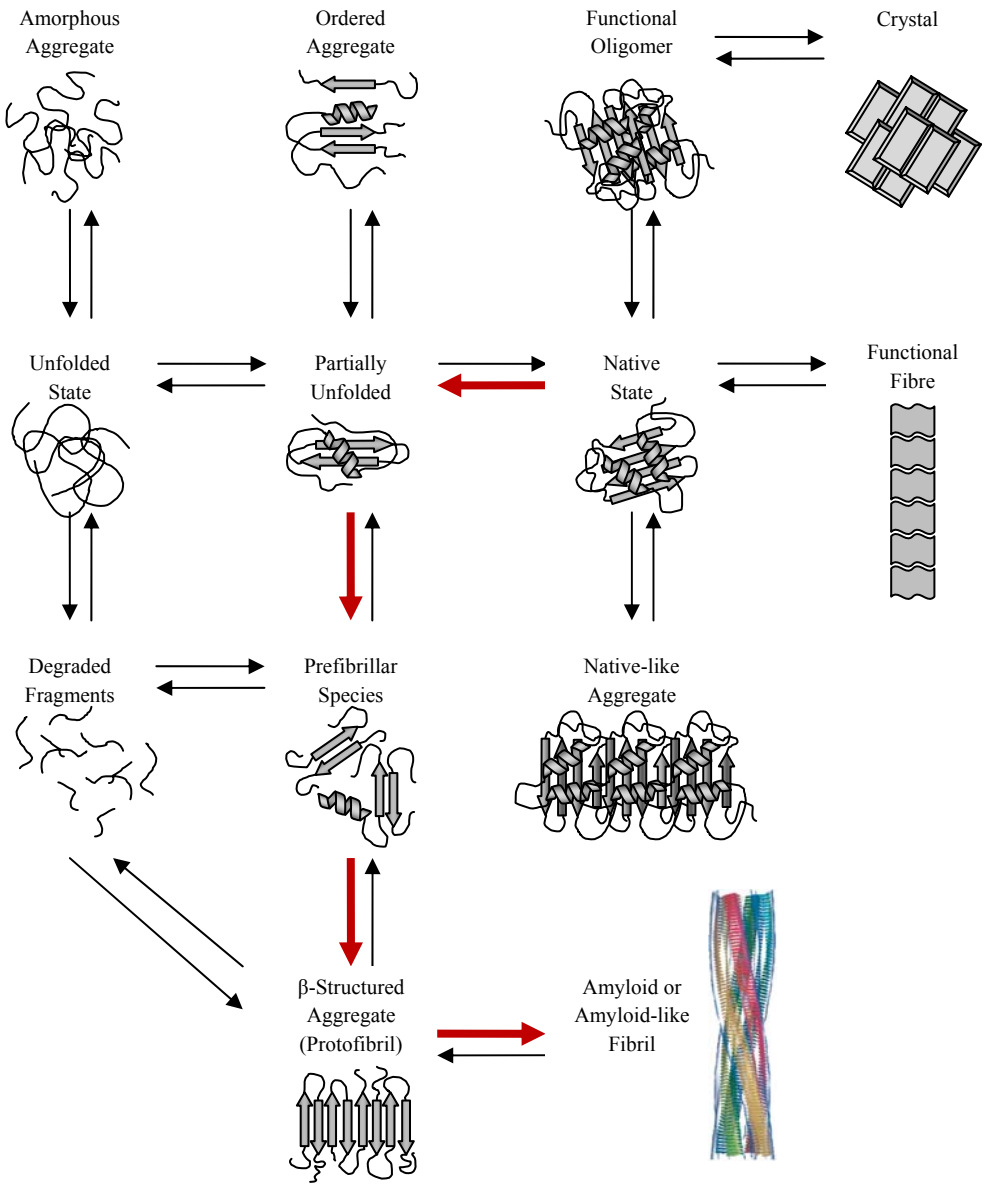

Figure 1.1

Protein misfolding states. *Following synthesis of proteins by the ribosome (not shown), the unfolded protein quickly establishes a native folded state, due to interactions between constituent amino acids and their environment. The native state can then associate with more native proteins to form one of two different structures, a functional oligomer (also known as a globular protein) or a functional fibre. The establishment of a native state is a dynamic pathway and the native state can unfold and fold in physiological conditions. If this pathway is disrupted, the protein may misfold, leading to the formation of disordered aggregate, the degradation of the protein into fragments, or the formation of prefibrillar species. Prefibrillar species associate to form amyloid fibrils via β-structured aggregates called protofibrils. Adapted from Dobson (2003), Chiti and Dobson (2006) and Murphy and Kendrick (2007).*

Many polypeptides can achieve the amyloid folding motif as a nearly ubiquitous alternative folded state, despite having different amino acid sequences and native folds (Rochet and Lansbury 2000; Wetzel *et al.* 2007). In fact, all proteins are thought to be able to access the amyloid fibril fold (Chiti and Dobson 2006). However, different proteins have different propensities for forming amyloid fibrils. Amyloid fibril forming propensity is governed by hydrophobicity, net charge, propensity of constituent amino acid residues to form β-sheets, and the presence of aromatic residues in the polypeptide (Gras 2007). For many proteins, fibril formation can be induced at high temperature and low pH, as these conditions provide the enthalpic driving force required to disrupt proteins from their native fold (Brange *et al.* 1997a) (Figure 1.2). In these denaturing conditions, non-covalent interactions such as hydrogen bonding can still occur within the polypeptide, which stabilise the amyloid fibril structure (Chiti *et al.* 1999). Amyloid fibrils are thus insoluble and stable, achieving their stability through both hydrophobic and electrostatic forces, in a similar way to globular proteins (Wetzel *et al.* 2007) (Figure 1.2).

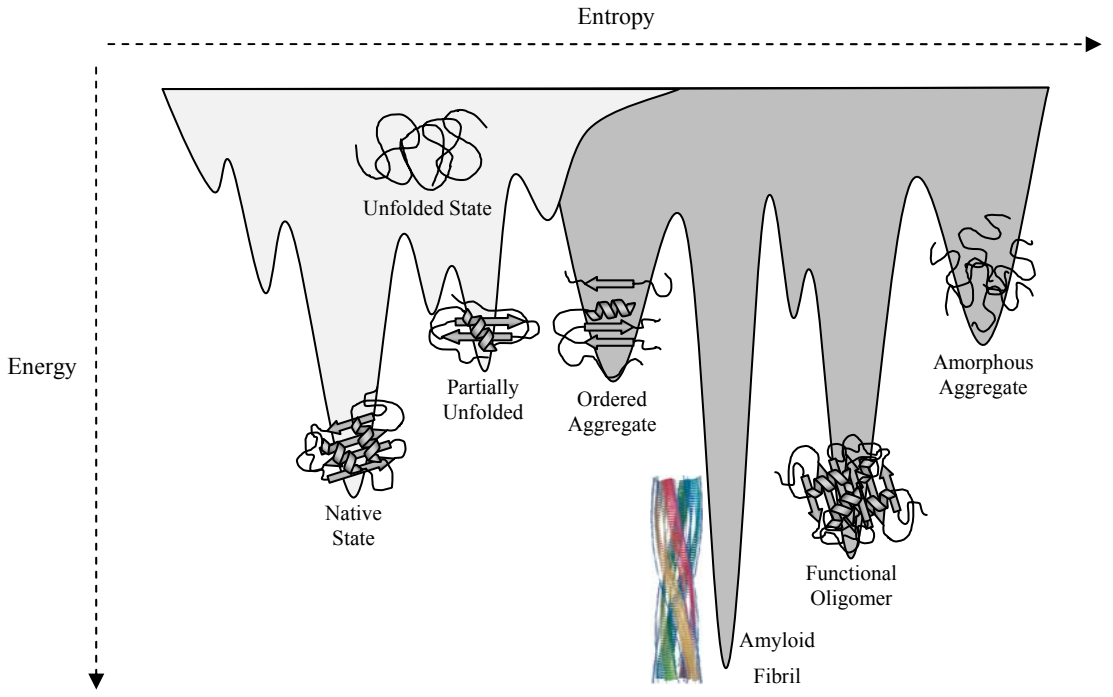

Figure 1.2

A combined schematic energy landscape for protein folding and aggregation. *The simple folding funnel (light grey) can describe the energy changes involved in establishing the native state of a polypeptide. The stability of the native state is indicated, where there is a large energy change needed to disrupt the native state. This simple folding funnel becomes more complex (dark grey) when intermolecular protein association is considered. The remarkable stability of the amyloid fibril fold is represented by the largest energy change needed to disrupt this fold. Adapted from Jahn and Radford (2008).*

1.3 Amyloid fibril structure

Amyloid fibrils have a diameter ranging from 5 nm for small fibrils, to 10 nm for larger fibrils, and are generally long, straight, rigid and un-branched (Rochet and Lansbury 2000; Cherny and Gazit 2008). The tertiary structure of the fibrils consists of β-strands perpendicular to the fibril axis in a 'cross-β' structure (Rochet and Lansbury 2000; Hamley 2007). This cross-β structure has been observed using infrared dichroism spectroscopy and X-ray diffraction (Sunde *et al.* 1997). Two steps govern the formation of amyloid fibrils, these are the rate of fibril growth and the rate of fibril nucleation (Lomakin *et al.* 1996). The formation of the β-rich nucleus is a thermodynamically unfavourable process, compared to the elongation process, which proceeds rapidly upon formation of the fibril nucleus (Jahn and Radford 2008). During the elongation process, the β-sheets self-assemble into protofilaments, which, in turn, coil into protofibrils (Hamley 2007) (Figure 1.3). Assembly of more than two protofilaments into a protofibril is considered a mature fibril (Groenning *et al.* 2007). In order for protofibril coiling to occur, there must be slight changes in the β-sheet, which is an intrinsically flat structure (Jiménez *et al.* 2002). For proteins with propensity for aggregation, such as insulin, the elongation process may occur within a few hours, whereas proteins with a lower amyloid propensity may take a lot longer (Gras 2007). It has recently been predicted that even the α-helix regions of polypeptides have β-sheet propensity, indicating that the protein must be partially unfolded from its secondary structure during amyloid fibril formation (Jahn and Radford 2008).

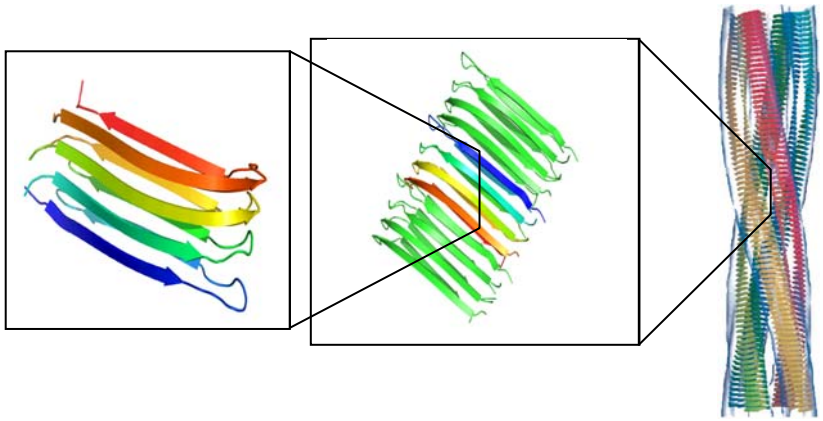

Figure 1.3

Amyloid fibril protofilament structure. *During the nucleation step of amyloid fibril formation, β-sheet rich pre-fibrillar species associate to form protofilaments, as shown in the protofilament structural motif (left inset). This structural motif is repeated to form a long protofilament during the elongation step of fibril formation (centre inset). The protofilaments then coil together, forming an amyloid fibril (right). Adapted from the "General amyloid structural motif", PDB file 2nnt (Ferguson* et al*. 2006) and the amyloid fibril model (Jiménez* et al*. 2002).*

1.4 Characterisation and purification of amyloid fibrils

Amyloid fibrils display a distinct X-ray diffraction pattern, consistent with a cross-β structure, which has become one of the accepted characteristics of amyloid fibril formation (Sunde *et al.* 1997). This distinct pattern also suggests that the amyloid fibrils share a degree of structural similarity, despite being formed from different polypeptide chains (Sunde *et al.* 1997). After X-ray diffraction, the best methods of fibril characterisation to date involve microscopic techniques. Amyloid fibrils have been visualised both with transmission electron microscopy (TEM) and atomic force microscopy (AFM) (Besteman *et al.* 2003; Hrapovic *et al.* 2004).

It is widely accepted that amyloid fibrils can be stained using histological dyes such as thioflavin T (ThT) and Congo red, which bind specifically to amyloid fibrils and change their fluorescence and absorbance properties, respectively (Klunk *et al.* 1989; LeVine III 1999). Positive identification of the formation of amyloid fibrils depends on the ability to distinguish between amyloid β-sheet structure from amorphous aggregates (LeVine III 1999). ThT elicits a distinctly different excitation and emission spectrum upon amyloid β-sheet binding, compared to the spectra produced by proteins with a high β-sheet content and the spectra produced by amyloid precursor monomers (LeVine III 1999). This is also found to be true for Congo red, where the dye will not stain other proteins with a minor β-sheet content (Klunk *et al.* 1989). The specificity of dye binding to amyloid fibrils is not well understood. However, several mechanisms have been proposed (Krebs *et al.* 2005). Recently, two amyloid fibril structure-specific ThT binding sites have been proposed, either between the protofilaments forming the protofibrils, or between the protofibrils forming the mature fibrils (Groenning *et al.* 2007). One limitation of the dye binding analysis is that pH and ionic strength are known to affect the time course of ThT binding, and thus both dye binding and microscopy studies will be used in this thesis to indicate the presence of amyloid fibrils (LeVine III 1999).

Exposure of amyloid fibril samples to pepsin, a protease which has high activity at low pH, will digest any non-fibrillar species, leaving the fibrils intact (Zurdo *et al.* 2001). This technique was developed to aid the separation of amyloid fibrils from other protein species, such as large aggregates, which was previously difficult to achieve using available biochemical techniques, such as electrophoresis or centrifugation (Zurdo *et al.* 2001). Separation is necessary due to heterogeneity introduced by the method of fibril formation *in vitro*, where the sample can contain soluble precursors that have not formed fibrils and non-fibrillar aggregates (Zurdo *et al.* 2001).

1.5 Amyloid fibrils in bionanotechnology

The amyloid fold has remarkable stability and insolubility, and thus offers great potential for biotechnology and nanotechnology (Gras 2007; Jahn and Radford 2008). This potential is derived from the unique properties of amyloid fibrils, specifically their ability to self-assemble under denaturing conditions, their inherent strength, and their ability to be functionalised by manipulation of their constituent amino acids (Waterhouse and Gerrard 2004; Garvey *et al.* 2009). These properties have lead to the suggestion that amyloid fibrils may be used as a scaffold for enzyme immobilisation (Gras 2007; Cherny and Gazit 2008). This has previously been achieved using green fluorescent protein and enzymes such as carbonic anhydrase and glutathione-S-transferase (Baxa *et al.* 2002; Cherny and Gazit 2008). In these experiments, the protein of interest was attached to the C-terminus of yeast Ure2 monomers. The yeast protein was then fibrillised, forming an amyloid fibril with native, functional protein attached (Baxa *et al.* 2002). Cytochrome b attachment has also been demonstrated after amyloid fibril formation, where modified fibrils acquired cytochrome b activity and incorporated heme groups (Baldwin *et al.* 2006).

1.6 Bovine insulin amyloid fibrils

Insulin is a small polypeptide, consisting of 51 residues, with an A chain of 21 amino acid residues linked to a B chain of 30 amino acid residues by three disulfide bridges (Figure 1.4) (Whittingham *et al.* 2002; Devlin *et al.* 2006). These disulfide bridges constrain structural flexibility in the molecule, creating a native fold which is resistant to thermal and chemical denaturation (Devlin *et al.* 2006). The native protein is largely α-helical in structure, and exists as a hexamer at physiological pH (Ahmad *et al.* 2005).

Under denaturing conditions, the termini of the component insulin chains become disordered and expose the helical core of the protein (Hua and Weiss 2004). This partially unfolded state is a prerequisite for the formation of prefibrillar species, leading to the formation of amyloid fibrils (Dobson 2003) (Figure 1.1). Insulin is known to form amyloid fibrils when subjected to high temperature and low pH (Devlin *et al.* 2006). When separated, both the A and B chain of human insulin form fibrils thus the fibril formation of whole insulin is attributed to both chains (Khurana *et al.* 2005). This has been indicated in cross-seeding experiments, where the addition of either A or B chain insulin fibrils seeds amyloid fibril formation in whole insulin (Devlin *et*

al. 2006). The fibrillation of insulin leads to problems in the medical industry with production, delivery and storage of soluble insulin for use in treating diabetic patients (Hong *et al.* 2006). This has resulted in insulin fibrils being comparatively well characterised, and thus insulin is a good model protein for amyloid fibril formation.

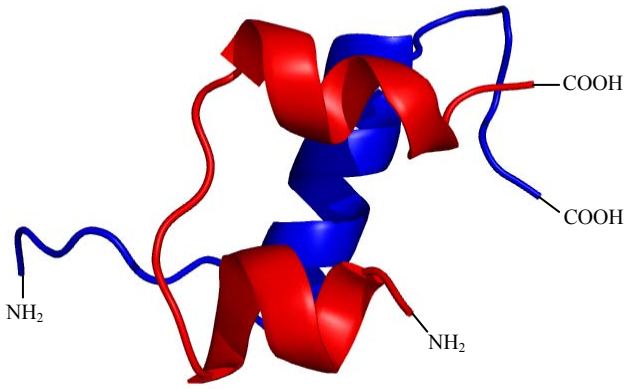

Figure 1.4

The insulin monomer. *The insulin molecule is made up of two chains, chain A (red) and chain B (blue). Adapted from "Bovine despentapeptide insulin", PDB file 1pid, from the crystal structure at 1.3 Å resolution, solved by Brange* et al. *(1997b).*

Insulin amyloid fibril formation occurs via a monomeric, partially unfolded intermediate rich in β-sheet structure, which is distinct from the native fold (Ahmad *et al.* 2005). Fibril formation requires the simultaneous aggregation of three to four insulin molecules *via* their hydrophobic surfaces, known as the nucleation step (Brange *et al.* 1997b). This nucleation step is followed by an extension step, to form long protofilaments. Mature insulin fibrils consist of between two and six protofilaments twisted into a fibrillar structure (Devlin *et al.* 2006) (Figure 1.3). The mature fibril measures 5-10 nm in diameter and up to several microns in length (Nielsen *et al.* 2001).

1.7 Bovine crystallin amyloid fibrils

Less is known about the structure of bovine crystallin fibrils in comparison to insulin fibrils; however, crystallins are a good source for amyloid fibrils, as eye lenses, from which crystallins are derived, are a waste material from the meat processing industry in New Zealand. To ensure feasibility for the use of amyloid fibrils in the production of new materials in

bionanotechnology, the amyloidogenic protein must be readily available and inexpensively sourced (Waterhouse and Gerrard 2004). Amyloid fibrils can be inexpensively produced from crude crystallin protein mixtures, and are a thus potential industrial source for protein nanofibres (Garvey *et al.* 2009).

The biological role of crystallins is to provide transparent structure to the eye lens (Bettelheim and Chen 1998). There are three constituent crystallins in the mammalian lens, α-, β-, and γ-crystallin (Carver *et al.* 1996). α-Crystallin, the most abundant lens protein, has two subunit components and exists as a large aggregate (approximately 800 kDa), β-crystallin has many subunits and is found as a smaller aggregate, and γ-crystallin is a monomer (Carver *et al.* 1996).

All three crystallins have been shown to form amyloid fibrils when subjected to conditions of high temperature and low pH (Meehan *et al.* 2004). Crystallin fibril formation in the eye lens is seen in age-related cataracts, where crystallin transparency is lost upon fibrillation (Carver *et al.* 1996). The formation of crystallin amyloid fibrils can be observed using TEM, X-ray fibre diffraction, and dye binding by Congo red and ThT, although the ThT method is compromised by high background binding to native crystallins (Meehan *et al.* 2004; Meehan *et al.* 2007; Garvey *et al.* 2009).

1.8 Glucose oxidase

Glucose oxidase (GOD) is an oxidoreductase enzyme found in some species of fungi such as *Aspergillus niger* and *Penicillium amagasakiense* and is also found in honey (Fuglsang *et al.* 1995). The natural function of GOD *in vivo* is proposed to provide protection against predators and other invasive species for fungi, and it acts as a natural antibiotic in honey (Vartiainen *et al.* 2005). GOD catalyses the oxidation of β-D-glucose by molecular oxygen, to hydrogen peroxide and glucono-1,5-lactone, which spontaneously hydrolyses to gluconic acid (Leskovac *et al.* 2005). The oxidation of β-D-glucose to glucono-1,5-lactone involves the reduction of the FAD (flavin adenine dinucleotide) cofactor to $FADH_2$. The reduced $FADH_2$ is oxidised by molecular oxygen, which is itself reduced to hydrogen peroxide. These reactions are coupled together to give an overall reaction shown in Scheme 1.1 (Leskovac *et al.* 2005).

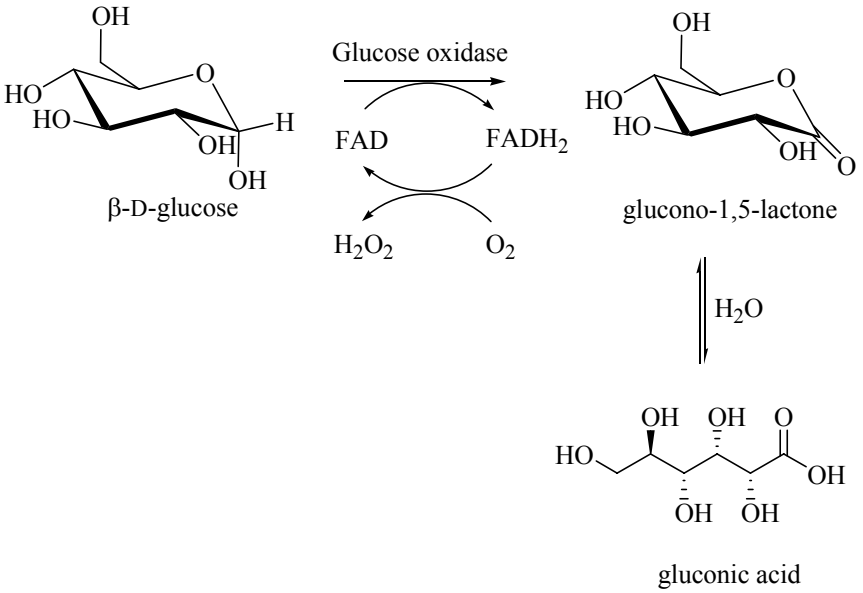

Scheme 1.1

The overall reaction catalysed by the GOD enzyme. *During the oxidation of glucose to gluconic acid by GOD, the FAD cofactor of GOD is reduced to $FADH_2$ and molecular oxygen is reduced to hydrogen peroxide. This leads to the re-oxidation of the cofactor and allows the reaction to cycle. Adapted from Lescovac* et al. *(2005).*

The redox active site of the enzyme is buried in the centre, close to the FAD cofactor. Other hexose sugars such as α-D-glucose, mannose and galactose form either fewer bonds or unfavourable contacts with neighbouring amino acids, explaining why the enzyme is specific for β-D-glucose (Wohlfahrt *et al.* 1999).

GOD is a slightly elongated, structurally rigid, flavin-containing glycoprotein, consisting of 583 amino acid residues (Wilson and Turner 1992; Hecht *et al.* 1993; Leskovac *et al.* 2005). It is a homodimer made up of two identical subunits (O'Malley and Weaver 1972), with a molecular weight of approximately 80 kDa each (Leskovac *et al.* 2005). GOD contains both α-helix and β-sheet structures. The active site contains three main active site residues, His516, His559 and Glu412 (Figure 1.5) (Leskovac *et al.* 2005). The dimer contains two disulfide bridges, one per monomer, though the significance of these bridges is still unknown (Wilson and Turner 1992). Each monomer also contains a flavin adenine dinucleotide (FAD) redox centre, which undergoes a two-electron transfer reaction (Figure 1.5) (Fairman and Åkerfeldt 2005).

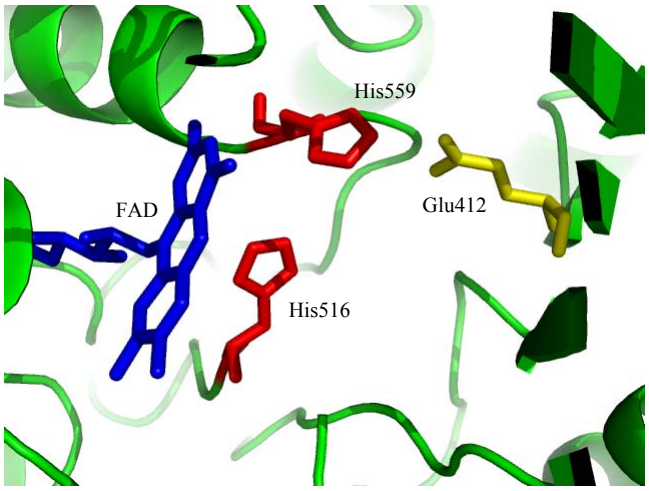

Figure 1.5

***Important structural features of the glucose oxidase monomer from* Aspergillus niger.** *The monomer contains one FAD molecule (blue) and three important active site residues, two histidines (red) and a glutamine (yellow). Adapted from "Glucose oxidase from* Aspergillus niger*", PDB file 1cf3, solved by Hecht* et al. *(1993) and Wohlfahrt* et al. *(1999).*

Upon binding of glucose, there is hydride and proton transfer from glucose to the FAD and His516 respectively (Leskovac *et al.* 2005). Proton transfer then occurs from His516 to molecular oxygen (Leskovac *et al.* 2005). His559 is hydrogen bonded to Glu412, leaving His516 exposed to the solvent (Leskovac *et al.* 2005).

The native enzyme has a glycoprotein shell which encases the protein core (Wilson and Turner 1992). The glycoprotein shell usually consists of 190 mannose residues and 16 *N*-acetylglucosamine residues, which are *N*- or *O*-glycosidically linked to the enzyme (Kalisz *et al.* 1991; Leskovac *et al.* 2005). These residues account for about 24% of the enzyme's molecular weight, depending whether glycosylation isoforms of the enzyme are present (Kalisz *et al.* 1991). According to the crystal structure of the deglycosylated enzyme at 2.3 Å resolution, the GOD monomer is a compact spheroid with the approximate dimensions of 60 Å x 52 Å x 37 Å and the GOD dimer has the approximate dimensions of 60 Å x 52 Å x 77 Å (Hecht *et al.* 1993). Scanning tunnelling microscopy (STM) images of the GOD dimer show the two subunits to be arranged in a butterfly shape, with two symmetric wings and a depressed bridge in the middle (Chi *et al.* 1994; Losic *et al.* 2002). Similarly, atomic force microscopy (AFM) has been used to visualise individual GOD molecules (Losic *et al.* 2004).

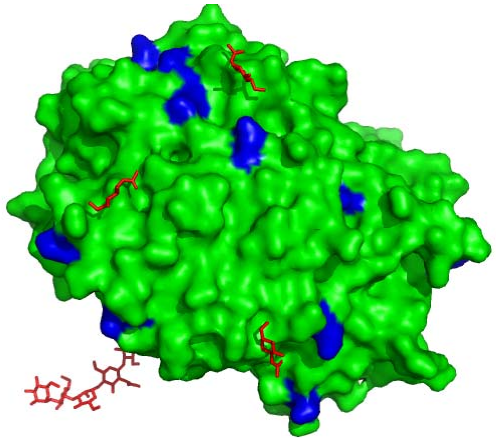

Figure 1.6

The glycoprotein shell of GOD. *Remaining carbohydrate residues following GOD deglycosylation (red) and surface lysine residues are indicated (blue). The visible side of the enzyme is the side that is not involved in the formation of the GOD dimer. The glycoprotein shell was removed by incubating with endoglycosidase H and α-mannosidase in order to achieve the crystal structure of the enzyme* (Kalisz et al*. 1991). The carbohydrate residues are not completely cleaved, showing the point of attachment of some residues of the carbohydrate shell to the protein. A mannose tail is also visible. In the GOD dimer, the two mannose tails are lined up at the same end. Image generated from the PDB file 1cf3, solved by Hecht* et al. *(1993) and Wohlfahrt* et al. *(1999).*

GOD is stable at temperatures up to 50 °C, and removal of the glycoprotein shell does not greatly affect its thermostability, as the enzyme still retains half of its activity after 5 minutes at 70 °C (Kalisz *et al.* 1991). It was first assumed that the role of the glycoprotein shell on the GOD enzyme was to provide stability by maintaining the functional conformational state. Deglycosylation of the GOD enzyme (Figure 1.6) has been achieved by treating with endoglycosidase and mannosidase, followed by electrophoretic assessment, which has shown that 95% of the carbohydrate had been cleaved (Sohail Akhtar and Bhakuni 2003). Early research on GOD from *A. niger* reported that removal of the glycoprotein shell had a minor effect on the kinetics of glucose oxidation and the stability of the enzyme at low pH, but did not affect the structure of the enzyme (Kalisz *et al.* 1991). In similar research on GOD from *P. amagasakiense*, removal of the glycoprotein shell did not affect the kinetics, but had a minor affect on pH and temperature stability (Kalisz *et al.* 1997). When GOD from *P. amagasakiense* is expressed recombinantly in *Escherichia coli* it is not glycosylated during post-translational modification and has a slightly decreased stability (Witt *et al.* 1998). This non-glycosylated enzyme still assumes the native GOD fold, indicating that the protein-bound carbohydrate moiety does not appear to be essential for the correct folding of GOD (Witt *et al.* 1998). The protein-bound carbohydrate does, however, appear to contribute to the high thermostability of

GOD, with the non-glycosylated recombinant enzyme being slightly less thermostable than native GOD from *P. amagasakiense* (Witt *et al.* 1998). Changes in glycosylation have been shown to directly affect the amount of hydrogen tunnelling in the hydrogen transfer step of the GOD-catalysed reaction (Kohen *et al.* 1997). Increased tunnelling is correlated with a lower enthalpy of activation (Kohen *et al.* 1997). It has since been concluded that any protein modification to the surface of the GOD molecule affects hydrogen transfer at the active site; however, the reason behind this is poorly understood (Seymour and Klinman 2002).

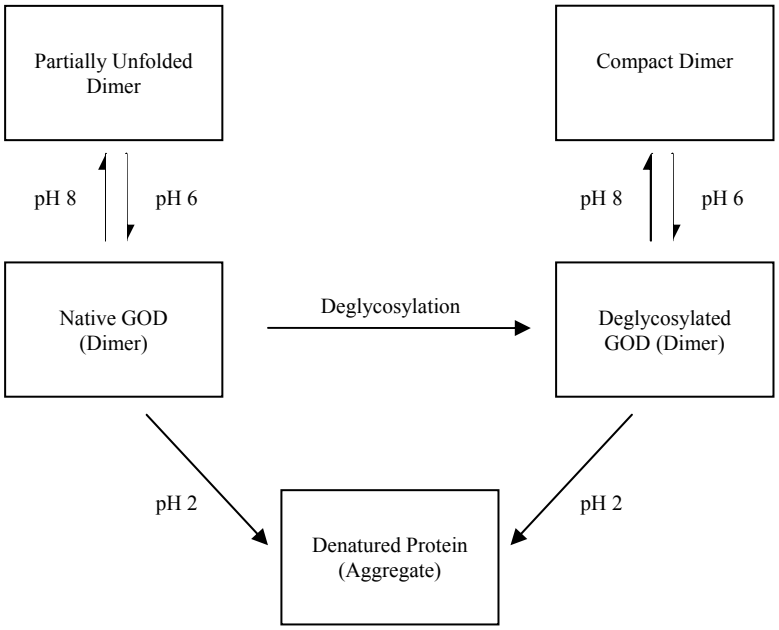

Figure 1.7

The effect of pH on GOD. *GOD forms its native dimeric state between a pH of 2 and 10. Below pH 2, the enzyme becomes denatured, and above pH 10, the enzyme forms a partially unfolded dimer. The partially unfolded dimer will resume the native dimeric state when the pH is lowered to 6. The deglycosylated enzyme behaves slightly differently, with the formation of a compact dimer at a pH above 10 (Sohail Akhtar and Bhakuni 2003).*

GOD is stable at 0 °C for two years after lyophilisation (Wilson and Turner 1992). In a water-ethanol mix with an ethanol content of above 90%, the enzyme has a greater stability than its stability in water, and still retains 100% of its activity after 30 minutes at room temperature (Lukachova *et al.* 1997). The enzyme is active at a pH range of between 2 and 8 and is very resistant to proteolysis (Wilson and Turner 1992). Dissociation of the subunits can only occur under denaturing conditions, and results in the loss of FAD to form an apo-enzyme (Leskovac *et al.* 2005). Thus the GOD enzyme is very stable relative to other enzymes. It has also been reported that both the deglycosylated and glycosylated enzyme have similar structural features

at physiological and acidic pH, but show different structural features at alkaline pH (Figure 1.7) (Sohail Akhtar and Bhakuni 2003). Recent thermal inactivation experiments show an increase in thermal inactivation and the loss of the FAD cofactor from the enzyme at 59 °C, with the enzyme retaining its secondary and tertiary structure at temperatures up to 62 °C (Gouda *et al.* 2003). This indicates that loss of the FAD cofactor is the important factor for initial thermal inactivation, rather than loss of secondary and tertiary structure (Gouda *et al.* 2003).

1.9 GOD assay methods

Hydrogen peroxide produced from the GOD-catalysed reaction has been reacted with *o*-dianisidine to produce a brown product in colorimetric diagnostic kits for the determination of glucose in the blood (Wilson and Turner 1992). Progression of the GOD-catalysed reaction can also be monitored using the intrinsic fluorescence increase of the FAD cofactor as it is reduced (De Luca *et al.* 2007). There are also commercially available kits that use the fluorescent agent resorufin (commercially known as Amplex Red (Invitrogen) or Ampiflu Red (Sigma)) to measure the progress of the GOD-catalysed reaction (Zhang *et al.* 2004). Resorufin was used in this thesis, as it is an extremely quick and sensitive method for assessment of GOD activity. The resorufin reaction also produces a fluorescent pink product, which is visible both by eye and by fluorescence measurement.

1.10 GOD immobilisation

Before an enzyme can be used effectively in many applications, it must first be immobilised. Immobilisation allows the enzyme to be reused, allows recovery of the enzyme and its product and more control over the enzymatic reaction, such as control of termination of the reaction (Krajewska 2004). Enzymes may be immobilised by a variety of methods, which may be broadly described as physical, where weak interactions between support and enzyme exist, such as entrapment within microgels and adsorption, and chemical, where covalent bonds are formed with the enzyme, such as cross-linking (Krajewska 2004). In some cases, such as with GOD, the enzyme has greater activity upon immobilisation, which may be due to the stabilisation of the active conformation of the enzyme by the supporting medium (Tiller *et al.* 2002).

The most common method of GOD immobilisation to date has been cross-linking *via* lysine residues on the GOD enzyme. The dimeric glycosylated GOD enzyme has 30 lysine residues in its sequence, with 24 of these residues located on the surface of the polypeptide (Baszkin *et al.* 1997). Around five of these surface lysine residues are available for cross-linking, as shown by covalently reacting the residues with *N*-hydroxysuccinimide (NHS) (Kriechbaum *et al.* 1989; Frederick *et al.* 1990; Baszkin *et al.* 1997). This indicates that some lysine residues on the surface of the enzyme are still accessible and are not completely covered by the glycoprotein shell. GOD has been previously cross-linked both to itself, in order to improve intramolecular stability, and to structures such as electrodes and films, for use in biosensing (Kozulic *et al.* 1987; Delvaux and Demoustier-Champagne 2003; Gade *et al.* 2006). GOD has been cross-linked using glutaraldehyde (GA) extensively in previous work (Ahmad *et al.* 2001; Sohail Akhtar and Bhakuni 2003). GA reacts with the free amino group of lysine (and arginine) residues on the surface of GOD (Figure 1.6). The exact mechanism remains unknown, and could progress *via* a Schiff base intermediate, although this would require further reaction and/or the presence of a reducing agent in order to form a stable covalent attachment. Another possible mechanism is the formation of a pyridinium cross-link, which is outlined in Scheme 1.2 (Meade *et al.* 2003).

In other research, GOD has been immobilised on metallic nanotubes using GA and a mixture of NHS and 1-ethyl-3-(3-diaminopropyl)carbodiimide hydrochloride (EDC), which cross-links the GOD enzyme in an analogous way to GA chemistry, *via* the lysine residues on GOD (Delvaux and Demoustier-Champagne 2003). Some research has also combined entrapment with cross-linking. This is achieved by entrapping the GOD in poly(vinyl pyridine), and then using a method such as exposure to UV light to cross-link the pyridine molecules (Gregg and Heller 1990).

GOD was most thermostable when immobilised using GA-activated supports (Betancor *et al.* 2006). Cross-linking of GOD to carbon nanotubes has also been achieved with carbodiimide (Lin *et al.* 2004). Ferrocene-modified polypyrrole was also used to immobilise GOD (Heller 1992). Some research that uses the entrapment immobilisation method alone involves the use of cross-linked polyacrylamide microgels in the immobilisation of GOD (Retama *et al.* 2003). Using scanning electron microscopy, Retama *et al.* (2003) were then able to visualise the difference between microgels containing cross-linked enzyme and those without, based on size.

Because GOD is a glycoprotein, conventional protein cross-linking techniques may not be the most effective method. Cross-linking the carbohydrate shell of GOD has been achieved by oxidising the constituent sugar molecules (Kozulic *et al.* 1987). This method is not ideal, however, due to the lack of data surrounding the exact composition of the glycoprotein shell of GOD, due to the necessary cleavage of the glycoprotein shell in order to get a crystal structure (Kalisz *et al.* 1991).

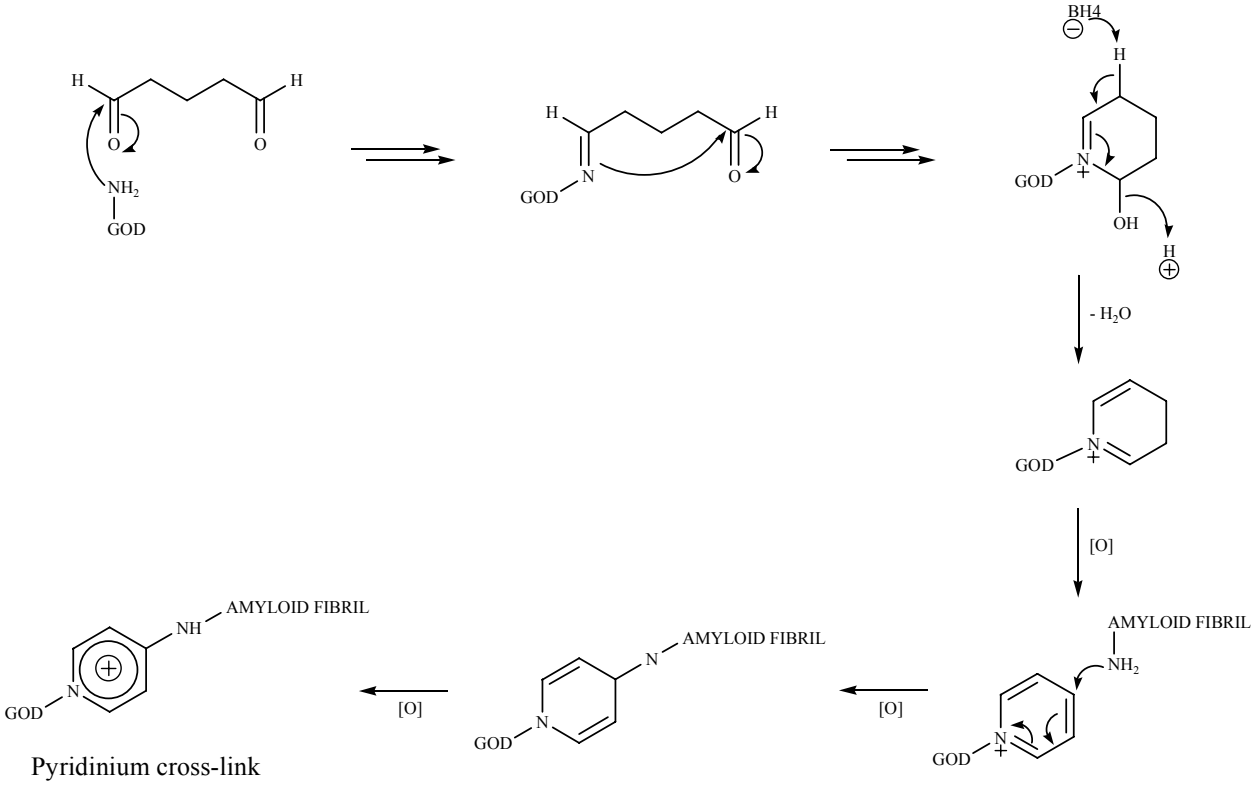

Scheme 1.2

Formation of a pyridinium cross-link with glutaraldehyde. *Glutaraldehyde reacts with lysine residues on the GOD enzyme. Following the completion of several steps, a pyridinium cross-link is formed. Adapted from Meade* et al. *(2003).*

1.11 Fibril cross-linking

As mentioned previously in Section 1.5, amyloid fibrils have the potential to be functionalised due to the reactivity of their constituent amino acids. The ability of amyloid fibrils to be cross-linked *via* these amino acids can be exploited as a method of enzyme immobilisation. Due to the fact that amyloid fibrils are of a high molecular weight and associate with each other, they are difficult to separate using standard protein separation methods, such as gel electrophoresis and

chromatography. It is therefore difficult to tell whether the enzyme has been cross-linked to the amyloid fibrils, or whether it is non-covalently associated with the fibrils. Microscopy currently offers the most convincing results for assessing enzyme attachment to carbon nanotubes. This is shown in research using atomic force microscopy (AFM) (Besteman *et al.* 2003). This research involved the use of single-walled carbon nanotubes (SWCNTs), which are long, thin tubes. The height of an unmodified SWCNT is constant over the length of the nanotube and slightly below one nanometre. Besteman *et al.* attached GOD to the outside of the SWCNT using glutaraldehyde chemistry, and compared the height of this functionalised nanotube to the unmodified nanotube. The functionalised SWCNT with immobilised GOD had a larger height measuring 2-4 nm. The GOD dimer has the dimensions 6 x 5.2 x 7.7 nm, as determined by crystallography (Section 1.8) (Hecht *et al.* 1993). However, this extra height is in agreement with the height of dehydrated GOD in addition to the height of the nanotube (Besteman *et al.* 2003). This indicates that enzyme immobilisation onto carbon nanotubes can be viewed using AFM, and suggests that this functionalised SWCNT could be used as a model for AFM studies of functionalised amyloid fibrils.

1.12 Poly(vinyl alcohol) film

Nanomaterials have unusual physical and chemical properties, and thus have potential for applications in biosensors, biocatalysts, bioelectronics and biomedicine (Liu *et al.* 2007). Blends of synthetic polymers and biopolymers are attractive and important, because the hybrids are potentially applicable as biochemical, biomedical, and biodegradable chemicals (Aoi *et al.* 2000). The sensitivity of a biosensor can be influenced by both the immobilisation method and the porosity, pore size distribution, mechanical properties, and operational stability of the host material used (Wong and Abdul-Aziz 2008). PVOH has useful properties for use as a bionanomaterial, such as good tensile strength, abrasion resistance and oxygen barrier properties under dry conditions (Chang and Kim 2007). PVOH has been widely used in biomaterial research because of its elasticity, good film-forming property, high degree of swelling in aqueous solutions, and water content similar to that of biological tissue (Wong and Abdul-Aziz 2008). PVOH is also able to form a hydrogel, and this has been reported to have selective permeability for low molecular weight substances such as glucose, the substrate of GOD (Wong and Abdul-Aziz 2008).

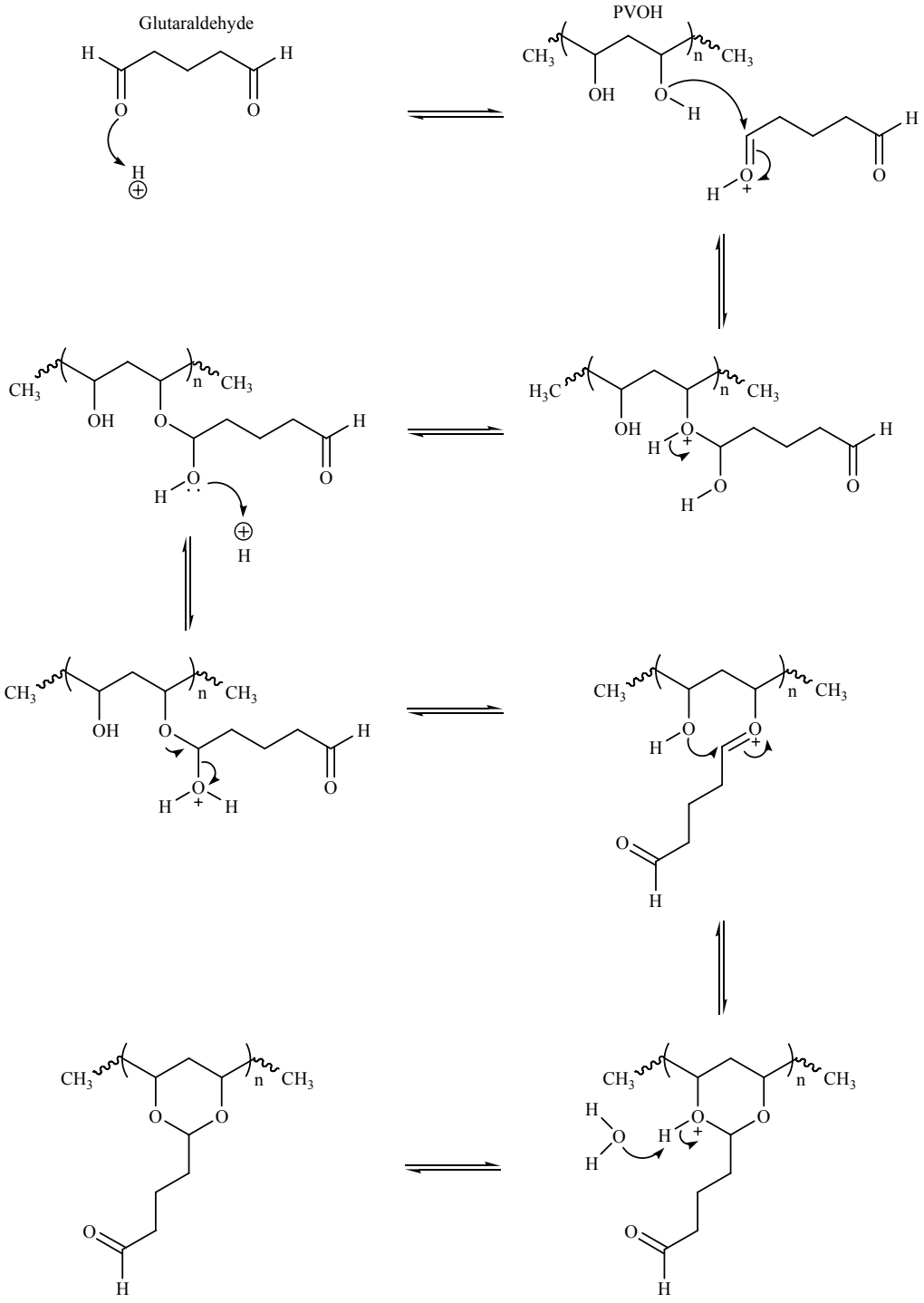

Scheme 1.3

Cross-linking of PVOH by glutaraldehyde. *One possible mechanism for glutaraldehyde cross-linking of PVOH is given above. All steps of the reaction are reversible. Another PVOH molecule can also react with the other end of the glutaraldehyde in the final product (Mansur* et al*. 2008).*

PVOH is an ideal material for enzyme immobilisation, as it has an abundance of hydroxyl groups, which provides an environment similar to the natural environment of an enzyme (Wong and Abdul-Aziz 2008). PVOH creates a stable environment for GOD by inhibiting the formation of non-functional conformations, by hydrogen bonding the H atoms of alcohol groups in the PVOH and the O atoms of the glycoprotein shell carbohydrate groups in GOD (Wong and Abdul-Aziz 2008). Despite this, PVOH films are very stiff and brittle due to high degree of crystallisation, and recently numerous plasticisers such as ethylene glycol have been studied and incorporated into films with the intention of improving the impact properties of the films (Chang and Kim 2007). Chemical cross-linkers such as GA have also been used in a similar way to introduce hydrophobicity and thus change the swelling properties of the film (Scheme 1.3) (Mansur *et al.* 2008). There is evidence to suggest that addition of amyloid fibrils to PVOH films may increase the tensile strength of the films, thus making PVOH films an attractive option for use in packaging (Rao 2008).

The incorporation of enzymes into PVOH films is a useful method of adding functionality to the films. Enzyme-film preparations are frequently unstable, due to the desorption or leeching out of enzyme (Gade *et al.* 2006). Therefore a cross-linking method *via* GA has frequently been chosen for immobilisation of the enzyme (Gade *et al.* 2006). GOD has been extensively researched for its incorporation into glucose biosensors (Liu *et al.* 2007). Chemical and physical stability of enzymes are essential requirements in enzyme sensors, as an enzyme must retain its activity in order to be used as a biosensor (Retama *et al.* 2003). GOD has been previously incorporated into a PVOH film, and was found to retain its activity, with an optimum activity level achieved at 2000 U/ml (Kumar and D'Souza 2008).

1.13 Antimicrobial applications

Antimicrobial enzymes are ubiquitous in nature, playing an important role in the defence mechanisms of an organism. Oxidoreductases, such as GOD, generate reactive molecules *in situ* and release these molecules into the surrounding environment as a defence mechanism. This has a cytotoxic effect on other organisms by destroying vital proteins (Rodriguez-Nogales 2004). Thus the antimicrobial effect of GOD is due to the hydrogen peroxide formed, and the production of gluconic acid may also influence the growth of some microorganisms by lowering pH levels (Rodriguez-Nogales 2004; Vartiainen *et al.* 2005). GOD is a naturally occurring enzyme in honey and originates from the hypopharyngeal glands of honey bees (Wong *et al.*

2008). The hydrogen peroxide produced in the GOD-catalysed reaction acts as a preservative (Taormina *et al.* 2001). Honey has been used for centuries as a wound dressing and these dressings are currently sold around the world for their antimicrobial properties (Sato and Miyata 2000; Taormina *et al.* 2001). GOD has been found to have antimicrobial activity against both Gram-negative and Gram-positive bacteria in whole egg and *Pseudomonas fluorescens*, *Acinetobacter calcoaceticum* and *Hansenula polymorpha* in shrimp, and thus has been an important focus for the production of novel biomaterials with antimicrobial properties (Fuglsang *et al.* 1995; Vartiainen *et al.* 2005).

GOD has been used in combination with lactoperoxidase in a commercial preservative system. Lactoperoxidase is a peroxidase enzyme found in milk, which uses hydrogen peroxide as a substrate. The lactoperoxidase uses hydrogen peroxide formed from the GOD-catalysed reaction to oxidise thiocyanate, iodine and bromine to form reactive species that have antimicrobial activity (Rodriguez-Nogales 2004).

It has been reported that hydrogen peroxide has an inhibitory effect on the immobilised GOD enzyme (Bao *et al.* 2003). Research into this inhibition has confirmed that the inhibition is competitive between hydrogen peroxide and molecular oxygen, and both substrates were found to bind with the same affinity (Bao *et al.* 2003). Because of the quick production of highly reactive hydrogen peroxide, either the enzyme or the substrate must be immobilised in order to prevent spoiling. GOD has been successfully microencapsulated in liposomes which removes the inhibitory effect of the hydrogen peroxide and increases the stability of the enzyme (Yoshimoto *et al.* 2005; Yoshimoto *et al.* 2006). Liposomes are small vesicles in which an aqueous volume is enclosed by a membrane made of lipid molecules (Rodriguez-Nogales 2004). This technology may also be useful for the sustained release of hydrogen peroxide as a preservative in food, cosmetics or toiletries (Rodriguez-Nogales 2004).

GOD has also been immobilised using GA chemistry onto polypropylene films, which were then found to have antimicrobial activity, and may be a useful biomaterial for novel antimicrobial food packaging (Vartiainen *et al.* 2005). In this paper, the antimicrobial activity of the polypropylene films was tested by culturing the test solution to look for surviving colonies of the bacteria *Bacillus subtilis* and *E. coli*.

Thermostability of enzymes is a significant problem in the production of food packaging, as the temperatures needed to make materials such as polypropylene films are very high and are likely

to denature the enzyme (Fuglsang *et al.* 1995). It has been stated that GOD is more likely to be involved in food processing than in packaging for shelf-life preservation due to the effect of hydrogen peroxide on the food, as it is known to cause rancidity due to lipid oxidation (Fuglsang *et al.* 1995). However, there is currently a large amount of research being undertaken in this area, with the opportunity to revolutionise the way consumables are preserved in the future.

1.14 Conclusion

The properties of both amyloid fibrils and GOD make them ideal for investigation of a new bionanomaterial. The ability of amyloid fibrils to be functionalised and the inherent strength of the fibrils make them useful for both adding enzyme function and strength to the bionanomaterial. GOD is extremely stable and catalyses a reaction that is useful in many areas, such as fermentation, blood glucose measurement and antimicrobial activity. PVOH is a useful material due to the environment it provides for enzyme immobilisation, and its availability. Thus these three constituents provide a good model for creation of a 'proof of concept' bionanomaterial based on enzyme immobilisation onto amyloid fibrils.

1.15 Thesis outline

Chapter Two describes the experimental methods used in this thesis. Chapter Three describes amyloid fibril formation from bovine insulin and bovine lens crystallins. Chapter Four assessed the attachment of GOD to amyloid fibrils using GA. Chapter Five investigated attachment of GOD to amyloid fibrils *via* the carbohydrate shell of the glycoprotein and the effect of removal of the glycoprotein shell on cross-linking *via* GA. In Chapter Six the functionalised amyloid fibrils were incorporated into a film system and this bionanomaterial was characterised for both its material and antimicrobial properties.

1.16 References

Ahmad, A., Akhtar, M. S. and Bhakuni, V. (2001). Monovalent cation-induced conformational change in glucose oxidase leading to stabilization of the enzyme. *Biochemistry* **40**: 1945-1955.

Ahmad, A., Uversky, V. N., Hong, D. and Fink, A. L. (2005). Early in the fibrillation of monomeric insulin. *Journal of Biological Chemistry* **280**: 42669-42675.

Aoi, K., Takasu, A. and Okada, M. (2000). DNA-based polymer hybrids. Part 1. Compatibility and physical properties of poly(vinyl alcohol)/DNA sodium salt blend. *Polymer* **41**: 2847-2853.

Baldwin, A. J., Bader, R., Christodoulou, J., MacPhee, C. E., Dobson, C. M. and Barker, P. D. (2006). Cytochrome display on amyloid fibrils. *Journal of the American Chemical Society* **128**: 2162-2163.

Bao, J., Furumoto, K., Yoshimoto, M., Fukunaga, K. and Nakao, K. (2003). Competitive inhibition by hydrogen peroxide produced in glucose oxidation catalyzed by glucose oxidase. *Biochemical Engineering Journal* **13**: 69-72.

Baszkin, A., Boissonnade, M. M., Rosilio, V., Kamyshny, A. and Magdassi, S. (1997). Adsorption of hydrophobized glucose oxidase at solution/air interface. *Journal of Colloid and Interface Science* **190**: 313-317.

Baxa, U., Speransky, V., Steven, A. C. and Wickner, R. B. (2002). Mechanism of inactivation on prion conversion of the Saccharomyces cerevisiae Ure2 protein. *Proceedings of the National Academy of Sciences of the United States of America* **99**: 5253-5260.

Besteman, K., Lee, J. O., Wiertz, F. G. M., Heering, H. A. and Dekker, C. (2003). Enzyme-coated carbon nanotubes as single-molecule biosensors. *Nano Letters* **3**: 727-730.

Betancor, L., López-Gallego, F., Hidalgo, A., Alonso-Morales, N., Dellamora-Ortiz, G., Guisán, J. M. and Fernández-Lafuente, R. (2006). Preparation of a very stable immobilized biocatalyst of glucose oxidase from *Aspergillus niger*. *Journal of Biotechnology* **121**: 284-289.

Bettelheim, F. A. and Chen, A. (1998). Thermodynamic stability of bovine α-crystallin in its interactions with other bovine crystallins. *International Journal of Biological Macromolecules* **22**: 247-252.

Brange, J., Andersen, L., Laursen, E. D., Meyn, G. and Rasmussen, E. (1997a). Toward understanding insulin fibrillation. *Journal of Pharmaceutical Sciences* **86**: 517-525.

Brange, J., Dodson, G. G., Edwards, D. J., Holden, P. H. and Whittingham, J. L. (1997b). A model of insulin fibrils derived from the x-ray crystal structure of a monomeric insulin (despentapeptide insulin). *Proteins: Structure, Function, and Genetics* **27**: 507-516.

Carver, J. A., Nicholls, K. A., Aquilina, A. J. and Truscott, R. J. W. (1996). Age-related changes in bovine α-crystallin and high-molecular-weight protein. *Experimental Eye Research* **63**: 639-647.

Chang, M. H. and Kim, B. C. (2007). Rheological investigation of the effects of introducing diethylene glycol on the physical properties of PVA solutions and PVA films. *Macromolecular Symposia* **249-250**: 591-600.

Cherny, I. and Gazit, E. (2008). Amyloids: Not only pathological agents but also ordered nanomaterials. *Angewandte Chemie International Edition* **47**: 4062-4069.

Chi, Q., Zhang, J., Dong, S. and Wang, E. (1994). Direct observation of native and unfolded glucose oxidase structures by scanning tunnelling microscopy. *Journal of the Chemical Society, Faraday Transactions* **90**: 2057-2060.

Chiti, F. and Dobson, C. M. (2006). Protein misfolding, functional amyloid, and human disease. *Annual Review of Biochemistry* **75**: 333-366.

Chiti, F., Webster, P., Taddei, N., Clark, A., Stefani, M., Ramponi, G. and Dobson, C. M. (1999). Designing conditions for *in vitro* formation of amyloid protofilaments and fibrils. *Proceedings of the National Academy of Sciences of the United States of America* **96**: 3590-3594.

Cohen, A. S. and Calkins, E. (1959). Electron microscopic observations on a fibrous component in amyloid of diverse origins. *Nature* **183**: 1202-1203.

De Luca, P., Lepore, M., Portaccio, M., Esposito, R., Rossi, S., Bencivenga, U. and Mita, D. G. (2007). Glucose determination by means of steady-state and time-course UV fluorescence in free or immobilized glucose oxidase. *Sensors* **7**: 2612-2625.

Delvaux, M. and Demoustier-Champagne, S. (2003). Immobilisation of glucose oxidase within metallic nanotubes arrays for application to enzyme biosensors. *Biosensors and Bioelectronics* **18**: 943-951.

Devlin, G. L., Knowles, T. P. J., Squires, A., McCammon, M. G., Gras, S. L., Nilsson, M. R., Robinson, C. V., Dobson, C. M. and MacPhee, C. E. (2006). The component polypeptide chains of bovine insulin nucleate or inhibit aggregation of the parent protein in a conformation-dependent manner. *Journal of Molecular Biology* **360**: 497-509.

Dobson, C. M. (2003). Protein folding and misfolding. *Nature* **426**: 884-890.

Fairman, R. and Åkerfeldt, K. S. (2005). Peptides as novel smart materials. *Current Opinion in Structural Biology* **15**: 453-463.

Ferguson, N., Becker, J., Tidow, H., Tremmel, S., Sharpe, T. D., Krause, G., Flinders, J., Petrovich, M., Berriman, J., Oschkinat, H. and Fersht, A. R. (2006). General structural motifs of amyloid protofilaments. *Proceedings of the National Academy of Sciences of the United States of America* **103**: 16248-16253.

Frederick, K. R., Tung, J., Emerick, R. S., Masiarz, F. R., Chamberlain, S. H., Vasavada, A., Rosenberg, S., Chakraborty, S., Schopfer, L. M. and Schopter, L. M. (1990). Glucose

oxidase from *Aspergillus niger*. Cloning, gene sequence, secretion from *Saccharomyces cerevisiae* and kinetic analysis of a yeast-derived enzyme. *Journal of Biological Chemistry* **265**: 3793-3802.

Fuglsang, C. C., Johansen, C., Christgau, S. and Adler-Nissen, J. (1995). Antimicrobial enzymes: Applications and future potential in the food industry. *Trends in Food Science and Technology* **6**: 390-396.

Gade, V. K., Shirale, D. J., Gaikwad, P. D., Savale, P. A., Kakde, K. P., Kharat, H. J. and Shirsat, M. D. (2006). Immobilization of GOD on electrochemically synthesized Ppy-PVS composite film by cross-linking *via* glutaraldehyde for determination of glucose. *Reactive and Functional Polymers* **66**: 1420-1426.

Garvey, M., Gras, S. L., Meehan, S., Meade, S. J., Carver, J. A. and Gerrard, J. A. (2009). Protein nanofibres of defined morphology prepared from mixtures of crude crystallins. *International Journal of Nanotechnology* **6**: 258-273.

Gouda, M. D., Singh, S. A., Rao, A. G. A., Thakur, M. S. and Karanth, N. G. (2003). Thermal inactivation of glucose oxidase: Mechanism and stabilisation using additives. *Journal of Biological Chemistry* **278**: 24324-24333.

Gras, S. L. (2007). Amyloid fibrils: From disease to design. New biomaterial applications for self-assembling cross-β fibrils. *Australian Journal of Chemistry* **60**: 333-342.

Gregg, B. A. and Heller, A. (1990). Cross-linked redox gels containing glucose oxidase for amperometric biosensor applications. *Analytical Chemistry* **62**: 258-263.

Groenning, M., Norrman, M., Flink, J. M., van de Weert, M., Bukrinsky, J. T., Schluckebier, G. and Frokjaer, S. (2007). Binding mode of Thioflavin T in insulin amyloid fibrils. *Journal of Structural Biology* **159**: 483-497.

Hamley, I. W. (2007). Peptide fibrillization. *Angewandte Chemie International Edition* **46**: 8128-8147.

Hecht, H. J., Kalisz, H. M., Hendle, J., Schmid, R. D. and Schomburg, D. (1993). Crystal structure of glucose oxidase from *Aspergillus niger* refined at 2.3 Å resolution. *Journal of Molecular Biology* **229**: 153-172.

Heller, A. (1992). Electrical connection of enzyme redox centers to electrodes. *Journal of Physical Chemistry* **96**: 3579-3587.

Hong, D. P., Ahmad, A. and Fink, A. L. (2006). Fibrillation of human insulin A and B chains. *Biochemistry* **45**: 9342-9353.

Hrapovic, S., Liu, Y., Male, K. B. and Luong, J. H. T. (2004). Electrochemical biosensing platforms using platinum nanoparticles and carbon nanotubes. *Analytical Chemistry* **76**: 1083-1088.

Hua, Q.-X. and Weiss, M. A. (2004). Mechanism of insulin fibrillation: The structure of insulin under amyloidogenic conditions resembles a protein-folding intermediate. *Journal of Biological Chemistry* **279**: 21449-21460.

Jahn, T. R. and Radford, S. E. (2008). Folding versus aggregation: Polypeptide conformations on competing pathways. *Archives of Biochemistry and Biophysics* **469**: 100-117.

Jiménez, J. L., Nettleton, E. J., Bouchard, M., Robinson, C. V., Dobson, C. M. and Saibil, H. R. (2002). The protofilament structure of insulin amyloid fibrils. *Proceedings of the National Academy of Sciences of the United States of America* **99**: 9196-9201.

Kalisz, H. M., Hecht, H. J., Schomburg, D. and Schmid, R. D. (1991). Effects of carbohydrate depletion on the structure, stability and activity of glucose oxidase from *Aspergillus niger*. *Biochimica et Biophysica Acta - Protein Structure and Molecular Enzymology* **1080**: 138-142.

Kalisz, H. M., Hendle, J. and Schmid, R. D. (1997). Structural and biochemical properties of glycosylated and deglycosylated glucose oxidase from *Penicillium amagasakiense*. *Applied Microbiology and Biotechnology* **47**: 502-507.

Kenney, J. M., Knight, D., Wise, M. J. and Vollrath, F. (2002). Amyloidogenic nature of spider silk. *European Journal of Biochemistry* **269**: 4159-4163.

Khurana, R., Coleman, C., Ionescu-Zanetti, C., Carter, S. A., Krishna, V., Grover, R. K., Roy, R. and Singh, S. (2005). Mechanism of thioflavin T binding to amyloid fibrils. *Journal of Structural Biology* **151**: 229-238.

Klunk, W. E., Pettegrew, J. W. and Abraham, D. J. (1989). Quantitative evaluation of Congo red binding to amyloid-like proteins with a beta-pleated sheet conformation. *Journal of Histochemistry and Cytochemistry* **37**: 1273-1281.

Kohen, A., Jonsson, T. and Klinman, J. P. (1997). Effects of protein glycosylation on catalysis: Changes in hydrogen tunneling and enthalpy of activation in the glucose oxidase reaction. *Biochemistry* **36**: 2603-2611.

Kozulic, B., Leustek, I., Pavlovic, B., Mildner, P. and Barbaric, S. (1987). Preparation of the stabilized glycoenzymes by cross-linking their carbohydrate chains. *Applied Biochemistry and Biotechnology* **15**: 265-278.

Krajewska, B. (2004). Application of chitin- and chitosan-based materials for enzyme immobilizations: a review. *Enzyme and Microbial Technology* **35**: 126-139.

Krebs, M. R. H., Bromley, E. H. C. and Donald, A. M. (2005). The binding of thioflavin-T to amyloid fibrils: localisation and implications. *Journal of Structural Biology* **149**: 30-37.

Kriechbaum, M., Heilmann, H. J., Wientjes, F. J., Hahn, M., Jany, K.-D., Gassen, H. G., Sharif, F. and Alaeddinoglu, G. (1989). Cloning and DNA sequence analysis of the glucose oxidase gene from *Aspergillus niger* NRRL-3. *FEBS Letters* **255**: 63-66.

Kumar, J. and D'Souza, S. F. (2008). Preparation of PVA membrane for immobilization of GOD for glucose biosensor. *Talanta* **75**: 183-188.

Kwan, A. H. Y., Winefield, R. D., Sunde, M., Matthews, J. M., Haverkamp, R. G., Templeton, M. D. and Mackay, J. P. (2006). Structural basis for rodlet assembly in fungal hydrophobins. *Proceedings of the National Academy of Sciences of the United States of America* **103**: 3621-3626.

Leskovac, V., Trivic, S., Wohlfahrt, G., Kandrac, J. and Perićin, D. (2005). Glucose oxidase from *Aspergillus niger*: The mechanism of action with molecular oxygen, quinones, and one-electron acceptors. *International Journal of Biochemistry and Cell Biology* **37**: 731-750.

LeVine III, H. (1999). Quantification of β-sheet amyloid fibril structures with thioflavin T. *Methods in Enzymology* **309**: 274-284.

Lin, Y., Lu, F., Tu, Y. and Ren, Z. (2004). Glucose biosensors based on carbon nanotube nanoelectrode ensembles. *Nano Letters* **4**: 191-195.

Liu, Q., Lu, X., Li, J., Yao, X. and Li, J. (2007). Direct electrochemistry of glucose oxidase and electrochemical biosensing of glucose on quantum dots/carbon nanotubes electrodes. *Biosensors and Bioelectronics* **22**: 3203-3209.

Lomakin, A., Chung, D. S., Benedek, G. B., Kirschner, D. A. and Teplow, D. B. (1996). On the nucleation and growth of amyloid beta-protein fibrils: Detection of nuclei and quantitation of rate constants. *Proceedings of the National Academy of Sciences of the United States of America* **93**: 1125-1129.

Losic, D., Shapter, J. G. and Gooding, J. J. (2002). Scanning tunneling microscopy studies of glucose oxidase on gold surfaces. *Langmuir* **18**: 5422-5428.

Losic, D., Short, K., Gooding, J. J. and Shapter, J. G. (2004). Scanning probe microscopy characterisation of immobilised enzyme molecules on a biosensor surface: Visualisation of individual molecules. *Journal of the Serbian Chemical Society* **69**: 93-106.

Luheshi, L. M., Crowther, D. C. and Dobson, C. M. (2008). Protein misfolding and disease: from the test tube to the organism. *Current Opinion in Chemical Biology* **12**: 25-31.

Lukachova, L. V., Karyakin, A. A., Karyakina, E. E. and Gorton, L. (1997). The improvement of polyaniline glucose biosensor stability using enzyme immobilization from water-organic mixtures with a high content of organic solvent. *Sensors and Actuators, B: Chemical* **44**: 356-360.

Mansur, H. S., Sadahira, C. M., Souza, A. N. and Mansur, A. A. P. (2008). FTIR spectroscopy characterization of poly (vinyl alcohol) hydrogel with different hydrolysis degree and chemically crosslinked with glutaraldehyde. *Materials Science and Engineering: C* **28**: 539-548.

Meade, S. J., Miller, A. G. and Gerrard, J. A. (2003). The role of dicarbonyl compounds in non-enzymatic crosslinking: a structure-activity study. *Bioorganic & Medicinal Chemistry* **11**: 853-862.

Meehan, S., Berry, Y., Luisi, B., Dobson, C. M., Carver, J. A. and MacPhee, C. E. (2004). Amyloid fibril formation by lens crystallin proteins and its implications for cataract formation. *Journal of Biological Chemistry* **279**: 3413-3419.

Meehan, S., Knowles, T. P. J., Baldwin, A. J., Smith, J. F., Squires, A. M., Clements, P., Treweek, T. M., Ecroyd, H., Tartaglia, G. G., Vendruscolo, M., MacPhee, C. E., Dobson, C. M. and Carver, J. A. (2007). Characterisation of amyloid fibril formation by

small heat-shock chaperone proteins human αA-, αB- and R120G αB-crystallins. *Journal of Molecular Biology* **372**: 470-484.

Nielsen, L., Frokjaer, S., Carpenter, J. F. and Brange, J. (2001). Studies of the structure of insulin fibrils by Fourier transform infrared (FTIR) spectroscopy and electron microscopy. *Journal of Pharmaceutical Sciences* **90**: 29-37.

O'Malley, J. J. and Weaver, J. L. (1972). Subunit structure of glucose oxidase from *Aspergillus niger*. *Biochemistry* **11**: 3527-3532.

Rao, S. P. (2008). PhD Thesis. Amyloid fibrils in bionanomaterials. *School of Biological Sciences, University of Canterbury, Christchurch*.

Retama, J. R., Lopez-Ruiz, B. and Lopez-Cabarcos, E. (2003). Microstructural modifications induced by the entrapped glucose oxidase in cross-linked polyacrylamide microgels used as glucose sensors. *Biomaterials* **24**: 2965-2973.

Rochet, J.-C. and Lansbury, P. T. (2000). Amyloid fibrillogenesis: themes and variations. *Current Opinion in Structural Biology* **10**: 60-68.

Rodriguez-Nogales, J. M. (2004). Kinetic behaviour and stability of glucose oxidase entrapped in liposomes. *Journal of Chemical Technology and Biotechnology* **79**: 72-78.

Sato, T. and Miyata, G. (2000). The nutraceutical benefit, part iii: honey. *Nutrition* **16**: 468-469.

Seymour, S. L. and Klinman, J. P. (2002). Comparison of rates and kinetic isotope effects using PEG-modified variants and glycoforms of glucose oxidase: The relationship of modification of the protein envelope to C-H activation and tunneling. *Biochemistry* **41**: 8747-8758.

Sohail Akhtar, M. and Bhakuni, V. (2003). Alkaline treatment has contrasting effects on the structure of deglycosylated and glycosylated forms of glucose oxidase. *Archives of Biochemistry and Biophysics* **413**: 221-228.

Sunde, M., Serpell, L. C., Bartlam, M., Fraser, P. E., Pepys, M. B. and Blake, C. C. F. (1997). Common core structure of amyloid fibrils by synchrotron X-ray diffraction. *Journal of Molecular Biology* **273**: 729-739.

Taormina, P. J., Niemira, B. A. and Beuchat, L. R. (2001). Inhibitory activity of honey against foodborne pathogens as influenced by the presence of hydrogen peroxide and level of antioxidant power. *International Journal of Food Microbiology* **69**: 217-225.

Tiller, J. C., Rieseler, R., Berlin, P. and Klemm, D. (2002). Stabilization of activity of oxidoreductases by their immobilization onto special functionalized glass and novel aminocellulose film using different coupling reagents. *Biomacromolecules* **3**: 1021-1029.

Vartiainen, J., Rátto, M. and Paulussen, S. (2005). Antimicrobial activity of glucose oxidase-immobilized plasma-activated polypropylene films. *Packaging Technology and Science* **18**: 243-251.

Waterhouse, S. H. and Gerrard, J. A. (2004). Amyloid fibrils in bionanotechnology. *Australian Journal of Chemistry* **57**: 519-523.

Wetzel, R., Shivaprasad, S. and Williams, A. D. (2007). Plasticity of amyloid fibrils. *Biochemistry* **46**: 1-10.

Whittingham, J. L., Scott, D. J., Chance, K., Wilson, A., Finch, J., Brange, J. and Guy Dodson, G. (2002). Insulin at pH 2: Structural analysis of the conditions promoting insulin fibre formation. *Journal of Molecular Biology* **318**: 479-490.

Wilson, R. and Turner, A. P. F. (1992). Glucose oxidase: An ideal enzyme. *Biosensors and Bioelectronics* **7**: 165-185.

Winklhofer, K. F., Tatzelt, J. and Haass, C. (2008). The two faces of protein misfolding: gain- and loss-of-function in neurodegenerative diseases. *EMBO Journal* **27**: 336-349.

Witt, S., Singh, M. and Kalisz, H. M. (1998). Structural and kinetic properties of nonglycosylated recombinant *Penicillium amagasakiense* glucose oxidase expressed in *Escherichia coli*. *Applied and Environmental Microbiology* **64**: 1405-1411.

Wohlfahrt, G., Witt, S., Hendle, J., Schomburg, D., Kalisz, H. M. and Hecht, H. J. (1999). 1.8 and 1.9 Å resolution structures of the *Penicillium amagasakiense* and *Aspergillus niger* glucose oxidases as a basis for modelling substrate complexes. *Acta Crystallographica Section D: Biological Crystallography* **55**: 969-977.

Wong, C. M., Wong, K. H. and Chen, X. D. (2008). Glucose oxidase: natural occurrence, function, properties and industrial applications. *Applied Microbiology and Biotechnology* **78**: 927-938.

Wong, F.-L. and Abdul-Aziz, A. (2008). Comparative study of poly(vinyl alcohol)-based support materials for the immobilization of glucose oxidase. *Journal of Chemical Technology & Biotechnology* **83**: 41-46.

Yoshimoto, M., Sato, M., Wang, S., Fukunaga, K. and Nakao, K. (2006). Structural stability of glucose oxidase encapsulated in liposomes to inhibition by hydrogen peroxide produced during glucose oxidation. *Biochemical Engineering Journal* **30**: 158-163.

Yoshimoto, M., Wang, S., Fukunaga, K., Fournier, D., Walde, P., Kuboi, R. and Nakao, K. (2005). Novel immobilized liposomal glucose oxidase system using the channel protein OmpF and catalase. *Biotechnology and Bioengineering* **90**: 231-238.

Zhang, W., Huang, Y., Dai, H., Wang, X., Fan, C. and Li, G. (2004). Tuning the redox and enzymatic activity of glucose oxidase in layered organic films and its application in glucose biosensors. *Analytical Biochemistry* **329**: 85-90.

Zurdo, J., Guijarro, J. I. and Dobson, C. M. (2001). Preparation and characterization of purified amyloid fibrils. *Journal of the American Chemical Society* **123**: 8141-8142.

2. CHAPTER TWO – METHODS

2.1 General materials and methods

Unless otherwise stated, all chemicals were obtained from Sigma Chemical Co., BDH Laboratory Supplies or Invitrogen. Bovine eye lenses were supplied by a local abattoir (CMP Canterbury Ltd, Seafield Road, Ashburton, New Zealand). Commercial grade glucose oxidase from *Aspergillus niger* (Type X-S) was obtained from Sigma Chemical Co.

Sodium dodecyl sulphate polyacrylamide gel electrophoresis was run using a NuPAGE system gel electrophoresis box, with precast 10 well NuPAGE Novex® 4 – 12% Bis-Tris gradient gels (1.0 mm) (Invitrogen). Samples were prepared by mixing with lithium salt of dodecyl sulfate (LDS) 4 x sample buffer and heating at 90 °C for 5 minutes to aid the reduction of disulfide bonds. An Invitrogen Novex® Sharp™ Pre-stained Wide-Range Protein Standard ladder was also run for each gel. Electrophoresis was carried out at a constant voltage of 200 V in NuPAGE 2-(*N*-morpholino)ethanesulfonic acid (MES)-SDS running buffer (50 mM MES, 50 mM Tris base, 0.1% SDS, 1 mM ethylenediaminetetraacetic acid (EDTA) at pH 7.4) at room temperature for 50 minutes. Gels were stained with Coomassie R-250 (2.5 g/l Coomassie R-250, 10% (v/v) glacial acetic acid, 45% (v/v) methanol and 45% (v/v) distilled water (dH_2O)) for 30 minutes, and then destained with destaining solution (30% (v/v) methanol, 10% (v/v) acetic acid and 60% (v/v) dH_2O) for at least one hour. Gel photographs were then taken using a BioImaging System (Syngene).

pH measurements were obtained using an UltraBasic UB10 pH meter (Denver Instrument Co.) (unless otherwise stated), fitted with a high-performance glass body pH/Tris electrode.

Protein concentrations of unknown solutions were measured on a Thermo Scientific NanoDrop™ ND-1000 Spectrophotometer (A_{280}) (Thermo Fischer Scientific), unless stated otherwise. Measurements of three replicates were averaged and corrected for a blank of the sample buffer.

Fluorescence and absorbance measurements were recorded by a BMG Labtech FLUOstar OPTIMA Platereader (Alphatech Systems Ltd.). For fluorescence measurements Nunc™ 96 flat well black, optical bottom plates were used, with Nunc™ 236707 sealing tape used when heating of samples was required. For absorbance measurements, SARSTEDT 96 flat well optical plates were used.

All fungi were supplied by Craig Galilee, School of Biological Sciences, University of Canterbury.

2.2 Amyloid fibril formation

Amyloid fibrils were formed from bovine insulin and from bovine eye lens crystallins. Following exposure to amyloid fibril forming conditions, the samples were tested for presence of amyloid fibrils using a thioflavin T assay (Section 2.2.6) and transmission electron microscopy (TEM) (Section 2.4.8).

2.2.1 Formation of amyloid fibrils by bovine insulin

Insulin amyloid fibrils were made from adapted in-house methods (Nielsen *et al.* 2001). Bovine insulin was dissolved at a concentration of 5.8 mg/ml in incubation buffer (0.1 M NaCl, adjusted to pH 1.6 with 1 M HCl) and incubated at 60 °C for at least 48 hours. The presence of fibrils was indicated using a thioflavin T assay (Section 2.2.6).

2.2.2 Crude crystallin extraction from bovine lenses

Two crystallin extraction methods were used in this thesis. First, an in-house method was followed with modifications from the literature (Garvey *et al.* 2009). The second method was devised to be gentler on the protein and achieve a greater yield of amyloid fibrils.

Method One

In the initial method, bovine lenses were removed from cow eyes obtained from an abattoir and stored at -20 °C. Crystallin proteins were extracted from bovine lenses by homogenisation in a

buffer containing 50 mM Tris, pH 7.2, 1 mM dithiothreitol (DTT) and 1 mM ethylenediaminetetraacetic acid (EDTA) using the Magic Bullet™ blender. The homogenate was centrifuged at 12,000 rpm for 30 minutes at 4 °C. The supernatant was removed and analysed for protein concentration using a Thermo Scientific NanoDrop™ ND-1000 Spectrophotometer (A_{280}) (Section 2.1). The crystallin extraction process was repeated multiple times with comparable protein concentrations. The extract was then filtered through a 0.22 μm MILLEX®GP Millipore Express® PES Membrane Filter Unit and retained as crude crystallin protein.

Method Two

To achieve a greater protein yield and minimise protein degradation, bovine lenses were removed from cow eyes obtained from an abattoir and stored at -20 °C. Crystallin proteins were extracted from bovine lenses by homogenisation in a buffer containing 50 mM Tris, pH 7.2, 1 mM DTT and 1 mM EDTA, using an IKA® Ultra Turrax® Tube Disperser with Tube ST-20. The lenses were homogenised for 1 minute, then left on ice for 1 minute. This cycle was repeated until the lens had been homogenised for 30 minutes. The homogenate was then centrifuged for 30 minutes at 13,000 x *g* in an Eppendorf® MiniSpin® Plus centrifuge. The supernatant was removed and pooled. The protein concentration of the supernatant was then measured using a Thermo Scientific NanoDrop™ ND-1000 Spectrophotometer (A_{280}) (Section 2.1). The crystallin extraction process was carried out multiple times with comparable protein concentrations. The extract was then stored at 4 °C for up to two weeks.

2.2.3 Purification of α-, β- and γ-crystallin

Crude bovine lens crystallin protein samples, prepared as described above, were purified by size-exclusion chromatography on a HiLoad™ 16/60 Superdex™ 200 prep grade column (Garvey *et al.* 2009). The elution speed was 0.5 ml/min, with 20 mM Tris (pH 8.0) at 4 °C. The absorbance at 280 nm was monitored, and 0.5 ml fractions were collected. The crystallin purification process was carried out multiple times and achieved a typical elution profile with high reproducibility. Samples were run on an SDS-PAGE gel (Section 2.1) to assess purity. The concentration of each sample was determined using a Thermo Scientific NanoDrop™ ND-1000 Spectrophotometer (A_{280}) (Section 2.1).

2.2.4 Formation of amyloid fibrils by crude crystallin and α-, β- and γ-crystallin

Amyloid fibrils were formed from crystallin proteins using adapted in-house methods (Garvey *et al.* 2009). Crude crystallin was diluted to a concentration of 5.8 mg/ml in 10% (v/v) trifluoroethanol (TFE) (adjusted to pH 2.0 with 1 M HCl). Bovine α-crystallin was dissolved at a concentration of 5.8 mg/ml in 10% (v/v) TFE (adjusted to pH 2.0 with 1 M HCl). The pH of the solution was tested, and further 0.1 M HCl was added dropwise until the pH of the solution was equal to 2.0. The solution was then incubated at 60 °C for 12 hours. This fibrillisation method was repeated with β- and γ-crystallin. Thioflavin T assays (Section 2.2.6) were performed on the samples, and the presence of fibrils was indicated using TEM (Section 2.4.8) (Burke and Rougvie 1972; LeVine III 1999; Whittingham *et al.* 2002).

2.2.5 Pepsin digestion of bovine crystallin amyloid fibrils

Pepsin was added to the crystallin amyloid fibril samples (1:100 w/w pepsin:crystallin) and incubated at 4 °C for one week (Zurdo *et al.* 2001). The digested sample was spun at 8,000 x *g* for 2 minutes and the fibril pellet re-suspended in nanopure water, previously adjusted to pH 2.0 with HCl. The presence of fibrils was then reassessed using TEM (Section 2.4.8). The results were repeated three times with high reproducibility.

2.2.6 Thioflavin T (ThT) assay

The ThT assay was carried out following in-house methods. 1 mM thioflavin T was made up fresh in nanopure water and added to 5.8 mg/ml amyloid fibril samples in a NUNC 96 well microplate to achieve a final concentration of 5 μM, in a final volume of 200 μl. ThT fluorescence emission intensity was measured using excitation/emission filters of 450 and 485 nm, respectively, using a BMG Labtech FLUOstar OPTIMA plate reader (LeVine III 1999) (Section 2.1). Fluorescence was measured for three replicates with a standard error of less than 5% for each assay.

Time-course ThT fluorescence measurements were carried out in a similar way, following in-house methods. 1 mM thioflavin T was made up fresh in nanopure water and added to 5.8 mg/ml protein samples in a NUNC 96 well microplate to achieve a final concentration of 5 μM,

in a final volume of 200 µl. ThT fluorescence emission intensity was measured using excitation/emission filters of 450 and 485 nm, respectively, using a BMG Labtech FLUOstar OPTIMA plate reader (LeVine III 1999) (Section 2.1). Fluorescence was measured every five minutes for 1250 minutes (250 cycles), for three replicates with a standard error of less than 5% for each assay.

2.3 Glucose oxidase assay

GOD activity was measured using an Invitrogen Amplex Red Glucose/Glucose Oxidase assay kit (Zhou *et al.* 1997). Samples containing 100 µM Amplex Red reagent, 0.2 U/ml horseradish peroxidase, 100 mM glucose and the appropriate amount of glucose oxidase in 50 mM sodium phosphate buffer, pH 7.4, were incubated for 8 minutes at 37 °C. Fluorescence was measured with a Labtech FLUOstar OPTIMA plate reader using excitation at 530 nm and fluorescence detection at 590 nm (Section 2.1). Background fluorescence determined for a control containing no GOD was subtracted from each value. A standard curve was created using a 0 – 10 mU GOD concentration range as shown in Figure 2.1. Fluorescence was measured for three replicates with a standard error of less than 5% for each assay.

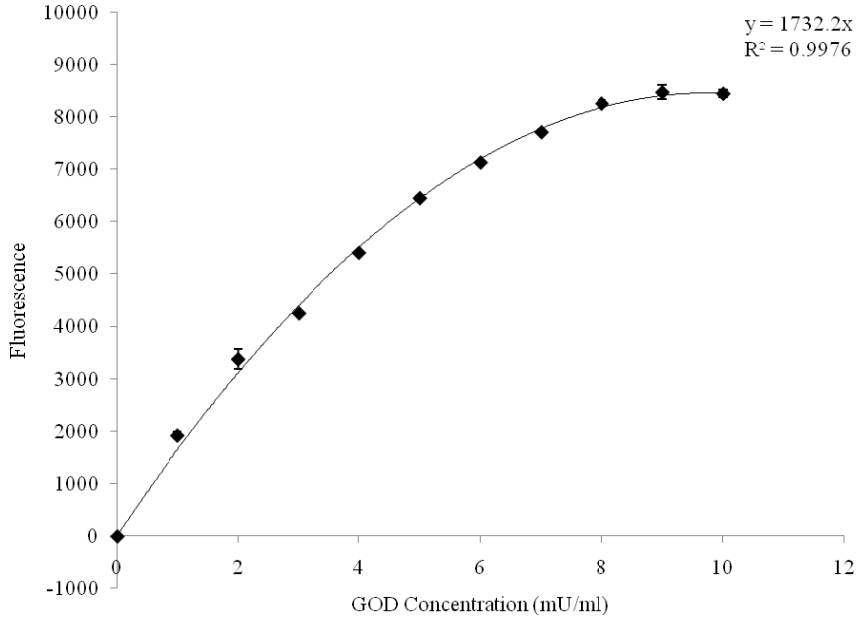

Figure 2.1

GOD standard curve. *Fluorescence of Amplex Red was measured at GOD concentrations ranging from 0-12 mU/ml. Error bars show standard error of the mean of three replicates and are less than 5%.*

2.4 Cross-linking of amyloid fibrils to GOD enzyme

Following amyloid fibril formation by protein from both bovine insulin and bovine eye lens crystallin sources, cross-linking experiments were undertaken to attach GOD to amyloid fibrils. Three methods were used, glutaraldehyde cross-linking, sugar oxidation by periodate, and glutaraldehyde cross-linking following deglycosylation. Several experimental techniques were then employed to assess the degree of GOD cross-linking to amyloid fibrils.

2.4.1 Glutaraldehyde cross-linking

Glutaraldehyde (GA) concentrations of 5, 10, 15, 20, 50, 100, 150, and 200 mM were used to determine the best concentration for cross-linking GOD to amyloid fibrils. Each GA concentration was added to 2 mg/ml GOD in 50 mM phosphate buffer at pH 7.4, and nanopure water adjusted to pH 2.0 with HCl in a ratio of 1:1:1. Samples were then run on an SDS-PAGE gel (Section 2.1). The chosen GA concentration (150 mM) from the gel was used in further experiments.

1.9 mg/ml insulin fibrils were added to an aliquot of 3% (v/v) GA to make a final concentration of 1% GA (150 mM), and mixed by inversion. 0.6 mg/ml GOD was then added and the samples were incubated for one hour at 25 °C. The pH of each cross-linked solution was tested to ensure a final pH of 7.0. Cross-linked samples were immediately run on an SDS-PAGE gel to assess degree of cross-linking (Section 2.1). This experiment was repeated with high reproducibility.

2.4.2 Deglycosylation of GOD

GOD (2 mg/ml) was incubated for 24 hours at 37 °C with 10 U α-mannosidase (E.C. 3.2.1.24) and 30 mU endoglycosidase H (E.C. 3.2.1.96) in 30 mM potassium phosphate buffer (pH 5) (Sohail Akhtar and Bhakuni 2003). The degree of deglycosylation was assessed by SDS-PAGE (Section 2.1).

2.4.3 Ninhydrin assay

The ninhydrin assay was performed using in-house methods (Friedman *et al.* 1984). Ninhydrin buffer was prepared by adding lithium acetate buffer (4M lithium acetate, adjusted to pH 5.2 with acetic acid) to ninhydrin solution (0.01 M ninhydrin, 0.01 M hydrindantin and 75% dimethyl sulfoxide (DMSO) to achieve a final ratio of lithium acetate buffer to ninhydrin solution of 1:3. The ninhydrin solution was then added to diluted protein samples, including a sample blank. The solution was heated at 100 °C for 10 minutes, vortexing the samples after five minutes. The solution was then cooled in an ice bath. 50% (v/v) ethanol was then added to each sample and vortexed. The absorbance of three sample replicates was read at 570 nm and corrected for the sample blank.

2.4.4 Periodate oxidation of GOD

GOD (2 mg/ml) was incubated for 24 hours at 4 °C with increasing molar concentrations of sodium periodate to mannose of 0.1:1, 0.2:1, 0.3:1, 0.5:1, 0.75:1, 1:1 and 2:1 (Section 5.3) (Kozulic *et al.* 1987). The degree of carbohydrate shell oxidation was assessed by SDS-PAGE, and the most effective concentration ratio of 2:1 was chosen. GOD oxidised with a molar concentration of sodium periodate to mannose of 2:1 was then reduced using increasing molar concentrations of sodium borohydride to mannose of 1:1, 10:1, 25:1, 50:1 and 100:1. The degree of carbohydrate shell reduction was assessed by SDS-PAGE, and the most effective concentration ratio of 100:1 was chosen. Sodium borohydride was then added to 2 mg/ml oxidised GOD and 5.8 mg/ml insulin amyloid fibrils at a molar concentration of sodium borohydride to mannose of 100:1 (Kozulic *et al.* 1987). The degree of cross-linking was then assessed by SDS-PAGE (Section 2.1).

2.4.5 Preparation of sucrose gradient

Cross-linked samples of GOD and fibrils as prepared above (Section 2.4.1, Section 2.4.2 and Section 2.4.4) were loaded onto 14 × 95 mm Ultra-Clear centrifuge tubes (Beckman) prepared with a step gradient formed by five layers containing 80%, 70%, 50%, 30%, and 0% sucrose, respectively. The tubes were centrifuged for 16 hours at 180,000 × g (33,000 rpm) at 4 °C using a SW40Ti rotor and a L-70 Beckman ultracentrifuge (Schrödel and De Marco 2005). The

centrifuge tube was then pierced using a 16 gauge needle, 1 cm from the bottom of the tube, and 1 ml fractions were removed. These fractions were then tested for GOD activity using the Amplex red assay (Section 2.3), the presence of amyloid fibrils using the ThT assay (Section 2.2.6), and for protein using the Bradford assay (Section 2.4.7).

2.4.6 Centrifugation of cross-linked samples

Cross-linked samples of GOD and fibrils as prepared in Section 2.4 were spun at 14,500 x *g* for 2 minutes. The supernatant was removed and the pellet resuspended in nanopure water. This washing cycle was repeated for five washes. Bradford, ThT and Amplex Red assays (Sections 2.4.7, 2.2.6, and 2.3, respectively) were then carried out on both supernatant and pellet samples.

2.4.7 Bradford assay

8 µl of cross-linked samples were added to a SARSTEDT 96 flat well optical plate and diluted with 152 µl nanopure water. Bradford reagent was diluted 1:4 (v/v) with water and added to samples to achieve a final dye concentration of 4%. Absorbance of the samples was then read at 540 nm using a Labtech FLUOstar OPTIMA plate reader (Bradford 1976) (Section 2.1). Absorbance was measured for three replicates with a standard error of less than 5% for each assay.

2.4.8 Transmission electron microscopy (TEM) studies

Bovine insulin and bovine lens crystallin fibrils (5.8 mg/ml) were stained with 1% uranyl acetate on Formvar-coated copper grids (200 mesh). Samples were then washed with nanopure water. Grids were then viewed at 89,000 x magnification (unless otherwise stated) using a Morgagni 268D TEM (FEI Company, Oregon, USA), operating at 80 kV and fitted with a 40 µm objective aperture (Burke and Rougvie 1972; Whittingham *et al.* 2002).

2.4.9 Differential scanning fluorimetry (DSF) of cross-linked samples

DSF was performed on cross-linked samples of GOD and fibrils as prepared in Section 2.4 using a BioRad IQ5 Multicolour Real-Time PCR Detection System. 10x SYPRO Orange dye was added to 0.5 mg/ml protein and 50 mM sodium phosphate buffer at pH 7.4 in a 96-well thin-wall PCR plate (Bio-Rad). The plate was sealed and heated in increments of 0.5 °C, with a 10 second dwell time. Fluorescence changes were monitored simultaneously with a charge-coupled device camera. The wavelengths for excitation and emission were 490 and 575 nm, respectively. Experiments were carried out in triplicate for each condition.

2.4.10 Thermal denaturation of cross-linked samples

Cross-linked samples were prepared as in Section 2.4. Each sample was heated at 50 °C for 5 minutes and placed on ice. This was then repeated with fresh cross-linked samples at 60, 70, 80 and 90 °C. GOD activity was then tested for each sample using the Amplex Red assay (Section 2.3). Experiments were carried out in triplicate for each condition.

2.4.11 Circular dichroism (CD) of cross-linked samples

CD spectra were generated on a Jasco J-815 spectrophotometer. The CD spectra were measured at a GOD concentration of 0.03 mg/ml and an insulin fibril concentration of 0.11 mg/ml in a 1 cm cell. Temperature scans were monitored at 220 nm, and data were collected at 0.5 °C intervals between 40 and 90 °C with a 1 second averaging time. Cuvettes were stopped to prevent evaporation. The values obtained were normalised by subtracting the baseline recorded for the sample buffer.

2.5 Poly(vinyl alcohol) (PVOH) films

PVOH films were made using Shiva Rao's in-house method (Rao 2008). PVOH was dissolved in water by heating to 60 °C to a concentration of 10% (w/v). 18 ml of cross-linked sample was then added to 6 ml PVOH to achieve a final concentration of 2.5%. Films were mixed by inversion, taking care to avoid air bubbles, and poured into 10 x 7 cm gel casting trays. The

trays were measured with a spirit level. The films were then covered with paper and dried under ambient conditions for seven days, removed from the trays and stored in separate plastic bags.

Films containing ThT were made using the same method, with 1 mM ThT added before mixing the films, to achieve a final concentration of 5 μM. Films were then cast as above.

2.5.1 Scanning electron microscopy (SEM)

Film samples were studied using the field emission scanning electron microscope (FE-SEM) (with assistance from Mike Flaws, Senior Technician, Department of Mechanical Engineering, University of Canterbury). Film samples from Section 2.5 were cut and prepared by splutter coating with gold and incubated at 60 °C overnight. Samples were then viewed using a 1,000 x objective on a JEOL JSM-7000F high resolution FE-SEM.

2.5.2 Confocal microscopy

1 x 1 cm pieces were cut from films prepared in Section 2.5 and mounted on slides using glycerol. Confocal optical sections of film samples were taken using a Leica Microsystems TCS SP5 confocal microscope with a Leica HCX PL APO 63 x 1.3 glycerol-immersion objective. An excitation of 405 nm and an emission detection of 430 – 520 nm were used.

2.6 Antibacterial experiments

Luria Bertani (LB) Agar (25 g/L LB and 15 g/L Select Agar) was prepared and autoclaved, using in-house methods. For glucose containing plates, 10 g/l glucose was added to the LB Agar before autoclaving. *E. coli* (XL1 Blue) was inoculated onto LB Agar plates. Each film sample was cut into circles of 1 cm diameter and two pieces of each film sample were placed on each plate. The plates were incubated at 37 °C for 48 hours. Three replicates of each plate were made, with high reproducibility.

2.7 Antifungal experiments

Potato dextrose agar (PDA) (39 g/L PDA and 5 g/L Select Agar) was prepared and autoclaved, using in-house methods. *Fusarium* (CANU-F14)*, Aspergillus* (CANU-M43) and *Rhizopus* (CANU-C245) were inoculated onto potato dextrose agar (PDA) plates. Each film sample was cut into circles of 1 cm diameter. One piece of film was placed on each plate. Fungi were incubated at 25 °C for one week to assess antimicrobial activity. Three replicates of each plate were made, with high reproducibility.

2.8 References

Bradford, M. M. (1976). A rapid and sensitive method for the quantitation of microgram quantities of protein utilizing the principle of protein dye binding. *Analytical Biochemistry* **72**: 248-254.

Burke, M. J. and Rougvie, M. A. (1972). Cross-β protein structures. I. Insulin fibrils. *Biochemistry* **11**: 2435-2439.

Friedman, M., Pang, J. and Smith, G. A. (1984). Ninhydrin-reactive lysine in food proteins. *Journal of Food Science* **49**: 10-13.

Garvey, M., Gras, S. L., Meehan, S., Meade, S. J., Carver, J. A. and Gerrard, J. A. (2009). Protein nanofibres of defined morphology prepared from mixtures of crude crystallins. *International Journal of Nanotechnology* **6**: 258-273.

Kozulic, B., Leustek, I., Pavlovic, B., Mildner, P. and Barbaric, S. (1987). Preparation of the stabilized glycoenzymes by cross-linking their carbohydrate chains. *Applied Biochemistry and Biotechnology* **15**: 265-278.

LeVine III, H. (1999). Quantification of β-sheet amyloid fibril structures with thioflavin T. *Methods in Enzymology* **309**: 274-284.

Nielsen, L., Frokjaer, S., Carpenter, J. F. and Brange, J. (2001). Studies of the structure of insulin fibrils by Fourier transform infrared (FTIR) spectroscopy and electron microscopy. *Journal of Pharmaceutical Sciences* **90**: 29-37.

Rao, S. P. (2008). PhD Thesis. Amyloid fibrils in bionanomaterials. *School of Biological Sciences, University of Canterbury, Christchurch*.

Schrödel, A. and De Marco, A. (2005). Characterization of the aggregates formed during recombinant protein expression in bacteria. *BMC Biochemistry* **6**.

Sohail Akhtar, M. and Bhakuni, V. (2003). Alkaline treatment has contrasting effects on the structure of deglycosylated and glycosylated forms of glucose oxidase. *Archives of Biochemistry and Biophysics* **413**: 221-228.

Whittingham, J. L., Scott, D. J., Chance, K., Wilson, A., Finch, J., Brange, J. and Guy Dodson, G. (2002). Insulin at pH 2: Structural analysis of the conditions promoting insulin fibre formation. *Journal of Molecular Biology* **318**: 479-490.

Zhou, M., Diwu, Z., Panchuk-Voloshina, N. and Haugland, R. P. (1997). A stable nonfluorescent derivative of resorufin for the fluorometric determination of trace hydrogen peroxide: Applications in detecting the activity of phagocyte NADPH oxidase and other oxidases. *Analytical Biochemistry* **253**: 162-168.

Zurdo, J., Guijarro, J. I. and Dobson, C. M. (2001). Preparation and characterization of purified amyloid fibrils. *Journal of the American Chemical Society* **123**: 8141-8142.

3. CHAPTER THREE - FORMATION OF AMYLOID FIBRILS FROM BOVINE INSULIN AND BOVINE LENS CRYSTALLIN

3.1 Introduction

Amyloid fibrils have potential for use in a number of industrial applications, as discussed in Section 1.5. The formation of insulin amyloid fibrils is well characterised, and was demonstrated in this chapter (Brange *et al.* 1997; Jiménez *et al.* 2002; Devlin *et al.* 2006). Crystallins are a good source of amyloid fibrils, as they are a waste material from the meat processing industry in New Zealand. Amyloid fibrils can be inexpensively produced from crude crystallin protein mixtures in significant quantity, which is important for use in commercial applications (Ecroyd and Carver 2008; Garvey *et al.* 2009). The ability to form amyloid fibrils from both crude and purified bovine lens crystallin proteins was assessed in this chapter. The method of crude crystallin extraction was modified to produce a greater protein yield and the properties of the resulting amyloid fibrils such as protease resistance and pH stability were then investigated.

3.2 Formation of insulin amyloid fibrils

Insulin amyloid fibrils were formed by subjecting bovine insulin to conditions of low pH and high temperature known to cause fibrillation, following literature methods (Section 2.2.1) (Nielsen *et al.* 2001). The time-course formation of amyloid fibrils was monitored using ThT. ThT is a fluorescent dye that elicits a distinctly different excitation and emission spectrum upon amyloid β-sheet binding (LeVine III 1993; LeVine III 1999). The time-course for amyloid fibril formation is given in Figure 3.1.

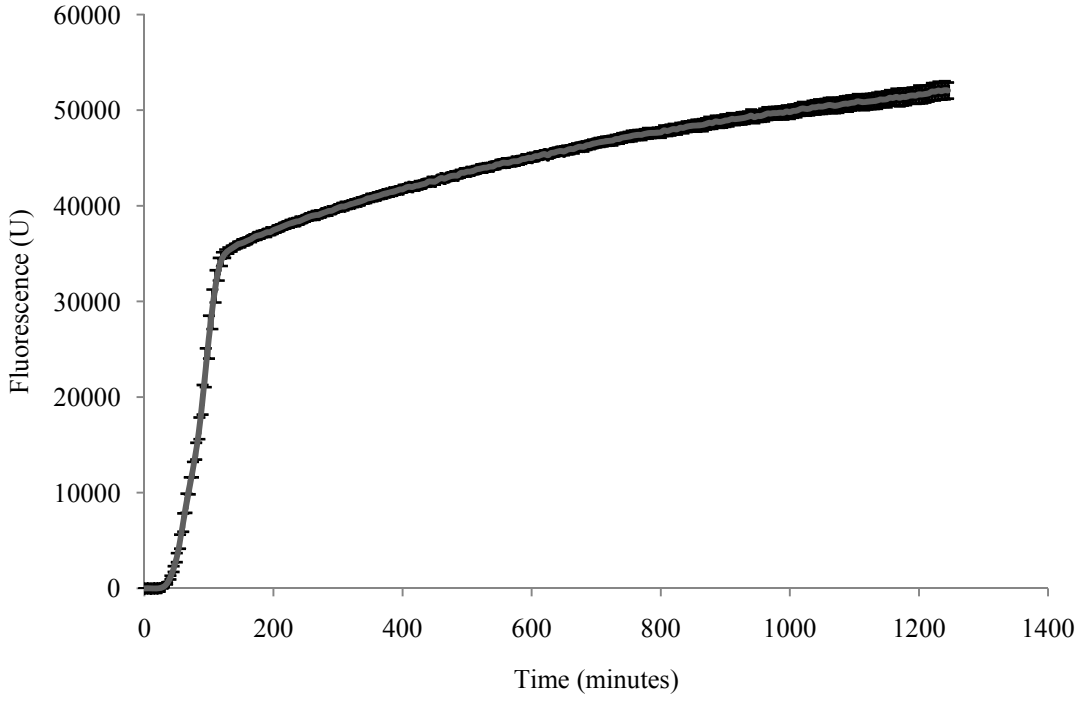

Figure 3.1

Time-course formation of amyloid fibrils by bovine insulin and bovine crystallin. *0.79 mg/ml ThT was added to 5.8 mg/ml bovine insulin in 0.1 M NaCl, adjusted to pH 1.6 with 1 M HCl, and incubated for 1400 minutes at 60 °C. Error bars indicate the standard error of the mean of four replicates, and are less than 5%.*

The results of the time-course incubation showed a steep increase in fluorescence for insulin within the first 120 minutes of incubation, consistent with literature reports (Hua and Weiss 2004; Ahmad *et al.* 2005).

TEM was also used for the identification and characterisation of insulin amyloid fibrils. The results are shown in Figure 3.2. These insulin amyloid fibrils have a straight, long, thin, unbranched morphology consistent with previous research, with a diameter of around 6 nm (Rochet and Lansbury 2000; Cherny and Gazit 2008).

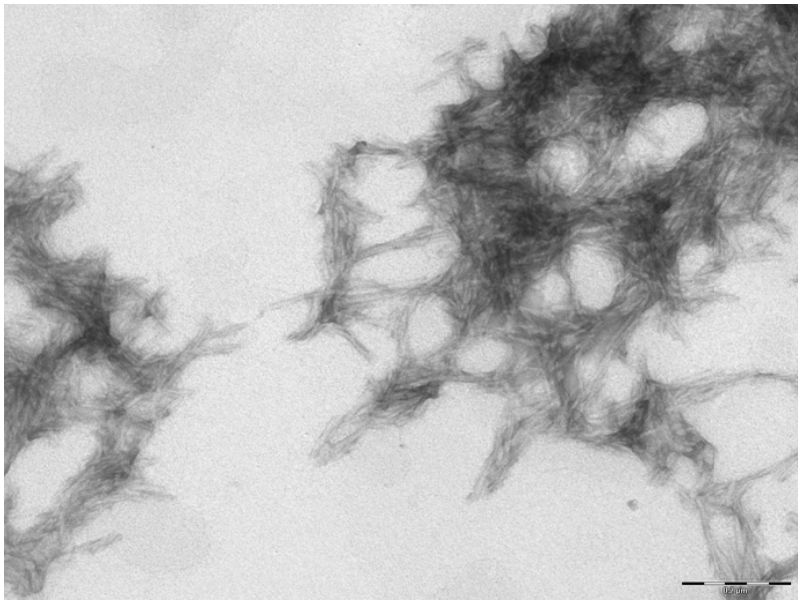

Figure 3.2

TEM image of insulin amyloid fibrils. *Representative TEM image of 5.8 mg/ml insulin in 0.1 M NaCl, adjusted to pH 1.6 with 1 M HCl at 60 °C for four days. Sample was stored frozen prior to imaging. Scale bar = 0.2 µm.*

3.3 Formation of crystallin amyloid fibrils

Crude crystallin was prepared using the initial in-house method described in Section 2.2.2 (Method One), and subjected to amyloid fibril forming conditions (Meehan *et al.* 2004). Previous research has shown that the amyloid-binding dyes Congo Red and ThT used to determine the presence of amyloid fibrils also bind to native crystallins *in situ* (Frederikse 2000). This suggests that the crystallin proteins in the mammalian eye lens are arranged in a supramolecular structure with amyloid-like properties (Frederikse 2000). Thus, because of the very high background reading of native crystallin proteins, the use of ThT is not reliable for the assessment of crystallin amyloid fibril formation. TEM was therefore used to identify the presence of crystallin amyloid fibrils (Figure 3.6) (Burke and Rougvie 1972; Whittingham *et al.* 2002).

Two distinct morphologies are present in the crude crystallin sample (Figure 3.3), the long, thin structures characteristic of amyloid fibrils, and short, curly structures. This is consistent with previous research (Meehan *et al.* 2004).

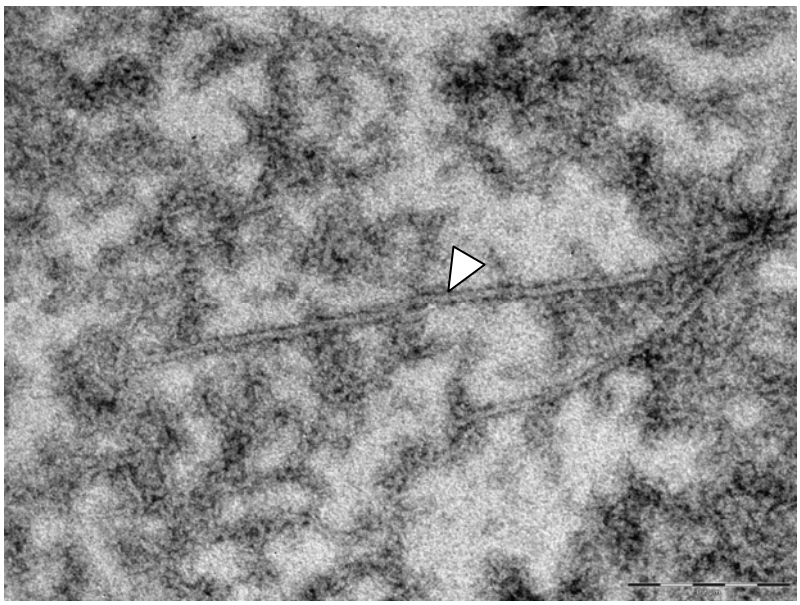

Figure 3.3

TEM image of insulin amyloid fibrils. *Representative TEM image of 5.8 mg/ml crude crystallin in 10% TFE, adjusted to pH 2.0 with 1 M HCl at 60 °C for four days. An amyloid fibril is indicated with an arrow. Scale bar = 0.2 μm.*

3.4 Purification of bovine crystallin

Crude bovine crystallin prepared in Section 2.2.2 (Method One) by the initial in-house method, was purified in order to achieve a homogenous fibril sample for use in cross-linking experiments. It was initially thought that the two morphologies seen in the crude sample may have been formed from different crystallin proteins. Thus purification was carried out in order to yield homogenous long, thin amyloid fibrils in a nanoscaffold formation for enzyme immobilisation. This separation gave a typical elution profile with six protein peaks, as shown in Figure 3.4. The fractions for each crystallin peak were pooled and lyophilised.

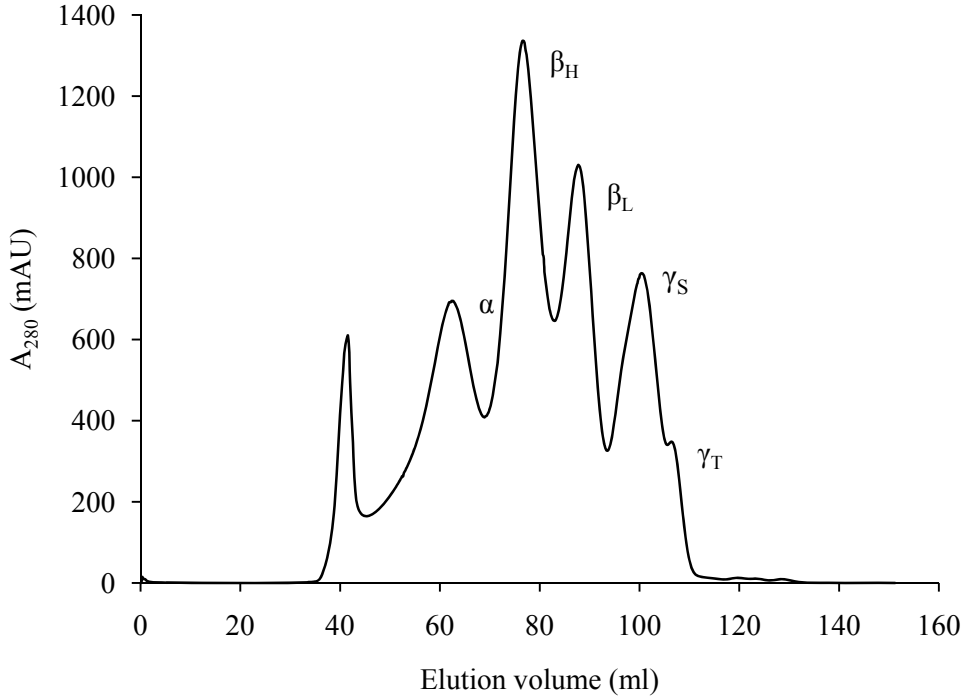

Figure 3.4

Purification of crude crystallin. *The α-crystallin peak corresponded to the fractions eluting between 50-65 ml, the β_H-crystallin peak corresponded to the fractions eluting between 70-80 ml, the β_L-crystallin peak corresponded to fractions eluting between 80-90 ml, the γ_S-crystallin peak corresponded to the fractions eluting between 95-105 ml, and the γ_T-crystallin peak corresponded to the fractions eluting between 107-109 ml.*

This elution profile shows separation between the crystallin fractions. The first peak (unlabelled) is high molecular weight protein aggregate. The second peak, α, consists of the two closely related subunits αA and αB. The third peak (β_H) is high molecular weight, or octameric, β-crystallin, and the fourth peak (β_L) is low molecular weight dimeric and trimeric β-crystallin. The fifth (γ_S) and sixth (γ_T) peaks consist of γ_S-crystallin and total γ-crystallins, respectively. This result shows a similar high degree of separation to crystallin purification reported in the literature (Carver *et al.* 1996). Following lyophilisation, fractions were reconstituted in nanopure water at a concentration of 5.8 mg/ml and run on an SDS-PAGE gel to assess purity (Figure 3.5).

The crude crystallin sample produced a number of bands (Lane 1). The α-crystallin sample in Lane 2 produced two bands, one band of ~19 kDa (Band a), and another band of 20 kDa (Band b). These bands are consistent with the molecular weight of the two mammalian α-crystallin subunits, which are ~20 kDa (Ecroyd and Carver 2008). The β_H-crystallin sample produced

three bands of ~20 kDa (Band c), ~25 kDa (Band d) and ~30 kDa (Band e) (Lane 3). These bands are consistent with the molecular weight of the seven mammalian β-crystallin subunits, which range from ~22 – 28 kDa (Ecroyd and Carver 2008). The β_L-crystallin sample in Lane 4 produced two of the three bands seen in the β_H-crystallin sample (Bands f and g). However, the larger subunit band of ~30 kDa is not visible. The γ_S-crystallin sample produced one band of ~20 kDa (Band h) (Lane 5). This is consistent with the molecular weight of the seven subunits of γ-crystallin, which is ~21 kDa (Ecroyd and Carver 2008). There is no band visible in the γ_T-crystallin fraction (Lane 6); however, this sample was later determined to be of very low protein concentration.

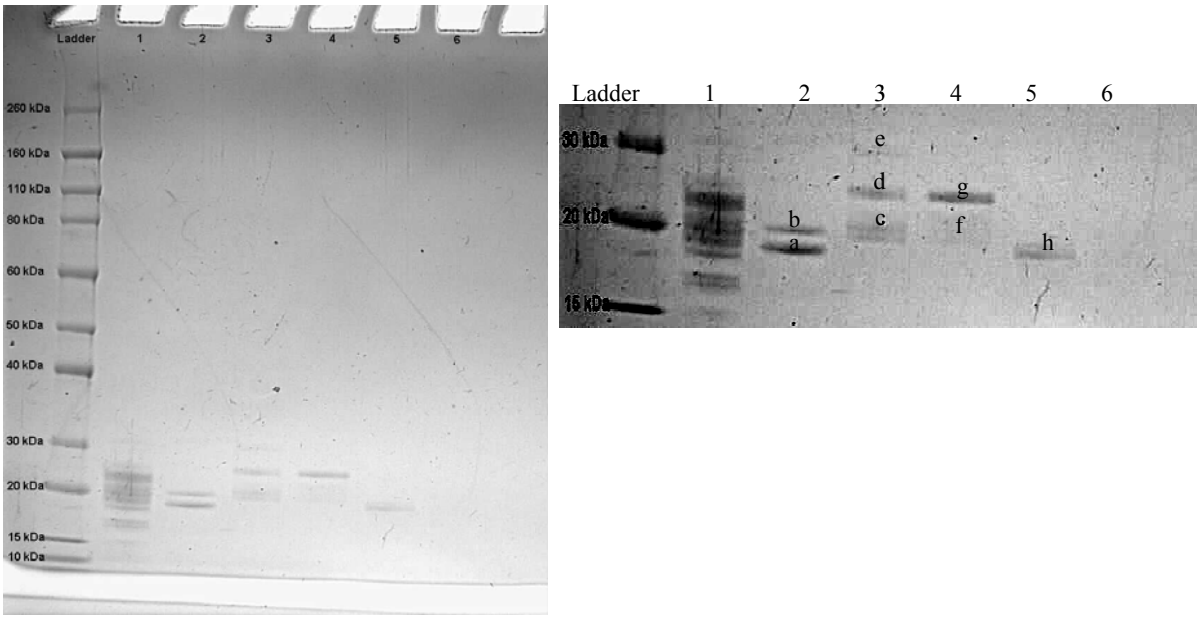

Figure 3.5

SDS-PAGE gel of purified crystallin samples. *Lane 1 is the 5.8 mg/ml crude crystallin sample, Lane 2 is the lyophilised α-crystallin sample made up at 5.8 mg/ml of lyophilised sample in nanopure water, Lane 3 is the lyophilised β_H-crystallin sample made up at 5.8 mg/ml, Lane 4 is the lyophilised β_L-crystallin sample made up at 5.8 mg/ml, Lane 5 is the lyophilised γ_S-crystallin sample made up at 5.8 mg/ml, Lane 6 is the lyophilised γ_T-crystallin sample made up at 5.8 mg/ml. The bands have been enlarged for greater clarity (inset).*

These results are consistent with crystallin separation results in previous research and confirm that size exclusion chromatography is a successful technique for the separation of crude crystallins into pure fractions (Garvey *et al.* 2009). Purified crystallin samples were then subjected to amyloid fibril forming conditions after appropriate concentration, and viewed by TEM.

3.5 TEM of purified crystallin amyloid fibrils

The α- and β_H-crystallin samples (Figure 3.6A and B, respectively) show long thin amyloid fibrils amongst amorphous aggregate, indicated with an arrow. These amyloid fibrils are consistent with the morphology of insulin amyloid fibrils, with a diameter of around 6 nm (Rochet and Lansbury 2000; Cherny and Gazit 2008). There are no long, thin fibrillar structures clearly visible in either the β_L-, γ_S- and γ_T-crystallin samples (Figure 3.6C, D and E, respectively), suggesting amorphous aggregate. This is inconsistent with previous results, which state that all the crystallin fractions were able to form amyloid fibrils (Garvey *et al.* 2009). This could be due to the conditions used to form amyloid fibrils, as amyloid fibrils have been found to have different morphologies in different conditions (Ecroyd and Carver 2008). The protein fractions were not dialysed following purification, and therefore contained a high concentration of Tris buffer, in comparison to previous methods where the purified crystallins were dialysed (Garvey *et al.* 2009). The protein fractions were also at a lower concentration than crystallin fractions used in previous research, which were all found to form amyloid fibrils (Meehan *et al.* 2004).

Further work was not done because the crude crystallin gave the best amyloid fibril formation, as judged by TEM. The amyloid fibrils were clearly defined and there was minimal aggregate present in comparison to purified samples. This confirms that amyloid fibrils can be readily prepared from this waste protein. Crude crystallin amyloid fibrils were therefore used for further experiments. To test the fibrillar nature of the short, curly structures, the crude crystallin sample was exposed to pepsin, a proteolytic enzyme. Before exposure to pepsin, the crude crystallin extraction method was modified to obtain a higher protein yield, and to reduce protein aggregation (Section 2.2.2 (Method Two)). This method used an Ultra Turrax™ without the grinding attachment, in place of the Magic Bullet, in order to gently homogenise the lenses. The tubes were placed on ice between homogenisation cycles to prevent aggregation. The samples were then centrifuged in 1.5 ml Eppendorf tubes to generate better separation between crystallin protein and other cellular matter. This adapted method gave a greater protein concentration than the previous in-house method (results not shown) and a higher proportion of long, thin amyloid fibrils compared to short, curly structures seen in Figure 3.3. This method of crude crystallin extraction and amyloid fibril formation was thus used for further experiments, including pepsin digestion experiments.

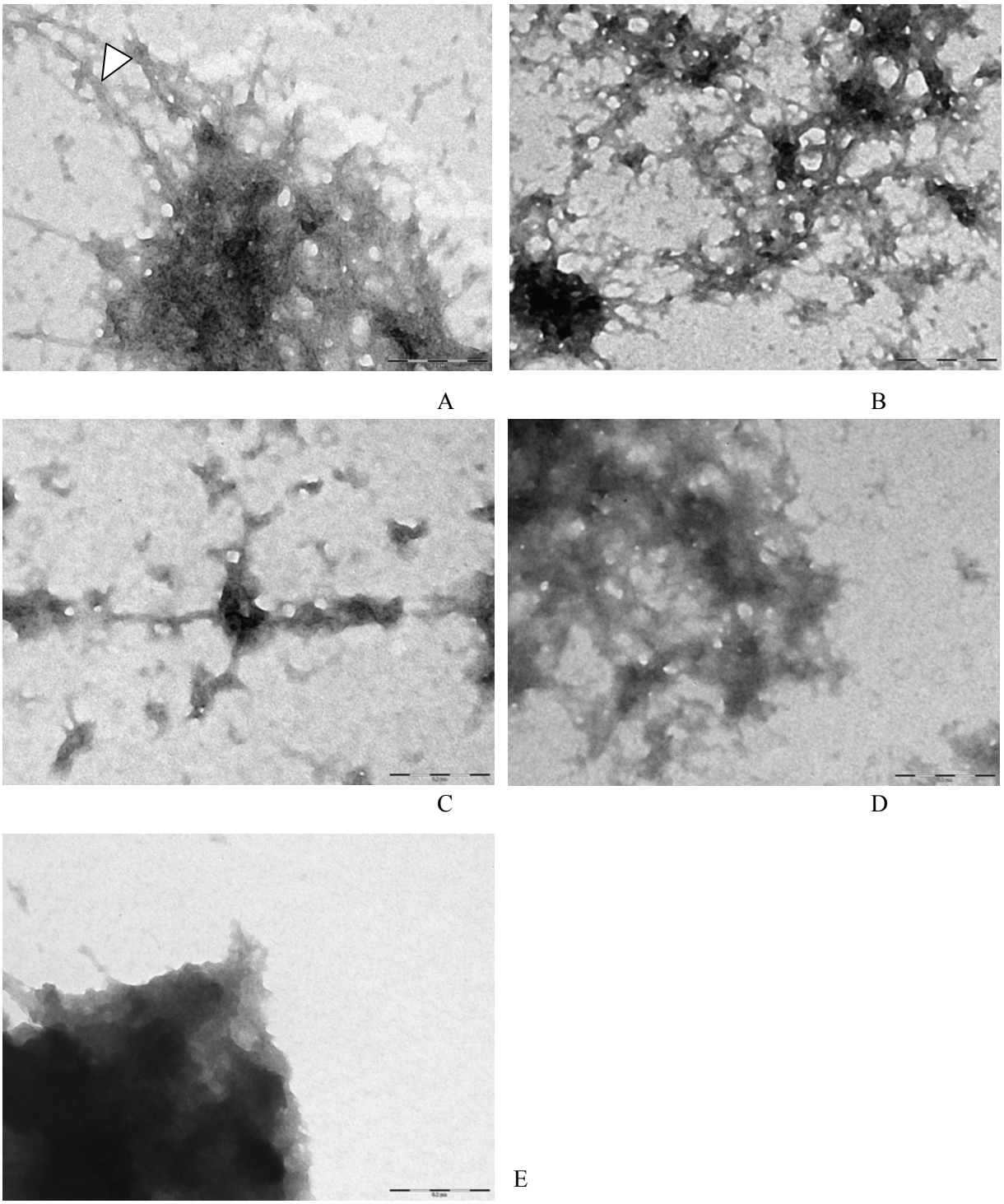

Figure 3.6

TEM images of purified crystallin amyloid fibrils. *Representative TEM images of purified crystallin fractions subjected to amyloid fibril forming conditions: α-crystallin (A) β_H-crystallin (B), β_L-crystallin (C), γ_s-crystallin (D) and γ_T-crystallin (E). Amyloid fibril-like structures are indicated with an arrow. Scale bar = 0.2 μm.*

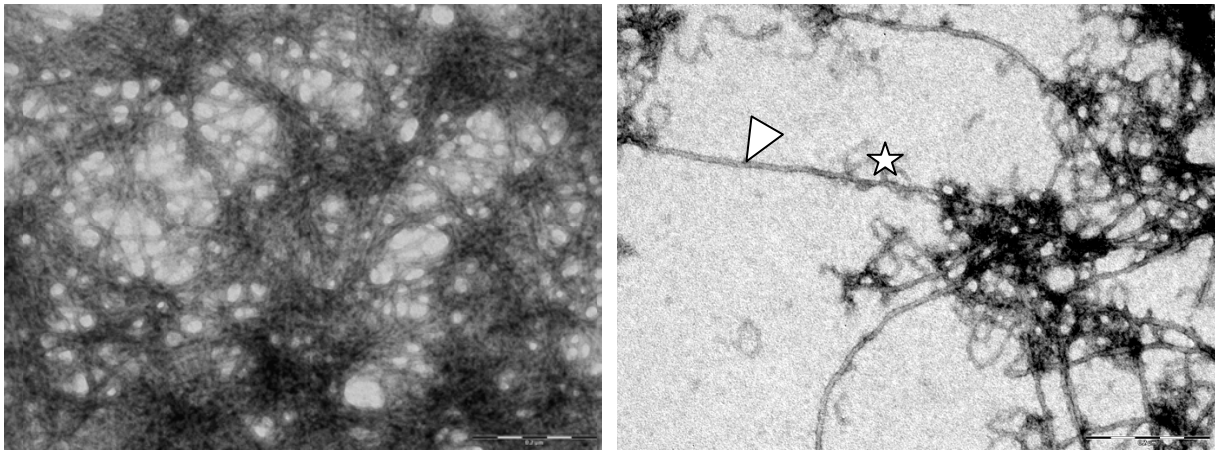

A B

Figure 3.7

TEM images of crude crystallin amyloid fibrils (Method Two). *Crude crystallin amyloid fibril scaffold at 5.8 mg/ml (A) and crude crystallin amyloid fibrils at 5.8 mg/ml (B). Scale bar = 0.2 µm. Long, thin amyloid fibrils are indicated with an arrow, and short curly structures are indicated with a star.*

The crude crystallin preparation produced large amyloid fibril scaffolds Figure 3.8 (A), with a mixture of long thin fibrils, and short curly fibrils. This was more clearly seen near the edges of fibril scaffold structures, where the amyloid fibrils were less concentrated Figure 3.8 (B). This scaffold structure is perfect for enzyme immobilisation, providing control over molecular architecture, which is important when incorporating enzymes into a polymer (Delvaux and Demoustier-Champagne 2003). This is an exciting result, since the scaffold is achieved directly from the crude crystallin protein. However, having the two types of amyloid fibrils introduces heterogeneity into the scaffold system, which is not ideal for further applications.

3.6 Crystallin pepsin digestion

The use of crude protein preparations for amyloid fibril formation introduces heterogeneity, where the sample can contain soluble precursors that have not fibrillised and non-fibrillar aggregate (Zurdo *et al.* 2001). Exposure of amyloid fibrils to pepsin will digest any non-fibrillar species, leaving the fibrils intact (Zurdo *et al.* 2001). Crude crystallin samples were exposed to pepsin, as described in Section 2.2.5, with representative TEM images shown in Figure 3.6.

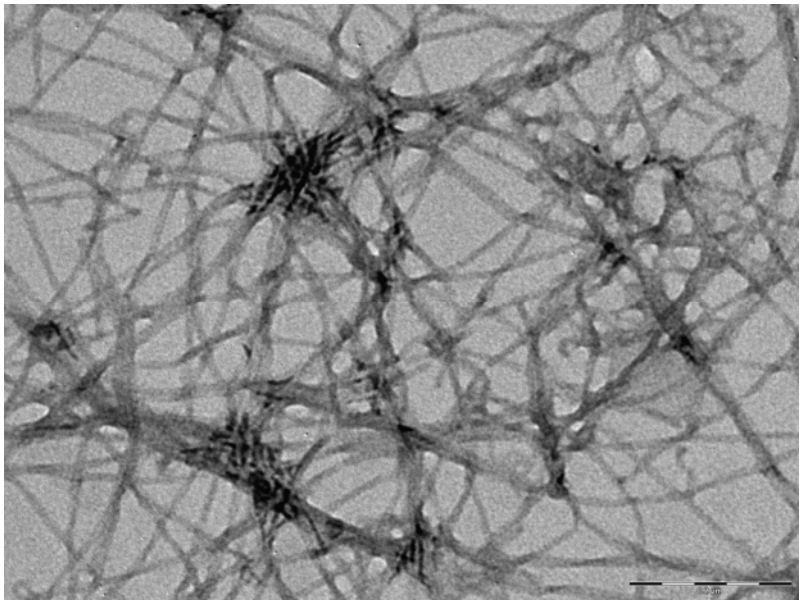

Figure 3.8

Pepsin digestion of crude crystallin amyloid fibrils. *2.9 mg/ml crystallin amyloid fibrils following digestion with pepsin. Scale bar = 0.2 µm.*

By nature, amyloid fibrils are resistant to proteolytic digestion (Zurdo *et al.* 2001). The short, curly fibrils were no longer visible following proteolytic digestion, whereas the long, thin amyloid fibrils were clearly visible Figure 3.8. This indicates that the short, curly structures seen in the TEM images were less resistant to proteolytic digestion than the long, thin fibrils, and thus may not be amyloid in nature. Another test to ensure the fibrillar nature of the short, curly structures is exposure to high pH, which is also important when cross-linking using glutaraldehyde, which requires an increase in pH for optimum reaction.

3.7 pH studies

Optimal cross-linking by glutaraldehyde occurs in basic conditions, where the amino groups of the protein are unprotonated, making the reaction of glutaraldehyde with free amino groups favourable (Wine *et al.* 2007). In contrast, the methods employed in this thesis involve the formation of both insulin and crystallin amyloid fibrils in acidic conditions (Section 2.2). In order to cross-link amyloid fibrils using glutaraldehyde effectively, the pH of the solution has to be increased. Insulin amyloid fibrils are known to be stable at pH extremes (Gras 2007); however, previous research has shown that when exposed to neutral pH, amyloid fibrils retain ThT binding ability but display different morphologies when visualised using TEM (Rao 2008).

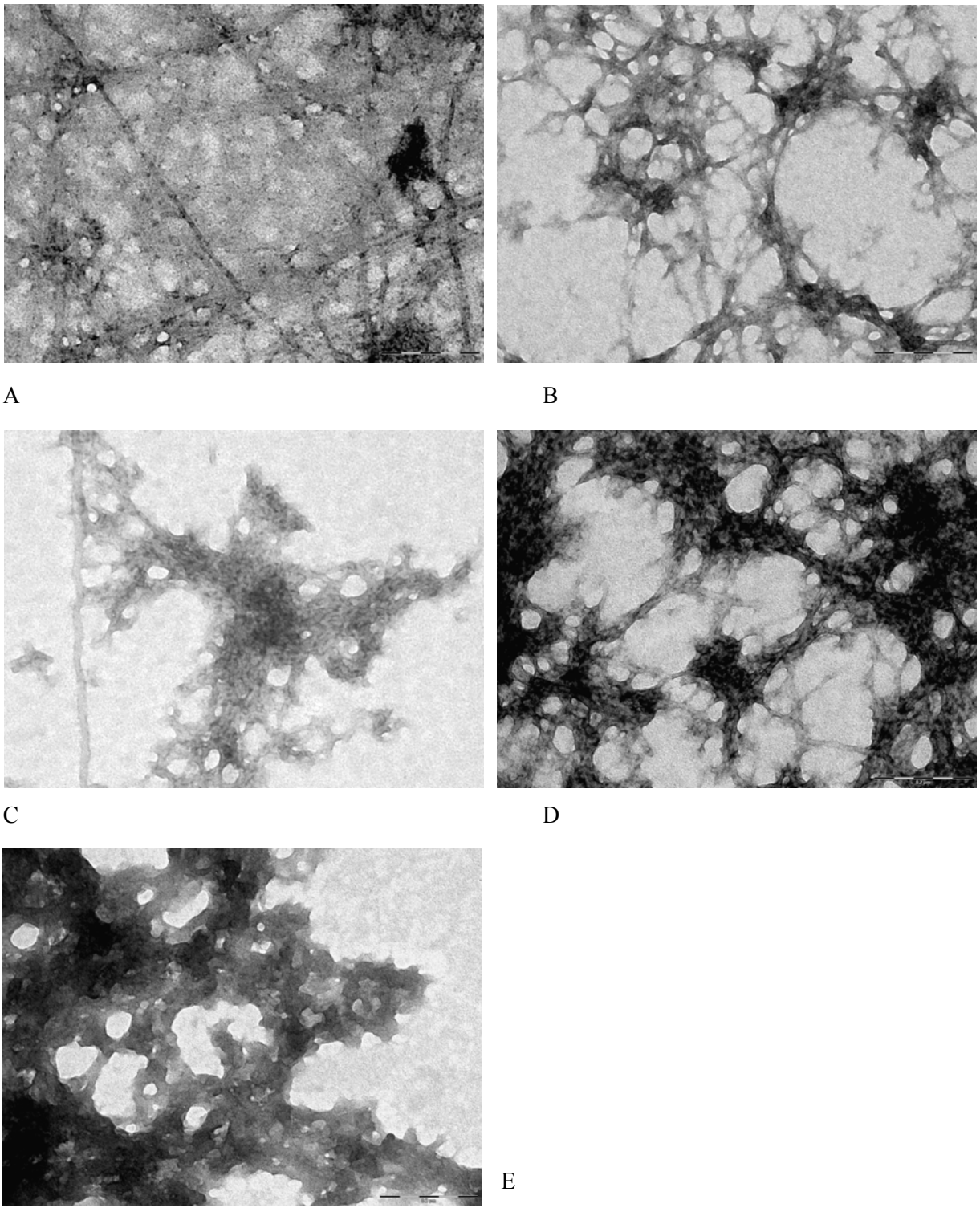

Figure 3.9

Effect of pH change on crude crystallin amyloid fibril morphology. *0.1 M sodium hydroxide was added to pre-fibrillised 5.8 mg/ml crude crystallin amyloid fibril samples to give increasing pH conditions; pH 2 (A), pH 3 (B), pH 4 (C), pH 5 (D) and pH 7 (E). Scale bar = 0.2 µm.*

Less is known about the pH stability of crystallin amyloid fibrils. Therefore, the effect of increasing pH on the morphology of pre-formed crystallin amyloid fibrils was assessed by adding sodium hydroxide before cross-linking experiments using glutaraldehyde were carried out (Figure 3.9).

The crude crystallin sample given in (Figure 3.9A) shows the long, thin fibrillar structures characteristic of amyloid fibrils. When the pH of the pre-formed fibrils is increased using NaOH, the definition of the amyloid fibrils becomes increasingly poor (Figure 3.9B – E). The increased clumping with increasing pH indicates that either the crude crystallin amyloid fibrils are affected by increase in pH, or that unfibrillised protein present in the heterogeneous crude sample is prone to aggregation upon increase of pH conditions. However, this effect could also be due to the increase of salt upon addition of NaOH. It has previously been stated that excessive salt in samples can obscure the identification of amyloid fibrils (Nilsson 2004). As mentioned in Section 2.4.8, samples were washed following staining to reduce the amount of salt on the TEM grids in order to reduce the amount of salt present in the sample. Despite this, the pH studies provide useful information for the use of crystallin amyloid fibrils for further applications (Chapter Six).

3.8 Conclusions

The ability to form amyloid fibrils from crude bovine lens crystallin protein was demonstrated in this chapter. Size exclusion chromatography was an effective method for purification of crude crystallin samples. The crude, α- and β_H-crystallin preparations formed amyloid fibrils, as determined by TEM. Short, curly structures that were also present were not resistant to proteolytic digestion or increase in pH, so were unlikely to be fibrillar. Development of the crude crystallin extraction method yielded a higher protein concentration and amyloid fibril samples containing a higher proportion of long, straight amyloid fibrils. The crude crystallin method was faster than the purification method and produced a more useful enzyme scaffold, so crude crystallins were used in further experiments to demonstrate the ability to functionalise a crude amyloid fibril scaffold system.

3.9 References

Ahmad, A., Uversky, V. N., Hong, D. and Fink, A. L. (2005). Early in the fibrillation of monomeric insulin. *Journal of Biological Chemistry* **280**: 42669-42675.

Brange, J., Andersen, L., Laursen, E. D., Meyn, G. and Rasmussen, E. (1997). Toward understanding insulin fibrillation. *Journal of Pharmaceutical Sciences* **86**: 517-525.

Burke, M. J. and Rougvie, M. A. (1972). Cross-β protein structures. I. Insulin fibrils. *Biochemistry* **11**: 2435-2439.

Carver, J. A., Nicholls, K. A., Aquilina, A. J. and Truscott, R. J. W. (1996). Age-related changes in bovine α-crystallin and high-molecular-weight protein. *Experimental Eye Research* **63**: 639-647.

Cherny, I. and Gazit, E. (2008). Amyloids: Not only pathological agents but also ordered nanomaterials. *Angewandte Chemie International Edition* **47**: 4062-4069.

Delvaux, M. and Demoustier-Champagne, S. (2003). Immobilisation of glucose oxidase within metallic nanotubes arrays for application to enzyme biosensors. *Biosensors and Bioelectronics* **18**: 943-951.

Devlin, G. L., Knowles, T. P. J., Squires, A., McCammon, M. G., Gras, S. L., Nilsson, M. R., Robinson, C. V., Dobson, C. M. and MacPhee, C. E. (2006). The component polypeptide chains of bovine insulin nucleate or inhibit aggregation of the parent protein in a conformation-dependent manner. *Journal of Molecular Biology* **360**: 497-509.

Ecroyd, H. and Carver, J. A. (2008). Crystallin proteins and amyloid fibrils. *Cellular and Molecular Life Sciences* **66**: 62-81.

Frederikse, P. H. (2000). Amyloid-like protein structure in mammalian ocular lenses. *Current Eye Research* **20**: 462-468.

Garvey, M., Gras, S. L., Meehan, S., Meade, S. J., Carver, J. A. and Gerrard, J. A. (2009). Protein nanofibres of defined morphology prepared from mixtures of crude crystallins. *International Journal of Nanotechnology* **6**: 258-273.

Gras, S. L. (2007). Amyloid fibrils: From disease to design. New biomaterial applications for self-assembling cross-β fibrils. *Australian Journal of Chemistry* **60**: 333-342.

Hua, Q.-X. and Weiss, M. A. (2004). Mechanism of insulin fibrillation: The structure of insulin under amyloidogenic conditions resembles a protein-folding intermediate. *Journal of Biological Chemistry* **279**: 21449-21460.

Jiménez, J. L., Nettleton, E. J., Bouchard, M., Robinson, C. V., Dobson, C. M. and Saibil, H. R. (2002). The protofilament structure of insulin amyloid fibrils. *Proceedings of the National Academy of Sciences of the United States of America* **99**: 9196-9201.

LeVine III, H. (1993). Thioflavine T interaction with synthetic Alzheimer's disease β-amyloid peptides: Detection of amyloid aggregation in solution. *Protein Science* **2**: 404-410.

LeVine III, H. (1999). Quantification of β-sheet amyloid fibril structures with thioflavin T. *Methods in Enzymology* **309**: 274-284.

Meehan, S., Berry, Y., Luisi, B., Dobson, C. M., Carver, J. A. and MacPhee, C. E. (2004). Amyloid fibril formation by lens crystallin proteins and its implications for cataract formation. *Journal of Biological Chemistry* **279**: 3413-3419.

Nielsen, L., Frokjaer, S., Carpenter, J. F. and Brange, J. (2001). Studies of the structure of insulin fibrils by Fourier transform infrared (FTIR) spectroscopy and electron microscopy. *Journal of Pharmaceutical Sciences* **90**: 29-37.

Nilsson, M. R. (2004). Techniques to study amyloid fibril formation *in vitro*. *Methods* **34**: 151-160.

Rao, S. P. (2008). PhD Thesis. Amyloid fibrils in bionanomaterials. *School of Biological Sciences, University of Canterbury, Christchurch*.

Rochet, J.-C. and Lansbury, P. T. (2000). Amyloid fibrillogenesis: themes and variations. *Current Opinion in Structural Biology* **10**: 60-68.

Whittingham, J. L., Scott, D. J., Chance, K., Wilson, A., Finch, J., Brange, J. and Guy Dodson, G. (2002). Insulin at pH 2: Structural analysis of the conditions promoting insulin fibre formation. *Journal of Molecular Biology* **318**: 479-490.

Wine, Y., Cohen-Hadar, N., Freeman, A. and Frolow, F. (2007). Elucidation of the mechanism and end products of glutaraldehyde crosslinking reaction by X-ray structure analysis. *Biotechnology and Bioengineering* **98**: 711-718.

Zurdo, J., Guijarro, J. I. and Dobson, C. M. (2001). Preparation and characterization of purified amyloid fibrils. *Journal of the American Chemical Society* **123**: 8141-8142.

4. CHAPTER FOUR - CROSS-LINKING GLUCOSE OXIDASE TO AMYLOID FIBRILS

4.1 Introduction

In this chapter, the attachment of GOD to amyloid fibrils using GA is explored. Cross-linking GOD to amyloid fibrils has potential to impart stability to the enzyme and functionality to the amyloid fibrils, as discussed in Sections 1.10 and 1.11. There is also evidence to suggest that immobilisation of GOD stabilises the active conformation of the enzyme (Tiller *et al.* 2002). Enzyme assays, thermal denaturation techniques and CD spectroscopy were employed in this chapter to assess the effect of attachment on GOD stability.

The effect of enzyme immobilisation on the integrity of amyloid fibrils must also be assessed, to test the theory that amyloid fibrils can be functionalised *via* the side chains of their constituent amino acids. To investigate the impact of cross-linking of GOD to amyloid fibrils on enzyme activity, any material that had not been cross-linked was separated from the cross-linked amyloid enzyme scaffold. Ideally, the best way to separate amyloid fibrils from cross-linked amyloid fibrils would be using protein separation techniques based on molecular weight. However, because amyloid fibrils have a very large molecular weight, they are difficult to separate *via* conventional biochemical separation techniques. The most effective techniques for separating large crude mixtures are gel electrophoresis and centrifugation. Thus, in this chapter, several centrifugation and electrophoretic techniques were investigated in order to separate cross-linked material. The samples were then viewed microscopically using TEM to visually assess cross-linked amyloid fibril morphology.

4.2 Cross-linking GOD by glutaraldehyde

GA was used in this chapter to cross-link GOD to amyloid fibrils. GA forms imine bonds between the free amine groups of surface lysine amino acids on proteins and the aldehyde groups on GA. Of the 24 lysine residues located on the surface of the GOD dimer, 5 residues have been shown to be available for cross-linking (Section 1.10) (Baszkin *et al.* 1997). This availability for cross-linking is influenced by the carbohydrate shell, which partially surrounds the GOD enzyme. As mentioned in Section 1.10, GA has been used to cross-link GOD extensively in previous research (Ahmad *et al.* 2001; Sohail Akhtar and Bhakuni 2003). Initial experiments were designed to test whether GOD could be cross-linked to itself using GA, and confirm that at least some of the lysine residues on the surface of the molecule are available for cross-linking. GOD and amyloid fibril concentrations were determined from previous in-house experiments and calculations, where GOD was in excess, to ensure optimum cross-linking (Sarah Roberts, Personal Communication). Several GA concentrations were investigated, as outlined in Section 2.4.1, with the most effective concentration being chosen for cross-linking experiments.

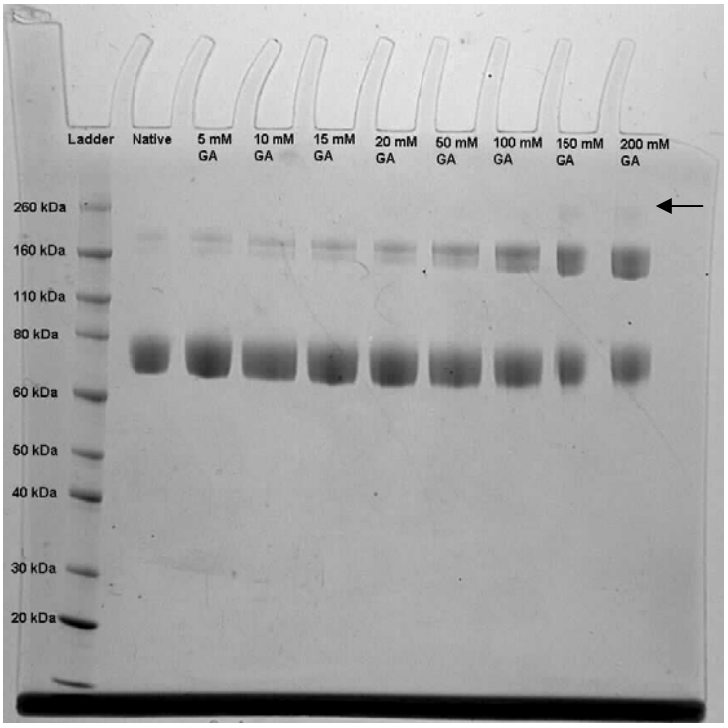

Figure 4.1

SDS-PAGE gel of GOD cross-linking. *2 mg/ml GOD was cross-linked using the following GA concentrations: 0 mM (native GOD), 5 mM, 10 mM, 15 mM, 20 mM, 50 mM, 100 mM, 150 mM and 200 mM for five minutes at 25°C. The samples were then run on an SDS-PAGE gel to assess the degree of cross-linking.*

SDS-PAGE separates proteins based on molecular weight. In Figure 4.1, the gel shows a band from 70-80 kDa, which corresponds to the molecular weight of the GOD monomer in all sample lanes. There is also a band around 160 kDa, which increases in intensity with increase in GA concentration in all cross-linked samples. This band corresponds to the molecular weight of the GOD dimer. This band is very faint in the sample that does not contain GA, suggesting that most of the GOD dimers have been denatured to monomers. In the cross-linked samples, the intensity of this band increases with GA concentration, indicating that increasing amounts of GOD dimer have been stabilised by intramolecular cross-links. There is also a faint band (labelled with an arrow) with a molecular weight of around 240 kDa at higher concentrations, which is consistent with the molecular weight of a GOD trimer. This suggests that there is also intermolecular GOD cross-linking at high concentrations of GA. 150 mM (1% v/v) GA was used in further cross-linking experiments, as it was the lowest concentration where both inter- and intramolecular cross-linking is observed.

4.3 Electrophoretic studies

SDS-PAGE denatures proteins using the detergent SDS and separates based on molecular weight. Amyloid fibrils are too large to enter the PAGE gel, and remain in the well at the top of the gel. GOD that has been cross-linked to the amyloid fibrils also remains in the well, attached to the amyloid fibrils. GOD that has not been cross-linked is free to move through the gel. The Experion™ capillary electrophoresis system works in a similar way to an SDS-PAGE gel, where denatured samples are run on a chip gel filtration column, and a gel photo is simulated from the resulting data (Minucci *et al.* 2008).

4.3.1 Gel electrophoresis

Experiments were optimised to limit intramolecular GOD cross-linking, with the addition of GA to amyloid fibrils first and enzyme added last, to ensure the pH of the solution was 7.4 from the phosphate buffer in the enzyme solution. Insulin amyloid fibril cross-linked samples and associated controls were run on an SDS-PAGE gel to assess the degree of cross-linking by GA. The results of this gel are shown in Figure 4.2. Native GOD resulted in two bands on an SDS-PAGE gel, at 80 kDa and between 110 and 160 kDa, corresponding to the molecular weight of the monomer and dimer, respectively. On a denaturing gel, only the monomer was expected,

although the GOD dimer was extremely stable and was not completely denatured, producing a faint band corresponding to the molecular weight of the dimer (Lane 1). Cross-linking of GOD by addition of GA increased the intensity of the 160 kDa band, indicating a higher stability of the dimeric state due to the presence of intramolecular cross-links (Lane 2), consistent with Figure 4.1. Insulin fibrils produced a low molecular weight band, which corresponds to the molecular weight of the unfibrillised insulin monomer of 5.7 kDa (Lane 3) (Nettleton *et al.* 2000). This band was no longer present upon addition of GA, suggesting cross-linking of unfibrillised protein to amyloid fibrils (Lane 4). Both the GOD band and the insulin monomer band are present in the insulin amyloid fibrils and GOD sample (Lane 5). The characteristic GOD bands were still visible upon addition of insulin amyloid fibrils and GA, but were significantly diminished in intensity, suggesting a lower protein concentration (Lane 6). This indicates that some GOD remained in the wells of the gel with the insulin amyloid fibrils, consistent with cross-linking.

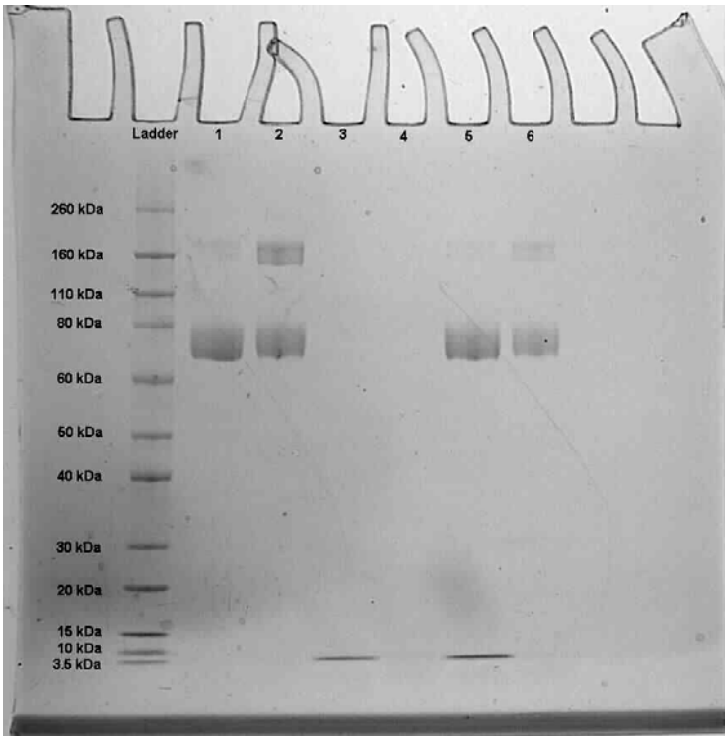

Figure 4.2

SDS-PAGE gel of cross-linking GOD to insulin amyloid fibrils using GA. *Bands produced by samples in lanes containing 0.6 mg/ml GOD (1), 0.6 mg/ml GOD and 1% GA (150 mM) (2), 1.9 mg/ml insulin amyloid fibrils (3), 1.9 mg/ml insulin amyloid fibrils and 1% GA (4), 1.9 mg/ml insulin amyloid fibrils and 0.6 mg/ml GOD (5), and 1.9 mg/ml insulin amyloid fibrils, 0.6 mg/ml GOD and 1% GA (6).*

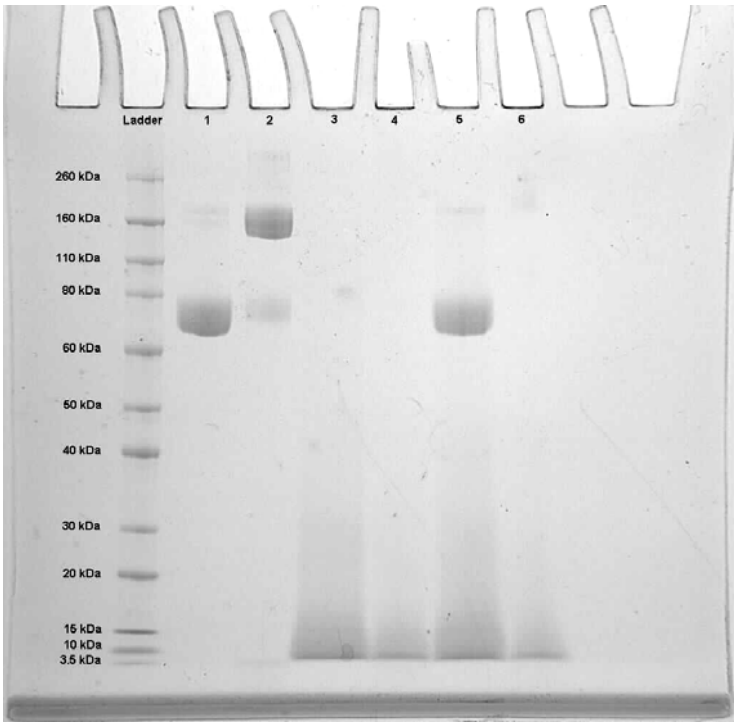

Figure 4.3

SDS-PAGE gel of cross-linking GOD to crystallin amyloid fibrils using GA. *Bands produced by samples in lanes containing 0.6 mg/ml GOD (1), 0.6 mg/ml GOD and 1% GA (2), 1.9 mg/ml crystallin amyloid fibrils (3), 1.9 mg/ml crystallin amyloid fibrils and 1% GA (4), 1.9 mg/ml crystallin amyloid fibrils and 0.6 mg/ml GOD (5), and 1.9 mg/ml crystallin amyloid fibrils, 0.6 mg/ml GOD and 1% GA (6).*

The results of the crystallin amyloid fibril cross-linked samples are given in Figure 4.3. Native GOD (Lane 1) produced two bands on an SDS-PAGE gel, at 80 kDa and at about 160 kDa, corresponding to the molecular weight of the monomer and dimer, which is consistent with the previous result for native GOD in Figure 4.2. Addition of GA increased the intensity of the 160 kDa band, indicating a higher stability of the dimeric state due to the presence of intra-molecular cross-links (Lane 2). This is also consistent with the results obtained in Figure 4.2. Crystallin amyloid fibrils produced a smeared band of low molecular weight, which was diminished in intensity upon addition of GA (Lane 3, 4). The characteristic GOD bands were still visible upon addition of crystallin amyloid fibrils (Lane 5). When GA was added to the sample, the characteristic GOD bands were no longer visible (Lane 6). This indicates that GOD has remained in the wells of the gel with the crystallin amyloid fibrils, consistent with cross-linking.

This gel was consistent with the cross-linking observed in the SDS-PAGE gel of GOD cross-linking to insulin fibrils using GA in Figure 4.2. These results indicate that intermolecular cross-links were present in the GOD molecules when reacted with GA, and that some GOD was also being retained in the wells of the gel with the amyloid fibrils in the cross-linked sample, suggesting successful attachment.

4.3.2 Capillary electrophoresis

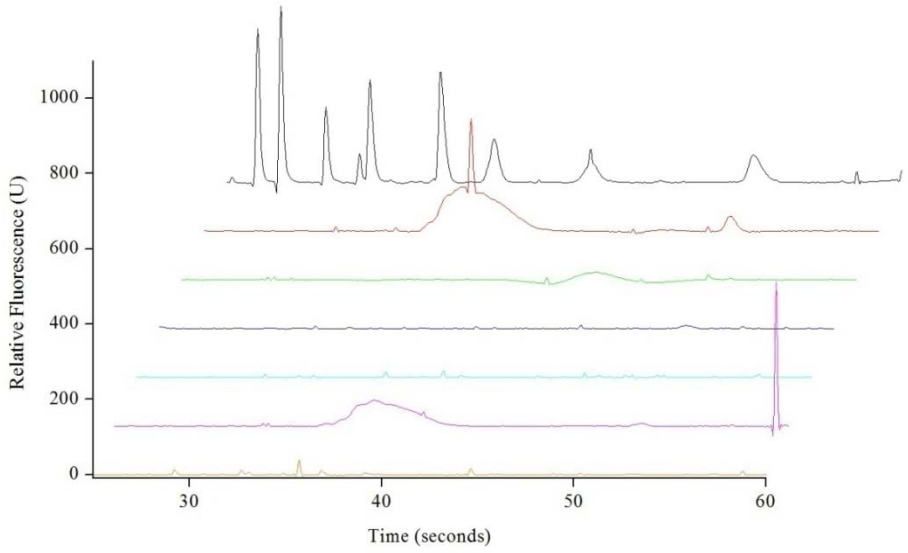

A

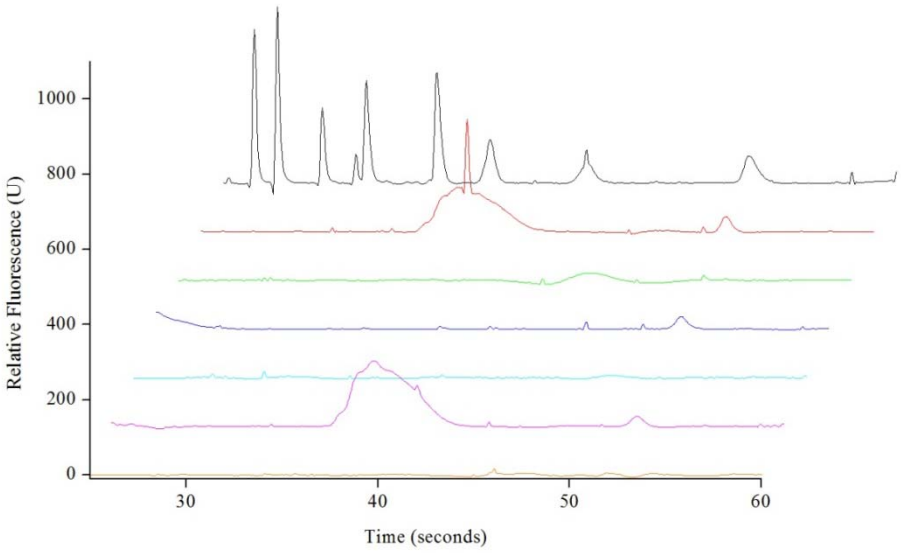

B

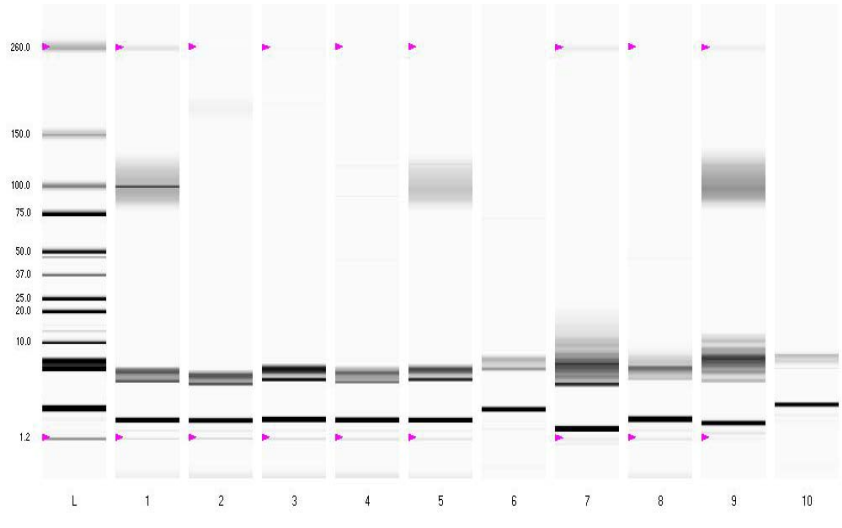

C

Figure 4.4

Experion™ capillary electrophoresis of GOD cross-linked to insulin and crystallin amyloid fibrils using glutaraldehyde. *Data are represented as chromatograms in (A) and (B) and as a simulated gel in (C). A: Ladder (black), 0.6 mg/ml GOD (red), 0.6 mg/ml GOD and 1% GA (green), 1.9 mg/ml insulin amyloid fibrils (dark blue), 1.9 mg/ml insulin amyloid fibrils and 1% GA (light blue), 0.6 mg/ml GOD and 1.9 mg/ml insulin amyloid fibrils (pink), and 0.6 mg/ml GOD and 1.9 mg/ml insulin amyloid fibrils and 1% GA (yellow). B: Ladder (black), 0.6 mg/ml GOD (red), 0.6 mg/ml GOD and 1% GA (green), 1.9 mg/ml crystallin amyloid fibrils (dark blue), 1.9 mg/ml crystallin amyloid fibrils and 1% GA (light blue), 0.6 mg/ml GOD and 1.9 mg/ml crystallin amyloid fibrils (pink), and 0.6 mg/ml GOD and 1.9 mg/ml crystallin amyloid fibrils and 1% GA (yellow). C: Lane L is the ladder produced by the protein molecular weight standards. Lane 1 contains 0.6 mg/ml GOD (pH 7.4). Lane 2 contains 0.6 mg/ml GOD and 1% GA. Lane 3 contains 1.9 mg/ml insulin fibrils. Lane 4 contains 1.9 mg/ml insulin fibrils and 1% GA. Lane 5 contains 1.9 mg/ml insulin fibrils and 0.6 mg/ml GOD. Lane 6 contains 1.9 mg/ml insulin fibrils and 0.6 mg/ml GOD and 1% GA. Lane 7 contains 1.9 mg/ml crystallin fibrils. Lane 8 contains 1.9 mg/ml crystallin fibrils and 1% GA. Lane 9 contains 1.9 mg/ml crystallin fibrils and 0.6 mg/ml GOD. Lane 10 contains 1.9 mg/ml crystallin fibrils and 0.6 mg/ml GOD and 1% GA.*

The chromatograms (Figure 4.4A and B) of the Experion™ data for cross-linked samples were used to generate a simulated gel photo (Figure 4.4C). The chromatogram for insulin amyloid fibril cross-linked samples (Figure 4.4A) showed a large peak at about 40 seconds in the GOD and GOD and insulin amyloid fibrils samples (red, pink), and a small peak at about 45 seconds; however, this peak was very small and hard to visualise in the simulated gel photo. Bands between 1.2 and 8 kDa are system peaks. Other peaks in the samples (excluding the peaks of the protein standards ladder (black)) were likely to be noise spikes. The chromatogram of the crystallin amyloid fibril cross-linked samples (Figure 4.4B) was very similar to the insulin amyloid fibril cross-linked samples, where there was a large peak at about 40 seconds

corresponding to the peak produced by the GOD sample in the GOD and crystallin amyloid fibril samples (red, pink).

The gel photo in Figure 4.4C showed a large band in the GOD, GOD and insulin amyloid fibrils and GOD and crystallin amyloid fibrils lanes (Lane 1, 5 and 9). This band had a molecular weight of between 80 and 120 kDa, consistent with the molecular weight of different glycoforms of the GOD monomer (Kalisz *et al.* 1991). This molecular weight result indicates that the sample was completely denatured, compared with the SDS-PAGE gels. There was a faint band in the GOD and GA sample that has a molecular weight of around 160 kDa (Lane 2). This corresponds to the weight of the GOD dimer, suggesting a small amount of intramolecular cross-links between GOD molecules that were resistant to denaturation. There were no bands in the insulin amyloid fibrils, GOD and GA lane (Lane 6), suggesting that the enzyme was retained with the amyloid fibrils, which have a large molecular weight and cannot enter the capillary. There were some low molecular weight bands in the crystallin amyloid fibrils and crystallin amyloid fibrils and GOD lanes, which are likely to be unfibrillised crystallin (Lane 7 and 9). These bands were not present in the crystallin amyloid fibrils and GA and crystallin amyloid fibrils, GOD and GA samples (Lane 8 and 10), indicating that they have been cross-linked, and were restricted from entering the gel with the amyloid fibrils. These results are consistent with the SDS-PAGE gels, although they indicate a higher degree association of GOD with the amyloid fibrils, as the GOD band is no longer visible upon addition of amyloid fibrils and GA, in comparison with SDS-PAGE, where a diminished GOD band is visible. This is consistent with SDS-PAGE being more effective at separating non-covalently associated GOD from amyloid fibrils than the Experion™. Further experiments in this chapter were designed to assess the degree of non-covalent GOD attachment to both insulin and crystallin amyloid fibrils. However, the activity of the cross-linked samples was first assessed to ensure that the cross-linked GOD was still functional.

4.4 Activity of cross-linked samples

The activity of cross-linked GOD was assessed using the Amplex Red assay, as discussed in Section 2.3 (Zhou *et al.* 1997). In this experiment, the presence of amyloid fibrils was measured using the ThT assay and overall protein concentration of the sample was also measured using the Bradford assay (Bradford 1976; LeVine III 1999). The results of the three assays are shown graphically in Figure 4.5.

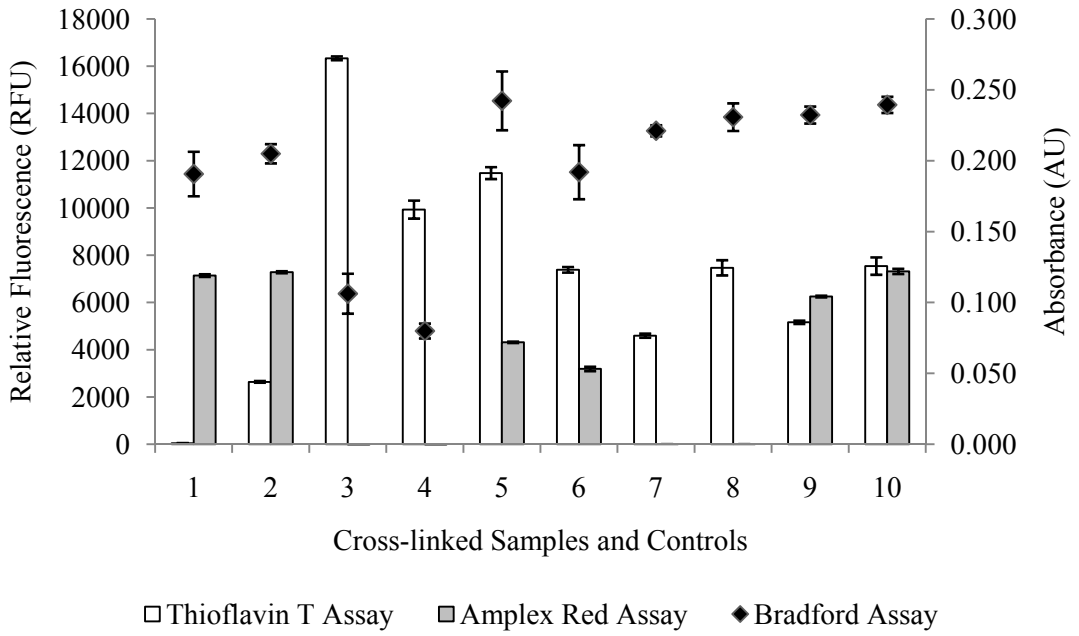

Figure 4.5

Amplex Red, thioflavin T and Bradford assays of GOD cross-linked to insulin and crystallin amyloid fibrils. *Cross-linked samples and controls: 0.6 mg/ml GOD (1), 0.6 mg/ml GOD and 1% GA (2), 1.9 mg/ml insulin amyloid fibrils (3), 1.9 mg/ml insulin amyloid fibrils and 1% GA (4), 0.6 mg/ml GOD and 1.9 mg/ml insulin amyloid fibrils (5), 0.6 mg/ml GOD, 1.9 mg/ml insulin amyloid fibrils and 1% GA (6),1.9 mg/ml crystallin amyloid fibrils (7), 1.9 mg/ml crystallin amyloid fibrils and 1% GA (8), 0.6 mg/ml GOD and 1.9 mg/ml crystallin amyloid fibrils (9) and 0.6 mg/ml GOD, 1.9 mg/ml crystallin amyloid fibrils and 1% GA (10). Thioflavin T and Amplex Red assay fluorescence readings (clear bars and grey bars, respectively) are plotted on the left axis and Bradford assay absorbance readings (dark diamonds) are plotted on the right axis. Error bars shown are standard error of three replicates and are less than 5%.*

GOD activity remained relatively unchanged upon addition of GA (Column 1 and 2), despite evidence of intramolecular cross-linking given in the SDS-PAGE and Experion™ experiments. This suggests that there is little conformational change at the active site of the enzyme during catalysis, which is consistent with previous reports, where GOD is described as a conformationally rigid protein (Wilson and Turner 1992). If there is little conformational change, the enzyme is unlikely to be affected by the presence of intramolecular cross-links, which can restrict conformational change in the enzyme (Kalisz *et al.* 1991). This result is consistent with previous research where GOD is shown to retain activity upon immobilisation (Tiller *et al.* 2002). GOD activity was also unchanged in the presence of crystallin amyloid fibrils, but decreased slightly in the presence of insulin amyloid fibrils (Column 6 and 10). This may indicate a slight loss of GOD activity upon addition of insulin amyloid fibrils. Possible

reasons for loss of activity could be less accessibility to substrate or product inhibition, due to the formation of a large amyloid fibril enzyme scaffold. GOD has previously been shown to be competitively inhibited by hydrogen peroxide, one of the products of the GOD-catalysed reaction (Bao *et al.* 2003). If hydrogen peroxide is unable to be released into solution due to an entrapment effect by the amyloid fibril scaffold, then increased inhibition would occur. Alternatively, this scaffold could restrict GOD access to glucose, the substrate of the enzyme needed for catalysis. This decrease in activity could be due to the formation of a tighter amyloid fibril scaffold by insulin, in comparison to that of crystallin, where a decrease was not observed. This can be seen in the TEM images of the scaffolds in Section 3.2 (Figure 3.2) and Section 3.3 (Figure 3.3). This would restrict the movement of small molecules such as glucose and hydrogen peroxide; however, further experiments would be required to investigate the cause of this effect.

Insulin amyloid fibrils gave a characteristic fluorescence reading in the presence of ThT (Column 3). The fluorescence of ThT upon binding to amyloid fibrils was decreased in the presence of GA (Column 4). This could be due to decreased ThT access to intercalate with insulin amyloid fibrils when cross-linked into a fibril scaffold. However, the fluorescence decrease seen in the insulin fibril samples upon addition of GA was not mirrored in the results of crystallin amyloid fibrils. Crystallin amyloid fibrils show increased fluorescence upon addition of GA (Column 7 and 8). GA has been shown to enhance fluorescence of proteins by production of an auto-fluorescent reaction product, characterised by a broad emission spectrum from around 475 to 700 nm, and has previously been used to induce auto-fluorescence in microscopy studies (Fester *et al.* 2008). This fluorescence would be detected at the filter wavelengths detected by the platereader (450 – 485 nm), and is thus a likely explanation for the increase in fluorescence seen in crystallin amyloid fibril samples, and also for the slight increase in fluorescence given by cross-linked GOD compared to free GOD (Column 2).

The protein concentration as determined by the Bradford assay decreased slightly upon addition of GA in the samples containing insulin amyloid fibrils (Column 3 and 4). This was due to the binding mechanism of the Bradford reagent to free amino groups on proteins (Bradford 1976). If these free amino groups have already been reacted with GA, then the Bradford reagent can no longer bind, producing a lower absorbance reading. This is not the case with crystallin fibrils however, which may indicate a lower level of insulin amyloid fibril cross-linking by GA, and with GOD, which may reflect the low number of available lysine residues for cross-linking or only a small amount of intermolecular cross-linking (Column 7 and 8).

4.5 Centrifugation studies

Amyloid fibrils have a large molecular weight, which causes formation of a pellet when centrifuged. This is useful as it allows the separation of amyloid fibrils from solution using centrifugation. Thus, free GOD can be separated from GOD cross-linked to amyloid fibrils, or non-covalently associated to amyloid fibrils, by centrifuging the sample. The experiments in this section investigate the use of centrifugation as an effective technique for separating free enzyme from cross-linked samples. In all cases, a relative measure of GOD activity, ThT fluorescence and protein concentration was required to compare individual fractions in a single experiment to locate the GOD activity. In the following figures, the scales are adjusted to emphasise this, and comparisons between figures cannot be directly made.

Free GOD gives a characteristic centrifugation profile (Figure 4.6), allowing the effect of cross-linking to be assessed. In the Amplex Red assay of the centrifugation samples for free GOD, there is a large amount of fluorescence produced in the supernatant of wash one. There is very little activity in any of the other remaining pellet and wash samples. In the ThT assay, there is no significant fluorescence in any of the samples. In the Bradford assay, there is a high absorbance in the pellet of the supernatant of wash one, correlating with the Amplex Red activity seen in this sample. There is no significant absorbance in any of the other remaining pellet and wash samples. GOD does not form a pellet during centrifugation at 8,000 rpm, and nearly all GOD is removed in the supernatant of the first wash.

The centrifugation profile for GOD and GA is shown in Figure 4.7. In the Amplex Red assay, there is a large fluorescence reading in the supernatant sample of the first wash. There is also a large absorbance reading for this sample in the Bradford assay. In the ThT assay, there is no significant fluorescence observed for any of the samples. This result is extremely similar to the profile of GOD alone, suggesting that the addition of GA does not affect the centrifugation profile of GOD or interfere with the fluorescence reading of the Amplex Red reagent. However, this result differs to the result seen for GOD and GA in Figure 4.5 (Column 2). Both experiments were repeated with high reproducibility. The difference seen between the two preparations may be due to the age of GA, as GA is known to polymerise in a process involving aldol condensation (Wine *et al.* 2007). This polymerization may affect the production of the auto-fluorescent reaction product.

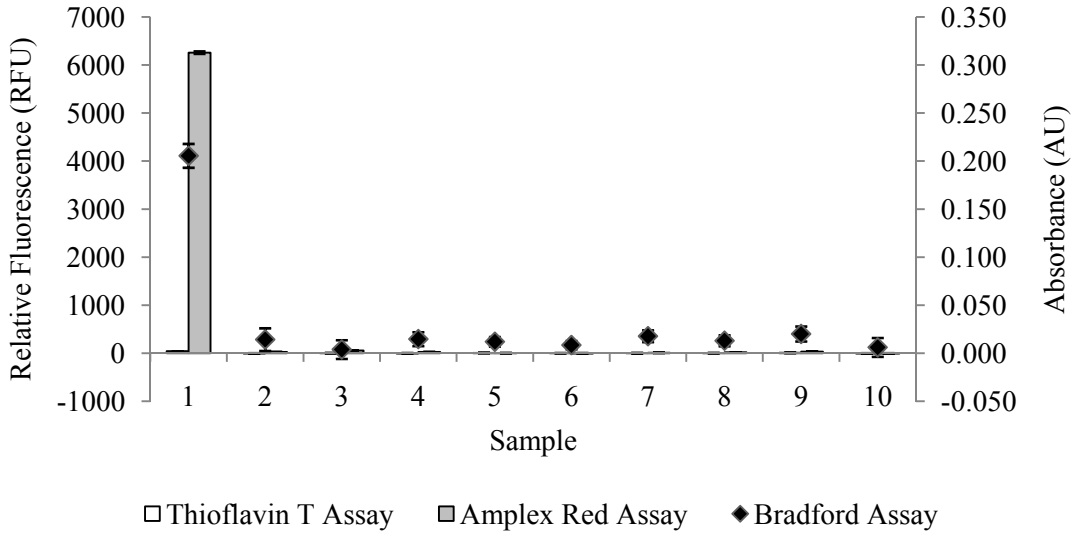

Figure 4.6

Centrifugation profile of GOD. *Thioflavin T and Amplex Red assay fluorescence readings (clear bars and grey bars, respectively) are plotted on the left axis and Bradford assay absorbance readings (dark diamonds) are plotted on the right axis. Samples are: wash one supernatant (1), wash one pellet (2), wash two supernatant (3), wash two pellet (4), wash three supernatant (5), wash three pellet (6), wash four supernatant (7), wash four pellet (8), wash five supernatant (9), wash five pellet (10). Error bars indicate the standard error of the mean of three replicates and are less than 5%.*

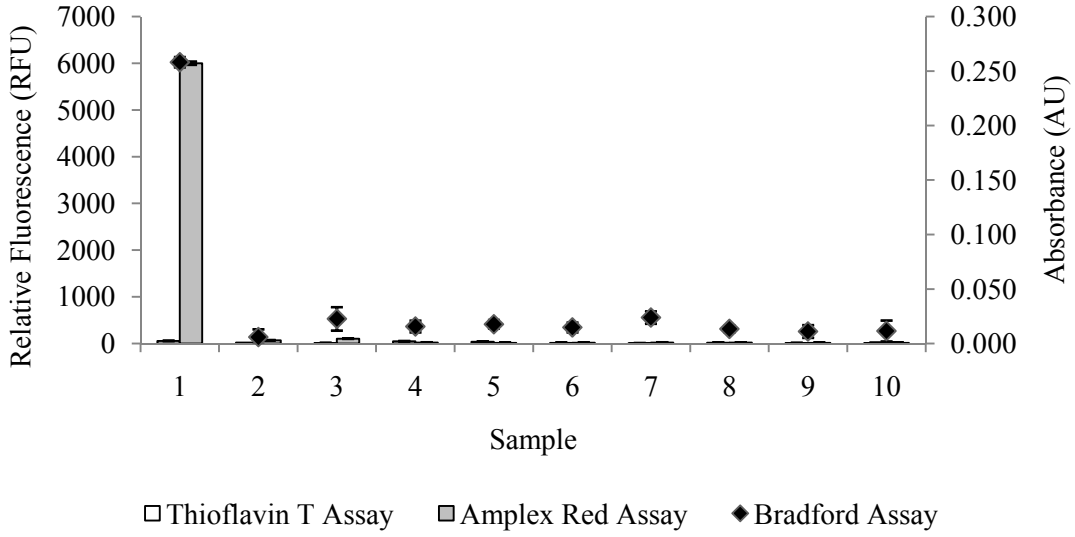

Figure 4.7

Centrifugation profile of GOD and GA. *Thioflavin T and Amplex Red assay fluorescence readings (clear bars and grey bars, respectively) are plotted on the left axis and Bradford assay absorbance readings (dark diamonds) are plotted on the right axis. Samples are: wash one supernatant (1), wash one pellet (2), wash two supernatant (3), wash two pellet (4), wash three supernatant (5), wash three pellet (6), wash four supernatant (7), wash four pellet (8), wash five supernatant (9), wash five pellet (10). Error bars indicate the standard error of the mean of three replicates and are less than 5%.*

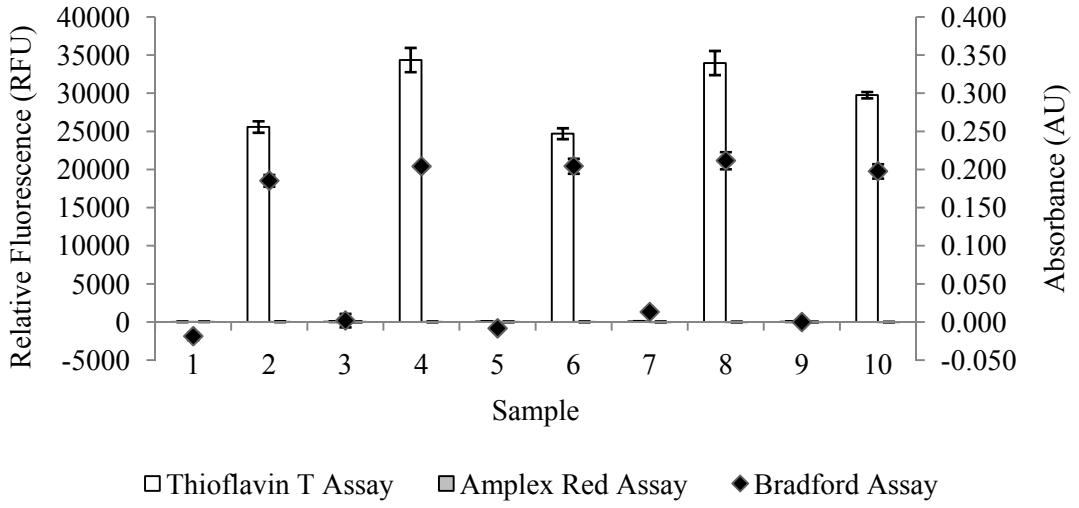

Figure 4.8

Centrifugation profile of insulin amyloid fibrils. *Thioflavin T and Amplex Red assay fluorescence readings (clear bars and grey bars, respectively) are plotted on the left axis and Bradford assay absorbance readings (dark diamonds) are plotted on the right axis. Samples are: wash one supernatant (1), wash one pellet (2), wash two supernatant (3), wash two pellet (4), wash three supernatant (5), wash three pellet (6), wash four supernatant (7), wash four pellet (8), wash five supernatant (9), wash five pellet (10). Error bars indicate the standard error of the mean of three replicates and are less than 5%.*

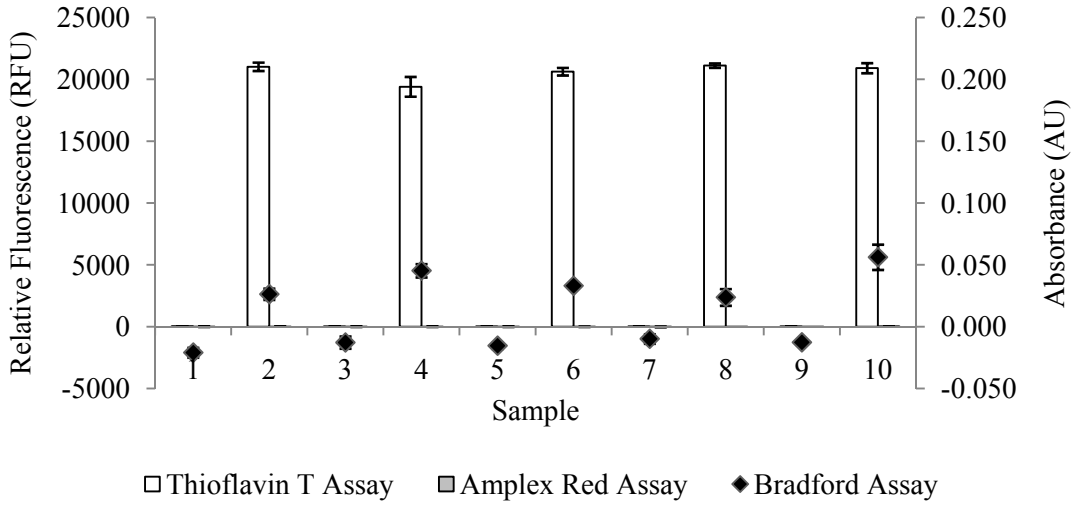

Figure 4.9

Centrifugation profile of insulin amyloid fibrils and GA. *Sample contains 1.9 mg/ml insulin amyloid fibrils, 1% GA, and 16 mM sodium phosphate, pH 7.4. Thioflavin T and Amplex Red assay fluorescence readings (clear bars and grey bars, respectively) are plotted on the left axis and Bradford assay absorbance readings (dark diamonds) are plotted on the right axis. Samples are: wash one supernatant (1), wash one pellet (2), wash two supernatant (3), wash two pellet (4), wash three supernatant (5), wash three pellet (6), wash four supernatant (7), wash four pellet (8), wash five supernatant (9), wash five pellet (10). Error bars indicate the standard error of the mean of three replicates and are less than 5%.*

There is a large amount of ThT fluorescence observed in all of the pellet samples and none of the wash samples of the insulin amyloid fibril centrifugation profile (Figure 4.8). These results show that amyloid fibrils form a pellet during centrifugation, and that the fibrils are retained through successive washes. There is no Amplex Red fluorescence observed in any of the samples, confirming that the presence of amyloid fibrils does not interfere with the Amplex Red reagent. The Bradford assay results are very similar to the results of the ThT assay, where there is a large protein concentration in the pellet and negligible protein in the supernatant.

Upon addition of GA (Figure 4.9), there is a large amount of fluorescence in the ThT assay in all of the pellet samples but none of the supernatant samples, like the centrifugation profile for amyloid fibrils alone. The fluorescence readings are lower than in the insulin amyloid fibril only profile, which is consistent with previous results in Figure 4.5, where the addition of GA lowers the fluorescence readings of the ThT assay. The results of the Bradford assay follow the same trend as the ThT assay and the Bradford assay from the insulin fibrils only profile in Figure 4.8; however, the absorbance values are much lower. This is due to the cross-linking of free amines from lysine residues by GA, resulting in limited binding by the Bradford reagent as discussed in Section 4.4.

In the Amplex Red assay in Figure 4.10, there is significant fluorescence in the supernatant of the first wash, and in all of the pellet samples. This indicates that some GOD is lost from the fibril pellet in the first wash, but not from the following washes. The remaining GOD is associated with the fibril pellet, suggesting there is significant non-covalent association occurring between GOD and the amyloid fibrils.

In Figure 4.11, the centrifugation profile for GOD, insulin amyloid fibrils and GA was very similar to the profile for GOD and insulin amyloid fibrils alone. In the Amplex Red assay, there was significant fluorescence in the supernatant of the first wash, and in all of the pellet samples. This indicates that some GOD was lost from the fibril pellet in the first wash, but not from the following washes. This implies that there is non-covalent association occurring between GOD and insulin amyloid fibrils. However, the absorbance readings for the Bradford assay were much lower upon addition of GA, suggesting that there is cross-linking occurring.

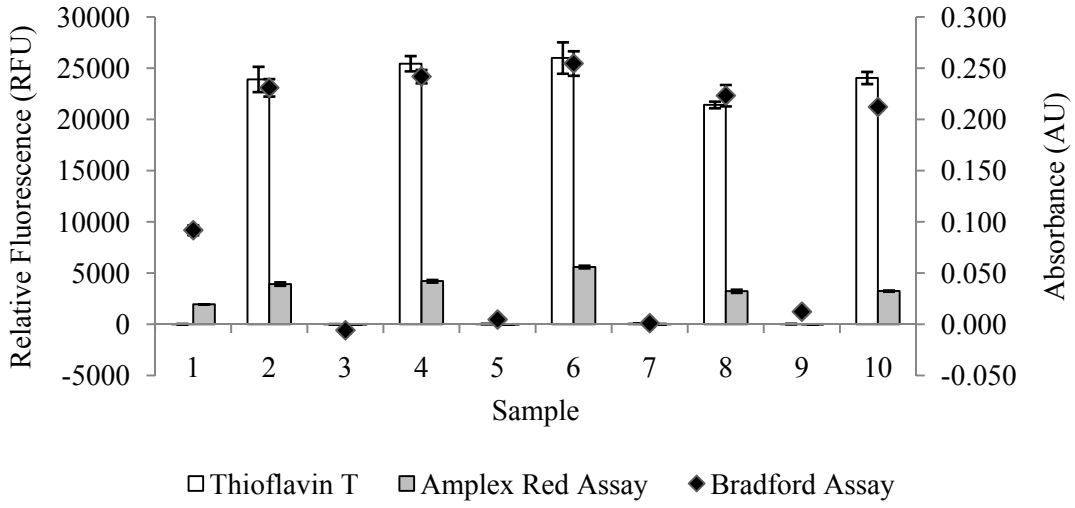

Figure 4.10

Centrifugation profile of GOD and insulin amyloid fibrils. *Sample contains 1.9 mg/ml insulin amyloid fibrils and 0.6 mg/ml GOD in 16 mM sodium phosphate, pH 7.4. Thioflavin T and Amplex Red assay fluorescence readings (clear bars and grey bars, respectively) are plotted on the left axis and Bradford assay absorbance readings (dark diamonds) are plotted on the right axis. Error bars indicate the standard error of the mean of three replicates and are less than 5%.*

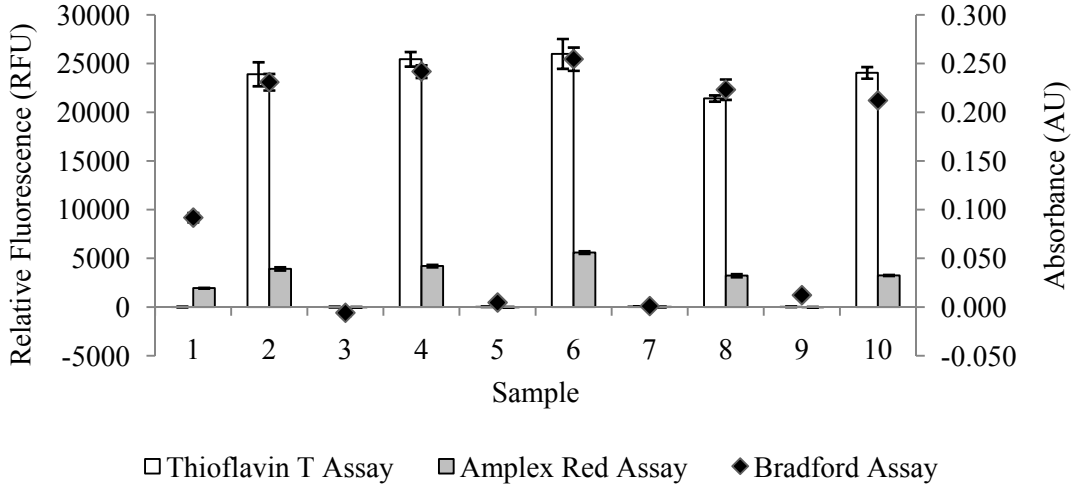

Figure 4.11

Centrifugation profile of GOD and insulin amyloid fibrils and GA. *Sample contains 1.9 mg/ml insulin amyloid fibrils, 0.6 mg/ml GOD in 16 mM sodium phosphate, pH 7.4, and 1% GA. Thioflavin T and Amplex Red assay fluorescence readings (clear bars and grey bars, respectively) are plotted on the left axis and Bradford assay absorbance readings (dark diamonds) are plotted on the right axis. Samples are as follows: wash one supernatant (1), wash one pellet (2), wash two supernatant (3), wash two pellet (4), wash three supernatant (5), wash three pellet (6), wash four supernatant (7), wash four pellet (8), wash five supernatant (9), wash five pellet (10). Error bars indicate the standard error of the mean of three replicates and are less than 5%.*

Crystallin amyloid fibrils displayed different characteristics to insulin amyloid fibrils; specifically, crystallins took longer to fibrillise and the resulting fibrils displayed different morphologies and showed greater sensitivity to pH (Section 3.6, Figure 3.7). This is reflected in the centrifugation profile of crystallin amyloid fibrils in Figure 4.12. Amyloid fibrils from both protein sources do not interfere with the Amplex Red assay, as there is no fluorescence seen in any of the samples for this assay. They both also formed a pellet and are not lost during consecutive washes, as shown by fluorescence in the ThT assay. In the Bradford assay, however, there is a significant absorbance reading in the supernatant of the first wash. This is likely to be washing unfibrillised protein from the pellet to the supernatant, as the crystallin sample is a crude preparation, consisting of several proteins. The large difference in ThT fluorescence between pellet samples is caused by heterogeneity of resuspended samples.

The centrifugation profile for crystallin amyloid fibrils and GA (Figure 4.13) is similar to the centrifugation profile for crystallin amyloid fibrils alone (Figure 4.12). Unfibrillised protein is still removed from the sample in the supernatant of the first wash, suggesting that there is little cross-linking between crystallin amyloid fibrils and unfibrillised protein. This is inconsistent with the SDS-PAGE gel of crystallin cross-linking in Figure 4.3. Taken together, the results suggest that some of the unfibrillised crystallin is remaining cross-linked in the fibril pellet, and some unfibrillised crystallin is not cross-linked.

The centrifugation profile for GOD and crystallin amyloid fibrils is shown in Figure 4.14. Compared with the centrifugation profile of GOD and insulin amyloid fibrils (Figure 4.10), there is less GOD retained in the crystallin amyloid fibril pellet. This indicates that there is less non-covalent association between crystallin amyloid fibrils and GOD than between insulin amyloid fibrils and GOD.

The centrifugation profile for GOD and crystallin amyloid fibrils and GA is given in Figure 4.15. In the Amplex Red assay, there is little fluorescence after the second wash (Sample 4). This suggests that there is less cross-linking occurring between GOD and crystallin amyloid fibrils than there is between insulin amyloid fibrils and GOD; however, evidence from other experiments carried out in this chapter indicates that cross-linking is occurring. This is likely to be due to differences in separation methods.

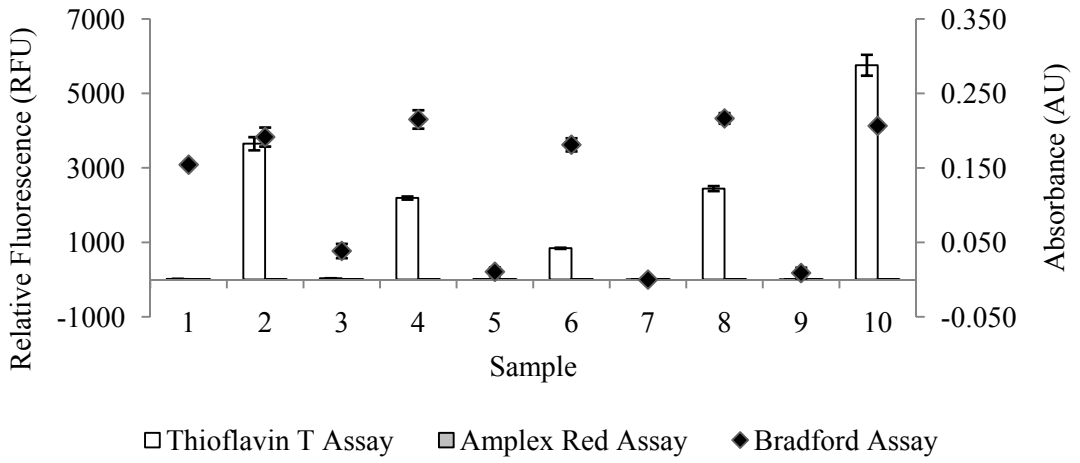

Figure 4.12

Centrifugation profile of crystallin amyloid fibrils. *Sample contains 1.9 mg/ml crystallin amyloid fibrils and 16 mM sodium phosphate, pH 7.4. Thioflavin T and Amplex Red assay fluorescence readings (clear bars and grey bars, respectively) are plotted on the left axis and Bradford assay absorbance readings (dark diamonds) are plotted on the right axis. Samples are as follows: wash one supernatant (1), wash one pellet (2), wash two supernatant (3), wash two pellet (4), wash three supernatant (5), wash three pellet (6), wash four supernatant (7), wash four pellet (8), wash five supernatant (9), wash five pellet (10). Error bars indicate the standard error of the mean of three replicates and are less than 5%.*

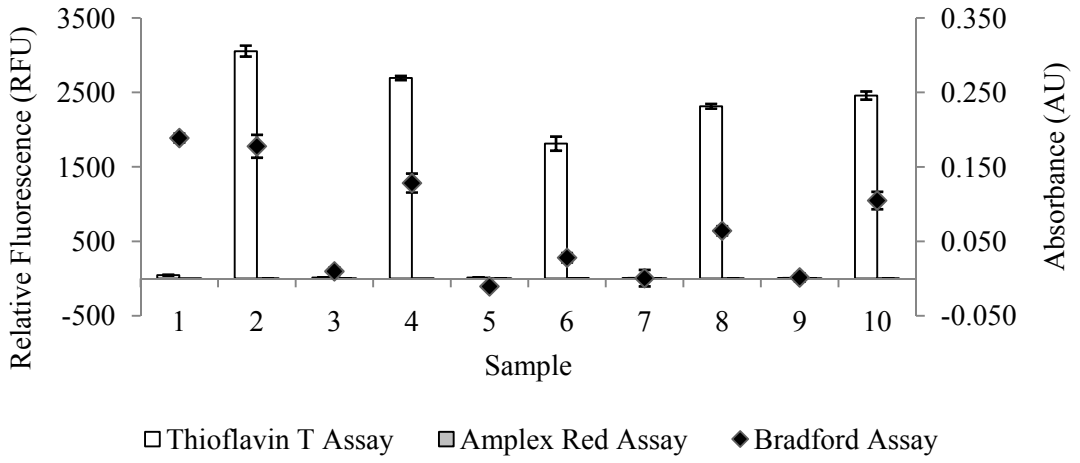

Figure 4.13

Centrifugation profile of crystallin amyloid fibrils and GA. *Sample contains 1.9 mg/ml crystallin amyloid fibrils and 1% GA in 16 mM sodium phosphate, pH 7.4. Thioflavin T and Amplex Red assay fluorescence readings (clear bars and grey bars, respectively) are plotted on the left axis and Bradford assay absorbance readings (dark diamonds) are plotted on the right axis. Samples are as follows: wash one supernatant (1), wash one pellet (2), wash two supernatant (3), wash two pellet (4), wash three supernatant (5), wash three pellet (6), wash four supernatant (7), wash four pellet (8), wash five supernatant (9), wash five pellet (10). Error bars indicate the standard error of the mean of three replicates and are less than 5%.*

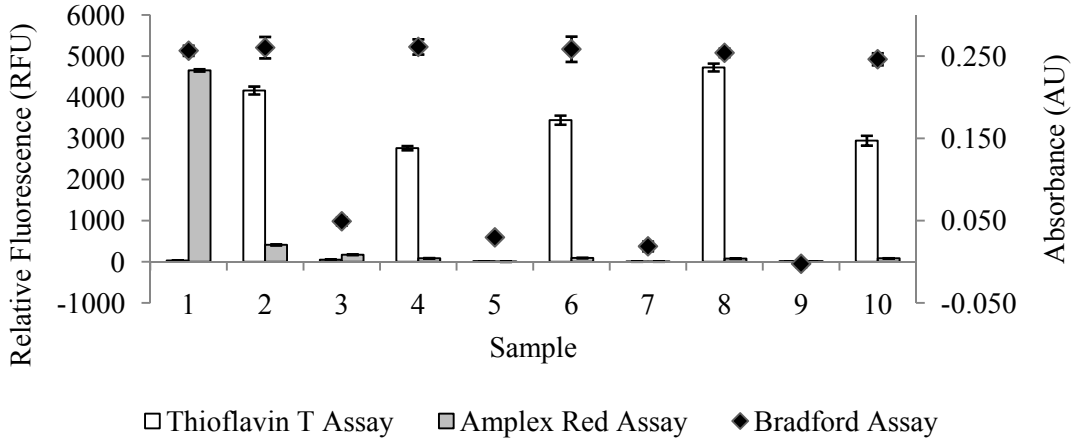

Figure 4.14

Centrifugation profile of GOD and crystallin amyloid fibrils. *Sample contains 1.9 mg/ml crystallin amyloid fibrils and 0.6 mg/ml GOD in 16 mM sodium phosphate, pH 7.4. Thioflavin T and Amplex Red assay fluorescence readings (clear bars and grey bars, respectively) are plotted on the left axis and Bradford assay absorbance readings (dark diamonds) are plotted on the right axis. Samples are as follows: wash one supernatant (1), wash one pellet (2), wash two supernatant (3), wash two pellet (4), wash three supernatant (5), wash three pellet (6), wash four supernatant (7), wash four pellet (8), wash five supernatant (9), wash five pellet (10). Error bars indicate the standard error of the mean of three replicates and are less than 5%.*

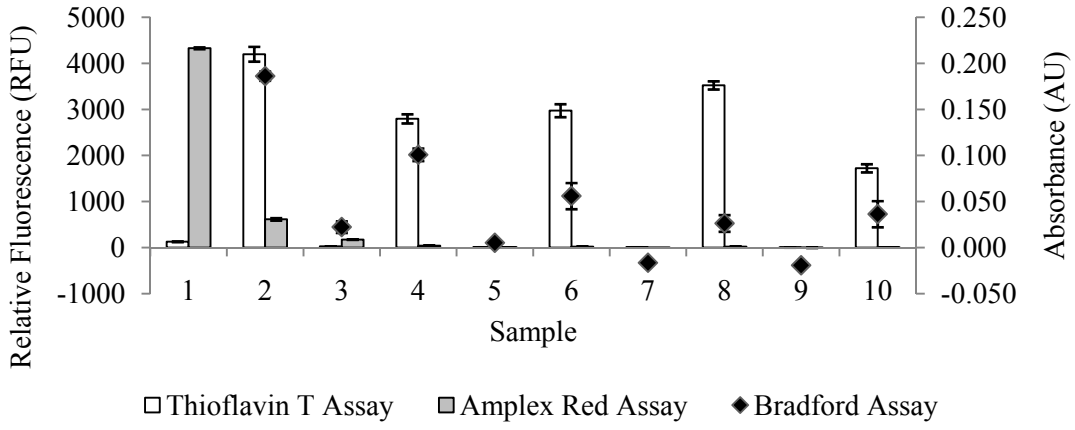

Figure 4.15

Centrifugation profile of GOD, crystallin amyloid fibrils and GA. *Sample contains 1.9 mg/ml crystallin amyloid fibrils, 1% GA and 0.6 mg/ml GOD in 16 mM sodium phosphate, pH 7.4. Thioflavin T and Amplex Red assay fluorescence readings (clear bars and grey bars, respectively) are plotted on the left axis and Bradford assay absorbance readings (dark diamonds) are plotted on the right axis. Samples are as follows: wash one supernatant (1), wash one pellet (2), wash two supernatant (3), wash two pellet (4), wash three supernatant (5), wash three pellet (6), wash four supernatant (7), wash four pellet (8), wash five supernatant (9), wash five pellet (10). Error bars indicate the standard error of the mean of three replicates and are less than 5%.*

4.6 Sucrose gradient studies

Sucrose gradients provide the ability to separate proteins due to different viscosities and densities of the sucrose, as a protein molecule will sediment through the gradient until the density of the particle matches that of the sucrose (Hirst and Cox 1976). Thus a sucrose gradient was used to separate free GOD from immobilised GOD due to differences in density. The sucrose gradient method was developed from an established method for separation of aggregate subclasses of GFP-GST fusion protein (Schrödel and De Marco 2005). The same sucrose densities and centrifugation parameters were used for separating amyloid fibrils, due to the large molecular weight of the ordered aggregate (Chapter One, Figure 1.1) (Chiti and Dobson 2006). Each of the samples prepared for the centrifugation experiments were also analysed by centrifugation through a sucrose gradient. Fractions from the gradient were then tested for GOD activity using the Amplex Red assay, the presence of amyloid fibrils using the ThT assay, and protein concentration using the Bradford assay. The density of GOD was considerably less than the density of amyloid fibrils, affording efficient separation.

The sucrose gradient results for free GOD are shown in Figure 4.16. In the Amplex Red assay, there was a large amount of fluorescence seen in the mid-range densities of the sucrose gradient (Fractions 4 and 5). This was mirrored in the results of the Bradford assay. There was no GOD activity seen in the fraction with the highest density of sucrose (Fraction 9), suggesting that there was little contamination between fractions. The low fluorescence observed in all fractions in the ThT assay indicates that sucrose does not interact with ThT.

Similar results were obtained for the sucrose gradient of GOD and GA (Figure 4.17). This was in agreement with the centrifugation profile of GOD and GA in Figure 7. There was a slight increase in ThT fluorescence in the fraction with the highest sucrose density; however, this was seen previously in another GOD and GA result (Figure 4.5), and is likely to be auto-fluorescent products of the GA reaction, which are visible at the wavelengths used to record ThT fluorescence, as described in Section 4.4.

The sucrose gradient results for insulin amyloid fibrils are given in Figure 4.18. There was a large amount of ThT fluorescence in the fraction with the highest sucrose density. The results of the Bradford assay also showed a high protein concentration in this fraction. There was no significant fluorescence seen in any of the fractions in the Amplex Red assay. This result was unchanged upon addition of GA, as shown in Figure 4.19.

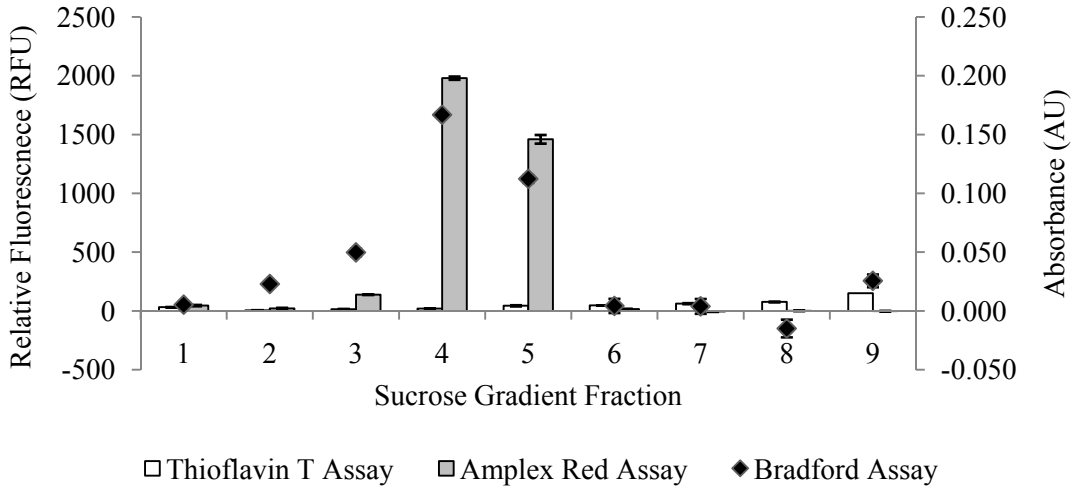

Figure 4.16

Sucrose gradient of GOD. *Sample contains 0.6 mg/ml GOD in 16 mM sodium phosphate, pH 7.4. Thioflavin T and Amplex Red assay fluorescence readings (clear bars and grey bars, respectively) are plotted on the left axis and Bradford assay absorbance readings (dark diamonds) are plotted on the right axis. The first fraction contains the lowest density of sucrose (0% before centrifugation) and the last fraction contains the highest density of sucrose (80% before centrifugation). Error bars indicate the standard error of the mean of three replicates and are less than 5%.*

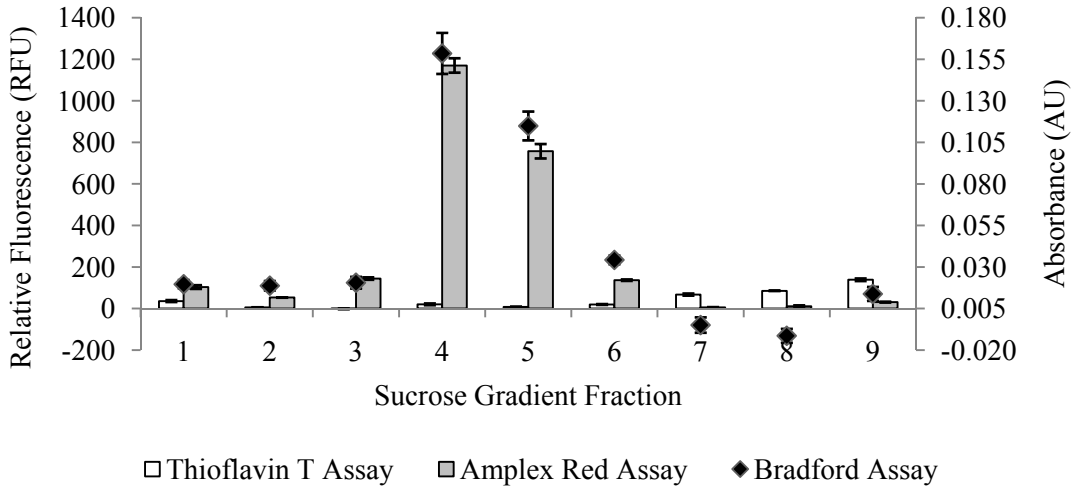

Figure 4.17

Sucrose gradient of GOD and GA. *Sample contains 0.6 mg/ml GOD in 16 mM sodium phosphate, pH 7.4 and 1% GA. Thioflavin T and Amplex Red assay fluorescence readings (clear bars and grey bars, respectively) are plotted on the left axis and Bradford assay absorbance readings (dark diamonds) are plotted on the right axis. The first fraction contains the lowest density of sucrose (0% before centrifugation) and the last fraction contains the highest density of sucrose (80% before centrifugation). Error bars indicate the standard error of the mean of three replicates and are less than 5%.*

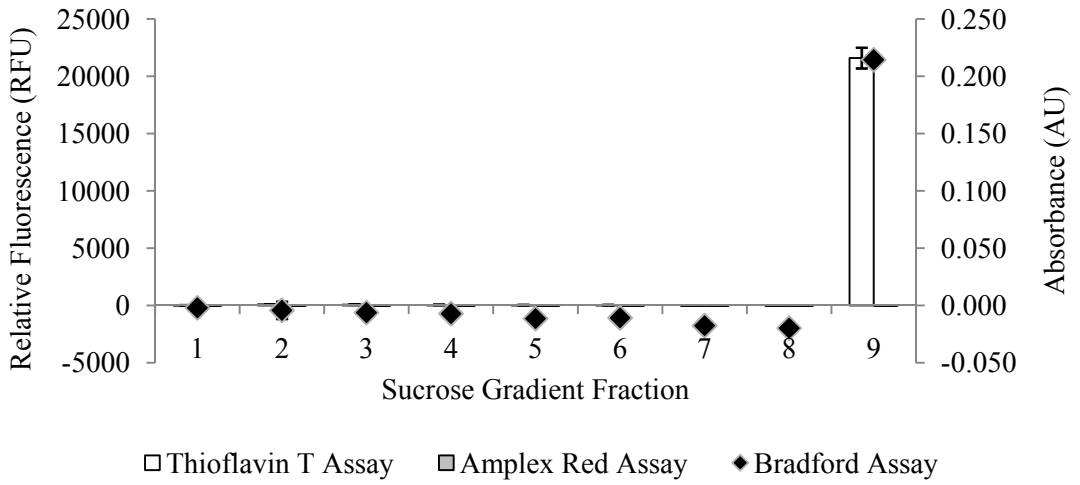

Figure 4.18

Sucrose gradient of insulin amyloid fibrils. *Sample contains 1.9 mg/ml insulin amyloid fibrils in 16 mM sodium phosphate, pH 7.4. Thioflavin T and Amplex Red assay fluorescence readings (clear bars and grey bars, respectively) are plotted on the left axis and Bradford assay absorbance readings (dark diamonds) are plotted on the right axis. The first fraction contains the lowest density of sucrose (0% before centrifugation) and the last fraction contains the highest density of sucrose (80% before centrifugation). Error bars indicate the standard error of the mean of three replicates and are less than 5%.*

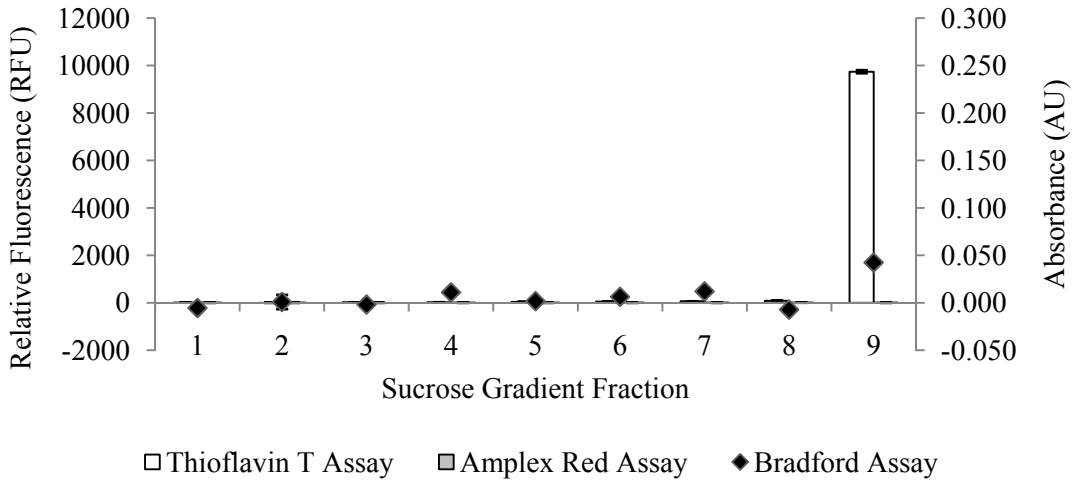

Figure 4.19

Sucrose gradient of insulin amyloid fibrils and GA. *Sample contains 1.9 mg/ml insulin amyloid fibrils in 16 mM sodium phosphate, pH 7.4 and 1% GA. Thioflavin T and Amplex Red assay fluorescence readings (clear bars and grey bars, respectively) are plotted on the left axis and Bradford assay absorbance readings (dark diamonds) are plotted on the right axis. The first fraction contains the lowest density of sucrose (0% before centrifugation) and the last fraction contains the highest density of sucrose (80% before centrifugation). Error bars indicate the standard error of the mean of three replicates and are less than 5%.*

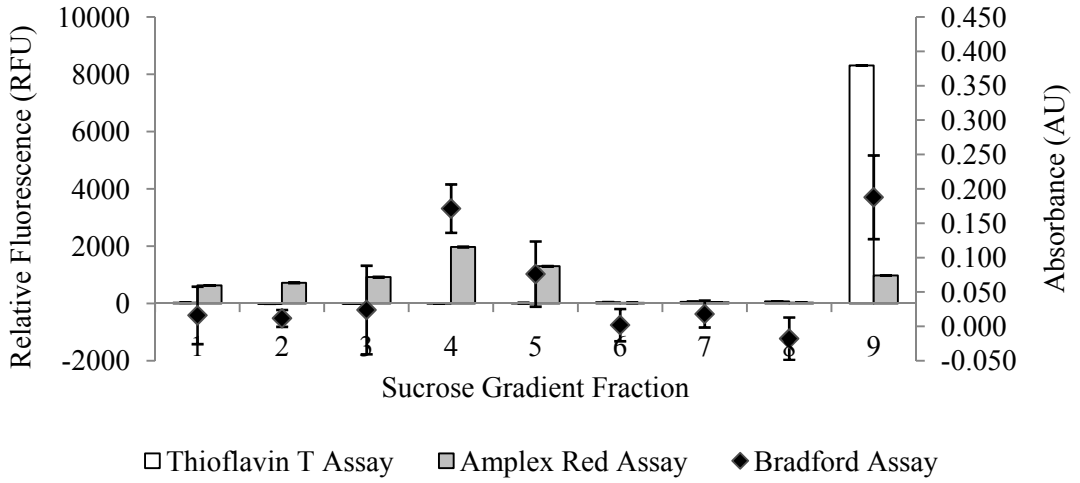

Figure 4.20

Sucrose gradient of GOD and insulin amyloid fibrils. *Sample contains 0.6 mg/ml GOD and 1.9 mg/ml insulin amyloid fibrils in 16 mM sodium phosphate, pH 7.4. Thioflavin T and Amplex Red assay fluorescence readings (clear bars and grey bars, respectively) are plotted on the left axis and Bradford assay absorbance readings (dark diamonds) are plotted on the right axis. The first fraction contains the lowest density of sucrose (0% before centrifugation) and the last fraction contains the highest density of sucrose (80% before centrifugation). Error bars indicate the standard error of the mean of three replicates and are less than 5%.*

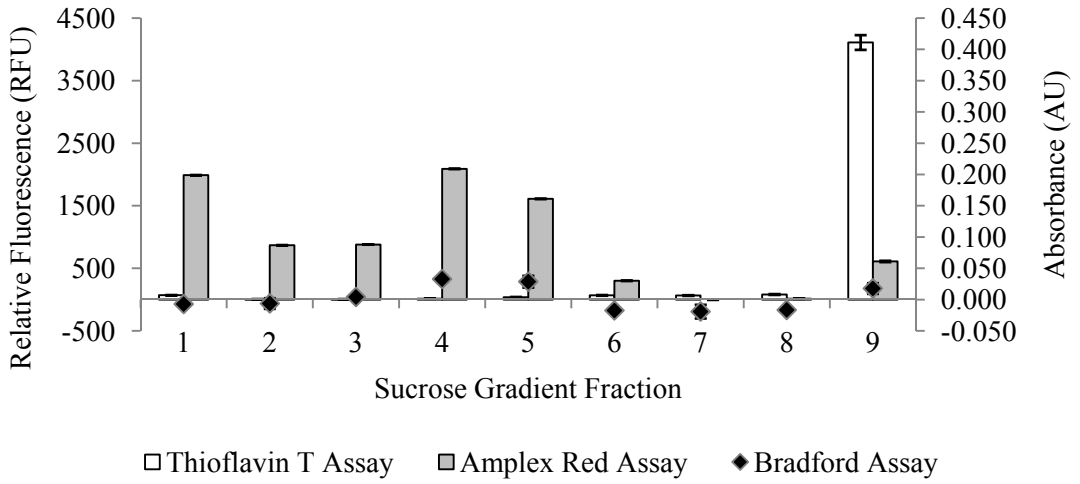

Figure 4.21

Sucrose gradient of GOD and insulin amyloid fibrils and GA. *Sample contains 0.6 mg/ml GOD and 1.9 mg/ml insulin amyloid fibrils in 16 mM sodium phosphate, pH 7.4 and 1% GA. Thioflavin T and Amplex Red assay fluorescence readings (clear bars and grey bars, respectively) are plotted on the left axis and Bradford assay absorbance readings (dark diamonds) are plotted on the right axis. The first fraction contains the lowest density of sucrose (0% before centrifugation) and the last fraction contains the highest density of sucrose (80% before centrifugation). Error bars indicate the standard error of the mean of three replicates and are less than 5%.*

The sucrose gradient results for GOD and insulin amyloid fibrils (Figure 4.20) were a combination of the sucrose gradient for GOD (Figure 4.16) and the gradient for insulin amyloid fibrils (Figure 4.18). There was a high Amplex Red fluorescence reading in the mid-density fractions, and a high ThT reading in the high density fraction. The Bradford assay had a high absorbance reading in both of these areas, reflecting the protein concentration of GOD in the mid-fractions and the protein concentration of amyloid fibrils in the high density fraction. There was a small amount of GOD in the amyloid fibril pellet in the high density fraction. This indicated that some of the GOD had been spun through the gradient with the amyloid fibrils. This could either be a contamination effect or a non-covalent association of GOD with the amyloid fibrils, consistent with earlier results (Section 4.5).

The results for the sucrose gradient of GOD and insulin amyloid fibrils and GA as given in Figure 4.21 were very similar to the results for GOD and insulin amyloid fibrils. The absorbance readings for the Bradford assay were slightly lower, indicating that there may be cross-linking occurring between GOD and insulin amyloid fibrils, as the free amino groups are no longer available to react with the Bradford reagent. However, this cross-linking effect on the Bradford reading is not seen in the GOD and GA samples. The reason for this trend is not known.

The results of the sucrose gradient for crystallin amyloid fibrils (Figure 4.22) showed a high fluorescence reading in the high density fraction, similar to the gradient for insulin amyloid fibrils (Figure 4.18). There was also a high absorbance reading for the low density fractions. This suggests that low molecular weight protein was removed from the fibril sample. This low molecular weight protein is likely to be unfibrillised crystallin proteins, due to the incomplete fibril formation by crude crystallin. This was also seen in the sucrose gradient results for crystallin amyloid fibrils and GA in Figure 4.23; however, all values were much lower. This could be due to incomplete resuspension of the crystallin amyloid fibril pellet in the sucrose gradient studies due to its transparency.

In the results for the sucrose gradient of GOD and crystallin amyloid fibrils there was low molecular weight, unfibrillised crystallins present in the low density fractions (Figure 4.24). There was also GOD present in the mid-density fractions, and in the highest density fraction with the crystallin amyloid fibrils. Upon addition of GA, there was a higher amount of GOD in the high density fraction, suggesting that cross-linking is occurring (Figure 4.25).

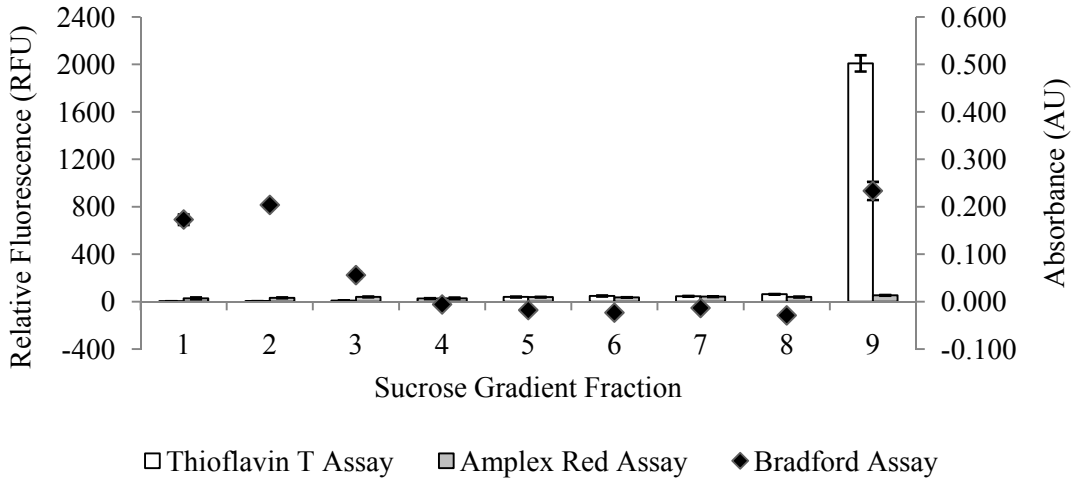

Figure 4.22

Sucrose gradient of crystallin amyloid fibrils. *Sample contains 1.9 mg/ml crystallin amyloid fibrils in 16 mM sodium phosphate, pH 7.4. Thioflavin T and Amplex Red assay fluorescence readings (clear bars and grey bars, respectively) are plotted on the left axis and Bradford assay absorbance readings (dark diamonds) are plotted on the right axis. The first fraction contains the lowest density of sucrose (0% before centrifugation) and the last fraction contains the highest density of sucrose (80% before centrifugation). Error bars indicate the standard error of the mean of three replicates and are less than 5%.*

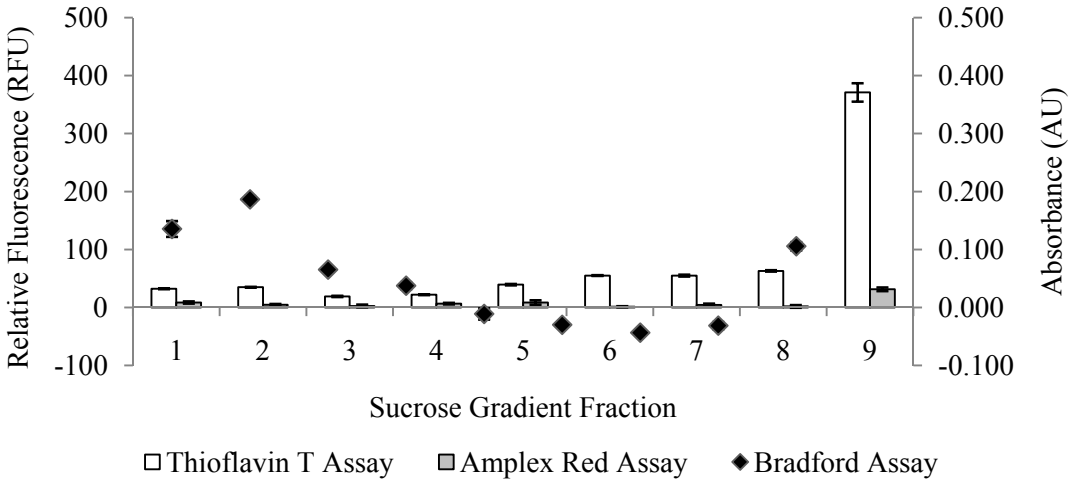

Figure 4.23

Sucrose gradient of crystallin amyloid fibrils and GA. *Sample contains 1.9 mg/ml crystallin amyloid fibrils in 16 mM sodium phosphate, pH 7.4 and 1% GA. Thioflavin T and Amplex Red assay fluorescence readings (clear bars and grey bars, respectively) are plotted on the left axis and Bradford assay absorbance readings (dark diamonds) are plotted on the right axis. The first fraction contains the lowest density of sucrose (0% before centrifugation) and the last fraction contains the highest density of sucrose (80% before centrifugation). Error bars indicate the standard error of the mean of three replicates and are less than 5%.*

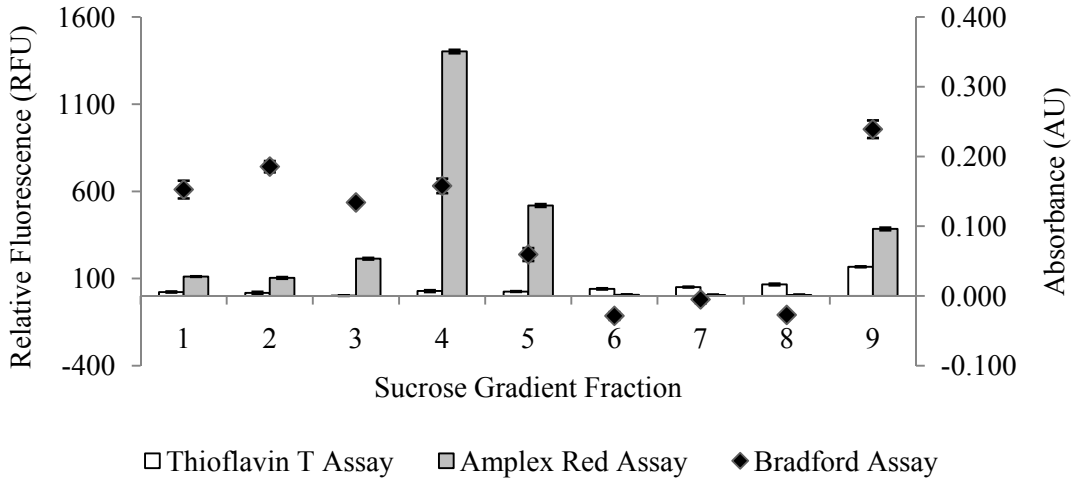

Figure 4.24

Sucrose gradient of GOD and crystallin amyloid fibrils. *Sample contains 0.6 mg/ml GOD and 1.9 mg/ml crystallin amyloid fibrils in 16 mM sodium phosphate, pH 7.4. Thioflavin T and Amplex Red assay fluorescence readings (clear bars and grey bars, respectively) are plotted on the left axis and Bradford assay absorbance readings (dark diamonds) are plotted on the right axis. The first fraction contains the lowest density of sucrose (0% before centrifugation) and the last fraction contains the highest density of sucrose (80% before centrifugation). Error bars indicate the standard error of the mean of three replicates and are less than 5%.*

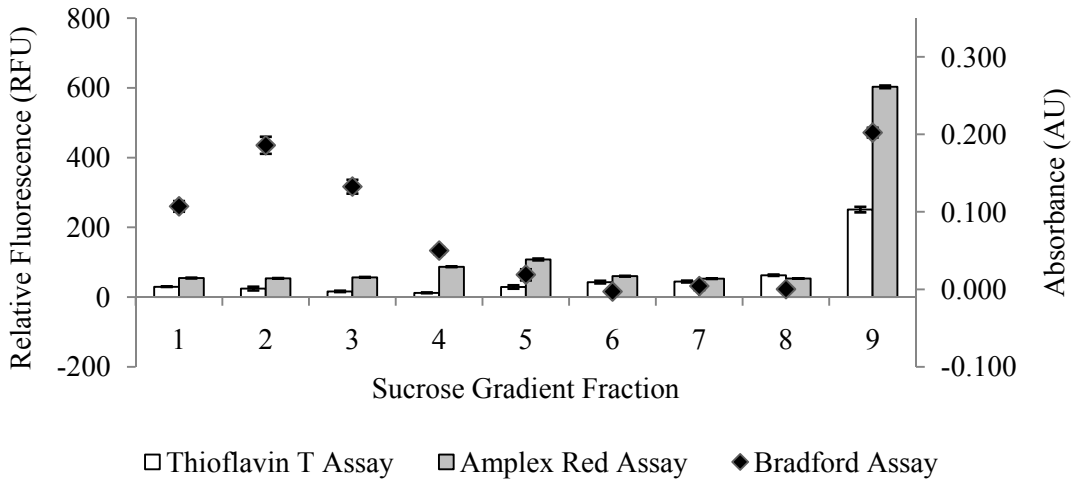

Figure 4.25

Sucrose gradient of GOD and crystallin amyloid fibrils and GA. *Sample contains 0.6 mg/ml GOD and 1.9 mg/ml crystallin amyloid fibrils and GA in 16 mM sodium phosphate, pH 7.4. Thioflavin T and Amplex Red assay fluorescence readings (clear bars and grey bars, respectively) are plotted on the left axis and Bradford assay absorbance readings (dark diamonds) are plotted on the right axis. The first fraction contains the lowest density of sucrose (0% before centrifugation) and the last fraction contains the highest density of sucrose (80% before centrifugation). Error bars indicate the standard error of the mean of three replicates and are less than 5%.*

These sucrose gradient results suggest that there is some cross-linking occurring both between GOD and insulin amyloid fibrils and GOD and crystallin amyloid fibrils. Overall, the sucrose gradient centrifugation method proved to be a successful technique for separating free GOD from immobilised GOD as there was minimal contamination and distinct separation of free GOD, immobilised GOD, and unfibrillised protein into sucrose fractions of different densities.

4.7 Microscopy studies

TEM is routinely used for the identification of amyloid fibrils, and has been used to assess the effect of enzyme immobilisation on other structures such as carbon nanotubes (Hrapovic *et al.* 2004; Nilsson 2004). The technique was employed to assess the effect of GOD immobilisation on the morphology of amyloid fibrils. The structures and morphologies of GOD-functionalised amyloid fibrils were viewed by TEM and representative images of cross-linked samples and controls are shown in Figure 4.26.

The GOD dimer has dimensions of approximately 6 x 5.2 x 7.7 nm, as determined by crystallography (Hecht *et al.* 1993), so may be able to be visualised by TEM. However, grid assembly and staining may cause the GOD dimer to be in a denatured anhydrous state. Previous work involving AFM of GOD cross-linked to carbon nanotubes reported the height of dry GOD to be around 1 nm (Besteman *et al.* 2003). The small rounded structures seen in the GOD and GOD and GA controls (Figure 4.26A and B, respectively) could be dry enzyme, as the average size of the small particles is around 1 nm in diameter. GOD gives a cloudy pattern when visualised by TEM, and the addition of GA causes the formation of denser cloud structures, consistent with the presence of intermolecular cross-links.

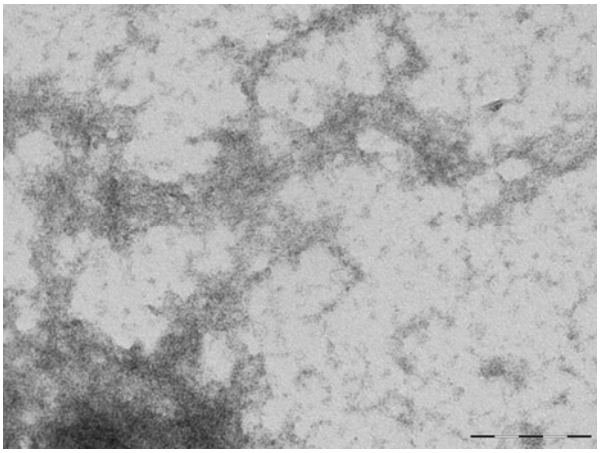

A

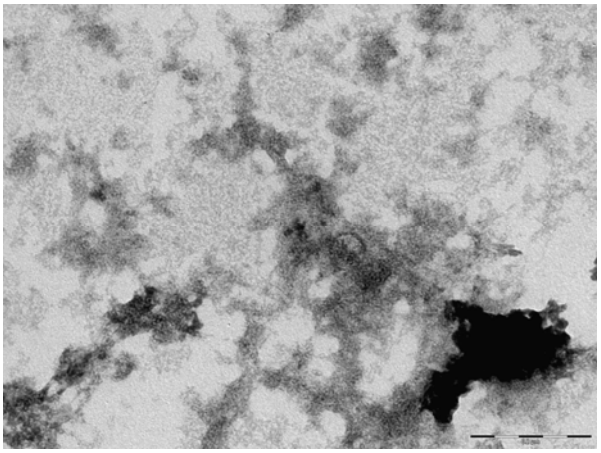

B

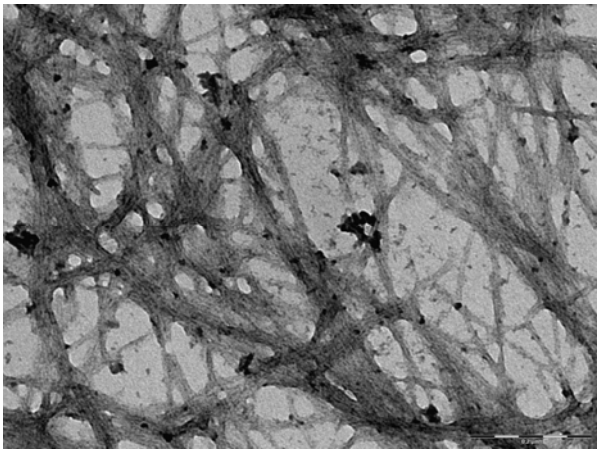

C

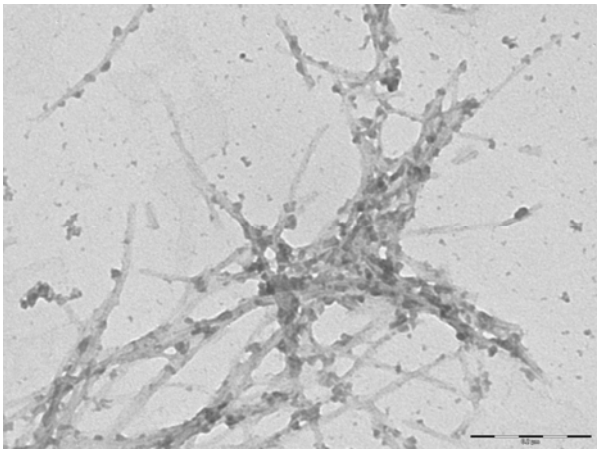

D

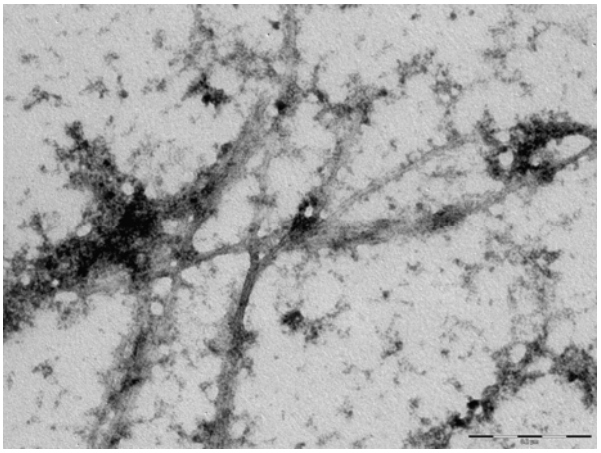

E

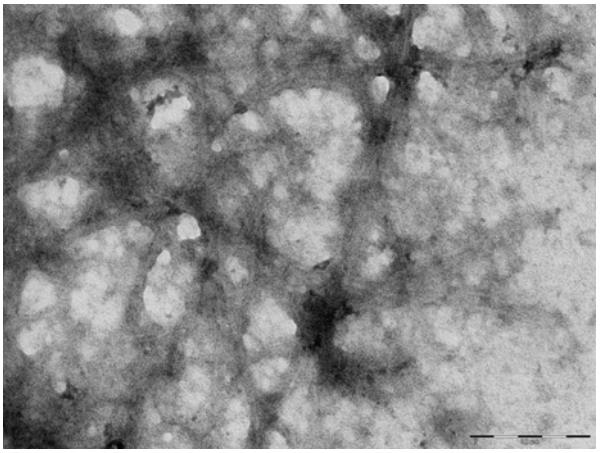

F

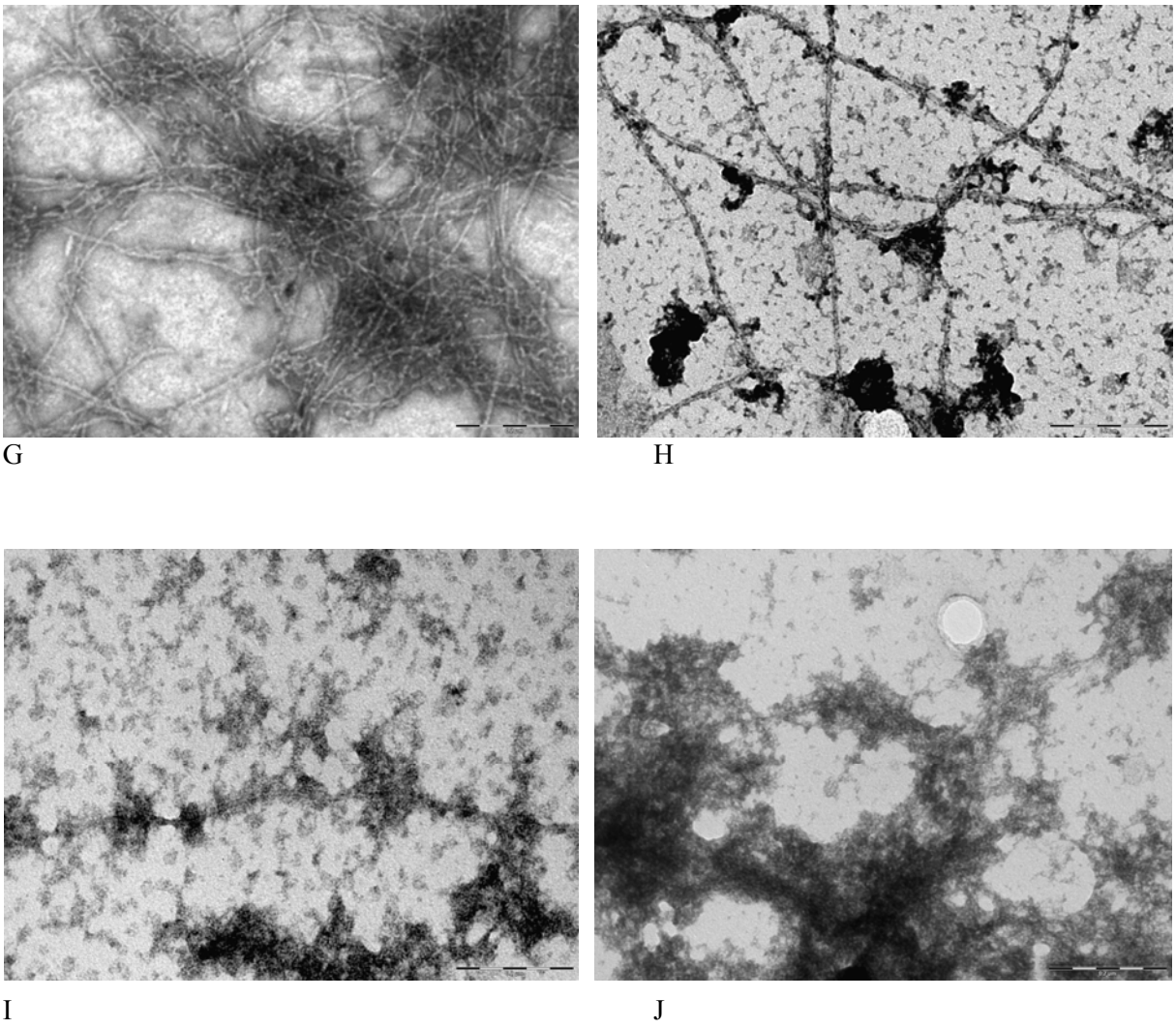

Figure 4.26

Representative TEM images of cross-linked samples and controls. *0.6 mg/ml GOD (A), 0.6 mg/ml GOD, 1% GA (B), 1.9 mg/ml insulin fibrils (C), 1.9 mg/ml insulin fibrils, 1% GA (D), 1.9 mg/ml insulin fibrils, 0.6 mg/ml GOD (E), 1.9 mg/ml insulin fibrils, 0.6 mg/ml GOD, 1% GA (F), 1.9 mg/ml crystallin fibrils (G), 1.9 mg/ml crystallin fibrils, 1% GA (H), 1.9 mg/ml crystallin fibrils, 0.6 mg/ml GOD (I), 1.9 mg/ml crystallin fibrils, 0.6 mg/ml GOD and 1% GA (J). Scale bar = 0.2 µm.*

4.8 Differential scanning fluorimetry (DSF)

DSF measures the temperature at which a protein unfolds using a dye called Sypro-orange, which has an affinity for hydrophobic protein, exposed as the protein unfolds (Niesen *et al.* 2007). The binding of the dye to unfolded protein produces a measurable fluorescence emission

(Ericsson *et al.* 2006). This technique was performed on cross-linked samples to test thermal stability of the cross-linked enzyme, as shown in Figure 4.27. Previously obtained values for the thermal denaturation of GOD, state that GOD loses tertiary structure at 61°C, with loss of the FAD cofactor at 61°C (Gouda *et al.* 2003). The result for GOD alone is consistent with these literature values, where thermal denaturation occurred at around 59°C. The sample containing GOD and insulin amyloid fibrils had a greater thermal stability than the sample containing native GOD, denaturing at around 67°C. Samples containing GA interfered with the Sypro-orange dye, giving a high initial fluorescence reading and thus a high signal to noise ratio and therefore no thermal denaturation temperature was obtained for these samples. There was no observed denaturation of amyloid fibrils, indicating their high stability.

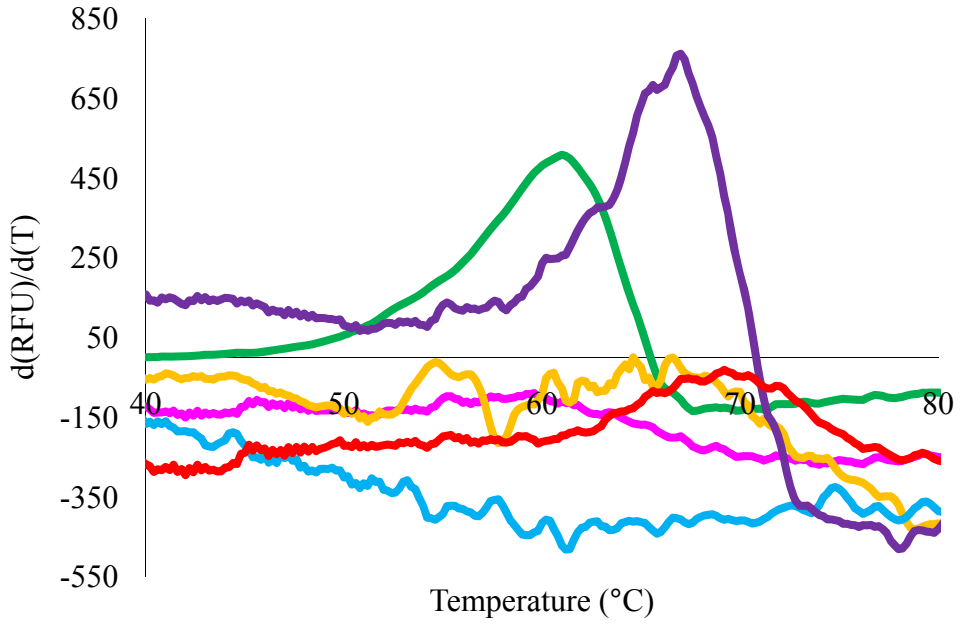

Figure 4.27

DSF of cross-linked samples. *Cross-linked samples and controls: Non-protein control (black), GOD (blue), GOD and GA (red), insulin amyloid fibrils (green), insulin amyloid fibrils and GA (purple), GOD and insulin amyloid fibrils (pink) and GOD, insulin amyloid fibrils and GA (orange). Curves are drawn from the average of three replicates.*

DSF data were corroborated by heating the samples in 10°C increments in an independent experiment and testing for GOD activity using the Amplex red assay, as shown in Figure 4.28. These results showed that the immobilisation of GOD onto insulin amyloid fibrils decreased the activity of GOD at lower temperatures. However, immobilisation of GOD onto amyloid fibrils was associated with the significantly higher activity observed at temperatures above 70 °C for

these samples, such as at 70 °C. The melting temperature results of the DSF and thermal denaturation studies are summarised in Table 4.1. These results show a similar melting temperature obtained from both studies.

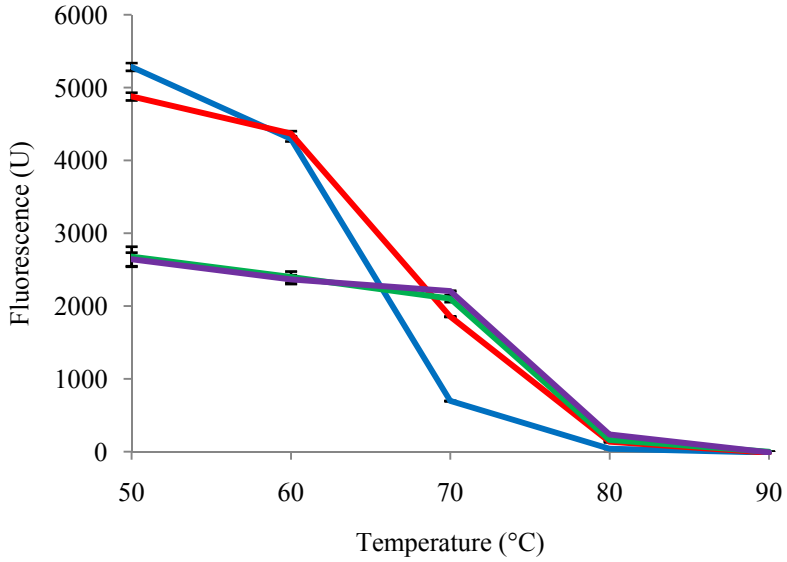

Figure 4.28

Thermal denaturation of cross-linked samples. *GOD (blue), GOD and GA (red), GOD and insulin amyloid fibrils (green) and GOD and insulin fibrils and GA (purple).*

Table 4.1

Melting temperature results of cross-linked samples. *The cross-linked samples and their melting temperature as determined by DSF and thermal denaturation experiments are given. DSC melting temperature is taken from peak maximum and thermal denaturation melting temperature is taken from point of decrease in GOD activity.*

Cross-linked Sample	DSF (°C)	Thermal Denaturation (°C)
GOD	61	60
GOD and GA	-	60
GOD and insulin amyloid fibrils	67	70
GOD, insulin amyloid fibrils and GA	-	70

To further corroborate the data from the DSF and thermal denaturation experiments, the samples were examined using a CD spectrometer, which measures protein unfolding along a temperature gradient. However, the samples had a very high absorbance and voltage threshold

for the CD spectrometer, and did not produce reliable results. Further experiments such as differential scanning colorimetry (DSC) are needed to ascertain the effect of immobilisation on the thermal stability of GOD. DSC uses measurement of heat input and output to assess protein denaturation, as opposed to the use of optical light by the CD spectrometer, and thus may be a more effective measure of thermal stability (Grant Pearce, Personal Communication).

4.9 Conclusion

The SDS-PAGE, centrifugation and TEM methods used in this chapter provided a suite of effective tools for assessing the degree of cross-linking in high molecular weight samples. These experiments also provide a model for assessment of cross-linking using other enzymes in the future. The melting temperature of immobilised GOD was found to be similar to that of free GOD. However, the techniques employed were subject to interference from the amyloid fibrils. The use of experiments which minimise this effect are required to confirm enzyme stability upon immobilisation in the future.

The results in this chapter show that GOD can be cross-linked to both bovine insulin and crystallin amyloid fibrils, to form an amyloid fibril enzyme scaffold that retains GOD activity, thus providing a 'proof of concept' model for enzyme attachment to amyloid fibrils.

The ability to increase the number of intermolecular cross-links between amyloid fibrils and GOD was investigated in Chapter Five *via* deglycosylation and *via* oxidation of the glycoprotein shell.

4.10 References

Ahmad, A., Akhtar, M. S. and Bhakuni, V. (2001). Monovalent cation-induced conformational change in glucose oxidase leading to stabilization of the enzyme. *Biochemistry* **40**: 1945-1955.

Bao, J., Furumoto, K., Yoshimoto, M., Fukunaga, K. and Nakao, K. (2003). Competitive inhibition by hydrogen peroxide produced in glucose oxidation catalyzed by glucose oxidase. *Biochemical Engineering Journal* **13**: 69-72.

Baszkin, A., Boissonnade, M. M., Rosilio, V., Kamyshny, A. and Magdassi, S. (1997). Adsorption of hydrophobized glucose oxidase at solution/air interface. *Journal of Colloid and Interface Science* **190**: 313-317.

Besteman, K., Lee, J. O., Wiertz, F. G. M., Heering, H. A. and Dekker, C. (2003). Enzyme-coated carbon nanotubes as single-molecule biosensors. *Nano Letters* **3**: 727-730.

Bradford, M. M. (1976). A rapid and sensitive method for the quantitation of microgram quantities of protein utilizing the principle of protein dye binding. *Analytical Biochemistry* **72**: 248-254.

Cherny, I. and Gazit, E. (2008). Amyloids: Not only pathological agents but also ordered nanomaterials. *Angewandte Chemie International Edition* **47**: 4062-4069.

Chiti, F. and Dobson, C. M. (2006). Protein misfolding, functional amyloid, and human disease. *Annual Review of Biochemistry* **75**: 333-366.

Ericsson, U. B., Hallberg, B. M., DeTitta, G. T., Dekker, N. and Nordlund, P. (2006). Thermofluor-based high-throughput stability optimization of proteins for structural studies. *Analytical Biochemistry* **357**: 289-298.

Fester, T., Berg, R. H. and Taylor, C. G. (2008). An easy method using glutaraldehyde-introduced fluorescence for the microscopic analysis of plant biotrophic interactions. *Journal of Microscopy* **231**: 342-348.

Gouda, M. D., Singh, S. A., Rao, A. G. A., Thakur, M. S. and Karanth, N. G. (2003). Thermal inactivation of glucose oxidase: Mechanism and stabilisation using additives. *Journal of Biological Chemistry* **278**: 24324-24333.

Hecht, H. J., Schomburg, D., Kalisz, H. and Schmid, R. D. (1993). The 3D structure of glucose oxidase from *Aspergillus niger*. Implications for the use of GOD as a biosensor enzyme. *Biosensors and Bioelectronics* **8**: 197-203.

Hirst, W. and Cox, R. A. (1976). The construction and analysis of sucrose gradients for use with zonal rotors. *Biochemical Journal* **159**: 259-265.

Hrapovic, S., Liu, Y., Male, K. B. and Luong, J. H. T. (2004). Electrochemical biosensing platforms using platinum nanoparticles and carbon nanotubes. *Analytical Chemistry* **76**: 1083-1088.

Kalisz, H. M., Hecht, H. J., Schomburg, D. and Schmid, R. D. (1991). Effects of carbohydrate depletion on the structure, stability and activity of glucose oxidase from *Aspergillus niger*. *Biochimica et Biophysica Acta - Protein Structure and Molecular Enzymology* **1080**: 138-142.

LeVine III, H. (1999). Quantification of β-sheet amyloid fibril structures with thioflavin T. *Methods in Enzymology* **309**: 274-284.

Minucci, A., Delibato, E., Castagnola, M., Concolino, P., Ameglio, F., Zuppi, C., Giardina, B. and Capoluongo, E. (2008). Identification of RFLP G6PD mutations by using microcapillary electrophoretic chips (Experion™). *Journal of Separation Science* **31**: 2694-2700.

Nettleton, E. J., Tito, P., Sunde, M., Bouchard, M., Dobson, C. M. and Robinson, C. V. (2000). Characterization of the oligomeric states of insulin in self-assembly and amyloid fibril formation by mass spectrometry. *Biophysical Journal* **79**: 1053-1065.

Niesen, F. H., Berglund, H. and Vedadi, M. (2007). The use of differential scanning fluorimetry to detect ligand interactions that promote protein stability. *Nature Protocols* **2**: 2212-2221.

Nilsson, M. R. (2004). Techniques to study amyloid fibril formation *in vitro*. *Methods* **34**: 151-160.

Rochet, J.-C. and Lansbury, P. T. (2000). Amyloid fibrillogenesis: themes and variations. *Current Opinion in Structural Biology* **10**: 60-68.

Schrödel, A. and De Marco, A. (2005). Characterization of the aggregates formed during recombinant protein expression in bacteria. *BMC Biochemistry* **6**.

Sohail Akhtar, M. and Bhakuni, V. (2003). Alkaline treatment has contrasting effects on the structure of deglycosylated and glycosylated forms of glucose oxidase. *Archives of Biochemistry and Biophysics* **413**: 221-228.

Tiller, J. C., Rieseler, R., Berlin, P. and Klemm, D. (2002). Stabilization of activity of oxidoreductases by their immobilization onto special functionalized glass and novel aminocellulose film using different coupling reagents. *Biomacromolecules* **3**: 1021-1029.

Wilson, R. and Turner, A. P. F. (1992). Glucose oxidase: An ideal enzyme. *Biosensors and Bioelectronics* **7**: 165-185.

Wine, Y., Cohen-Hadar, N., Freeman, A. and Frolow, F. (2007). Elucidation of the mechanism and end products of glutaraldehyde crosslinking reaction by X-ray structure analysis. *Biotechnology and Bioengineering* **98**: 711-718.

Zhou, M., Diwu, Z., Panchuk-Voloshina, N. and Haugland, R. P. (1997). A stable nonfluorescent derivative of resorufin for the fluorometric determination of trace hydrogen peroxide: Applications in detecting the activity of phagocyte NADPH oxidase and other oxidases. *Analytical Biochemistry* **253**: 162-168.

5. CHAPTER FIVE - ALTERNATIVE METHODS OF CROSS-LINKING GLUCOSE OXIDASE TO AMYLOID FIBRILS

5.1 Introduction

In Chapter Three, the ability to attach native GOD to amyloid fibrils using GA was investigated. Cross-linking by glutaraldehyde is dependent on the presence of free amino groups on the surface of the enzyme, provided by the amino acids lysine and arginine (Wine *et al.* 2007). The glycoprotein shell on native GOD may influence the binding of glutaraldehyde to surface lysine residues, by limiting access of the cross-linker to free amine groups, as the structure of the carbohydrate shell remains unknown (Kalisz *et al.* 1991). Thus, in this chapter, the ability to modify the glycoprotein shell to achieve a higher degree of cross-linking was investigated. Two methods were used to modify the glycoprotein shell, deglycosylation and oxidation. Deglycosylation involves removal of the shell using sugar-cleaving enzymes, and oxidation involves the formation of aldehyde groups on the sugar molecules using periodate. Methods used in this chapter to assess the degree of cross-linking were SDS-PAGE and sucrose gradient centrifugation, as described in Chapter Four.

5.2 Deglycosylation of GOD

Native GOD consists of a protein core which is partially surrounded by a carbohydrate shell (Wilson and Turner 1992). GOD was deglycosylated using the enzymes α-mannosidase and endoglycosidase H, a combination that has been widely used for the removal of the glycoprotein shell of GOD (Sohail Akhtar and Bhakuni 2003). As mentioned in Section 1.8, the carbohydrate shell of GOD consists of 190 mannose residues and 16 *N*-acetylglucosamine residues, which are

N- or *O*-glycosidically linked to the enzyme (Kalisz *et al.* 1991). α-Mannosidase is a non-linkage specific glycosidase, and endoglycosidase H is useful for the cleavage of mannose (Tarentino and Maley 1974; Burrows and Rastall 1998).

5.2.1 Ninhydrin

The effect of deglycosylation on the availability of lysine residues for cross-linking was assessed using a ninhydrin test. The number of ε-amino groups and N-terminal amines can be determined by reaction with ninhydrin solution following denaturation at high temperature (Friedman and Williams 1973). Thus the ninhydrin test can be used to compare the number of lysine residues available for cross-linking before and after deglycosylation. This test has been previously used to test the number of free amines of chitosan, before and after GOD immobilisation (Wei *et al.* 2002).

The ninhydrin test was carried out on deglycosylated GOD cross-linked samples and native GOD cross-linked samples. Control curves were created for BSA and native GOD, where the absorbance of GOD was higher than that of BSA, reflecting the amino acid content. BSA has been used in previous research as a standard for ninhydrin-based assays (Starcher 2001). The results obtained for the cross-linked samples are given in Table 5.1.

Table 5.1

Ninhydrin results for cross-linked GOD and deglycosylated cross-linked GOD. *The GOD sample and associated ninhydrin absorbance readings are given below. The error values show the standard error of the mean of three replicates of less than 5%.*

Sample	Absorbance at 570 nm	Calculated Molar Concentration (Lysine) (M)	Absorbance/Available Lysine
0.6 mg/ml GOD	0.100 ± 0.003	1.87×10^{-5}	5.33×10^{3}
0.6 mg/ml GOD, 1.9 mg/ml insulin amyloid fibrils and 1% GA	0.024 ± 0.002	-	-
0.075 mg/ml deglycosylated GOD	0.950 ± 0.001	1.41×10^{-5}	6.70×10^{4}
0.075 mg/ml deglycosylated GOD, 0.24 mg/ml insulin amyloid fibrils and 0.125% GA	0.244 ± 0.002	-	-

The number of free amine groups can be calculated from the ninhydrin absorbance data in Table 5.1 and the reported of available surface lysine residues in the literature (Baszkin *et al.* 1997). The results of these calculations are summarised in Table 5.2.

Table 5.2

Calculation of available lysine residues from ninhydrin data. *The number of available lysine residues in deglycosylated GOD can be calculated from the reported number of available lysine residues given for native GOD in the literature and the calculated absorbance per lysine residue from Table 5.1, and* vice versa*.*

Sample	Available Lysine (Literature)	Calculated Available Lysine
0.6 mg/ml GOD	7	0.39
0.075 mg/ml deglycosylated GOD	26	302

These results showed that the degree of ninhydrin reaction greatly increased upon deglycosylation of GOD. However, the calculated number of lysine residues before deglycosylation is significantly lower than the literature value, and the number of lysine residues available after deglycosylation is significantly higher than the literature value, based on the amino acid sequence of GOD (30 lysine residues). The number of lysine residues contributed by small quantities of cleavage enzymes (calculation not shown), is negligible and does not account for the significant difference.

If the obtained value for deglycosylated GOD is assumed to be correct, the calculated number of available lysine residues in native GOD suggests variation between glycoforms of GOD used in the literature compared to this thesis. Conversely, if the obtained value for GOD is assumed to be correct, the calculated number of free lysine residues suggests that hydrolysis is occurring within the protein, accounting for a large number of N-terminal amino groups in the sample. From these results, it was concluded that the use of ninhydrin to quantify the number of free lysine residues in GOD may be inaccurate. However, qualitatively, the results given in Table 5.1 indicate that deglycosylation is successful and, further, the number of free amino groups has decreased upon addition of GA in both the native and deglycosylated GOD samples, suggesting that cross-linking is occurring. Further experiments are required to quantify the degree of this cross-linking.

5.2.2 Electrophoretic studies

The deglycosylated enzyme was cross-linked using glutaraldehyde and run on an SDS-PAGE gel, as described for the native enzyme in Section 2.4.1. The results for the SDS-PAGE gel of the cross-linked samples and controls are given in Figure 5.1.

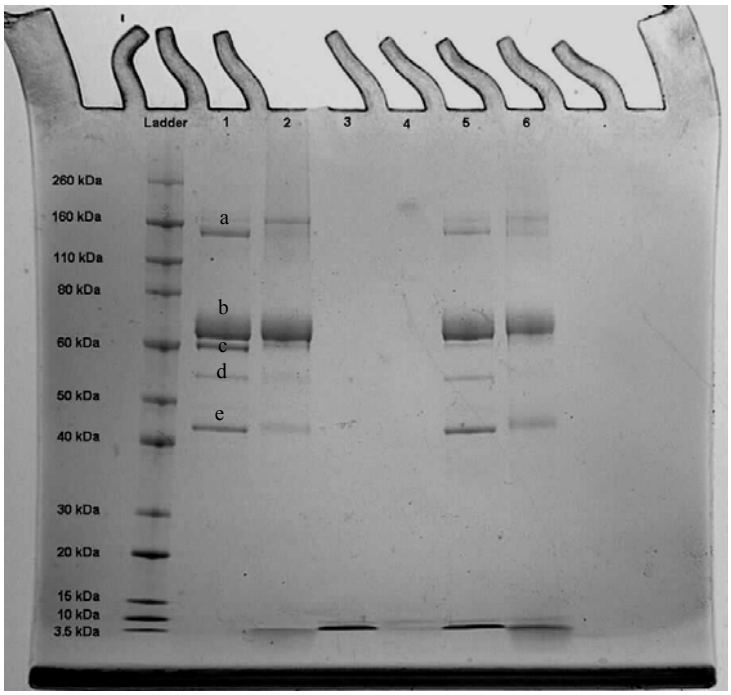

Figure 5.1

SDS-PAGE of deglycosylated GOD cross-linking to insulin amyloid fibrils. *Bands produced by samples in lanes containing 0.6 mg/ml deglycosylated GOD in 10 mM potassium phosphate buffer at pH 5.0 adjusted to pH 7.0 (1), deglycosylated GOD and 1% GA adjusted to pH 7.0 (2), 1.9 mg/ml insulin amyloid fibrils adjusted to pH 7.0 (3), 1.9 mg/ml insulin amyloid fibrils and 1% GA adjusted to pH 7.0 (4), 1.9 mg/ml insulin amyloid fibrils and 0.6 mg/ml deglycosylated GOD in 10 mM potassium phosphate buffer adjusted to pH 7.0 (5), and 1.9 mg/ml insulin amyloid fibrils, 0.6 mg/ml deglycosylated GOD and 1% GA adjusted to pH 7.0 (6).*

In Figure 5.1, deglycosylated GOD resulted in several bands ranging from low to high molecular weight (Lane 1). The molecular weight for deglycosylated GOD has been previously reported as 61 kDa for the monomer and 110 kDa for the dimer (Kalisz *et al.* 1991). Two of the bands in Lane 1 (Bands a, b), at 65 kDa and 140 kDa, were consistent with the molecular weight of the deglycosylated GOD monomer and dimer, respectively. The dimer band (Band a) has a higher value than the literature (Leskovac *et al.* 2005), which could be due to a slightly lower

efficiency of deglycosylation. This shows a 12 – 18 % drop in molecular weight from the native enzyme, where the molecular weight of the monomer was ~80 kDa and the molecular weight of the dimer was 160 kDa (Section 1.8). This result is in agreement with the molecular weight of the GOD amino acid sequence, calculated at 63.2 kDa (Frederick *et al.* 1990). There were smaller bands at around 66 kDa and 44 kDa (Bands c, e), which are consistent with the molecular weights of the α-mannosidase monomers. α-Mannosidase is a heterotetramer containing a two subunits of 66 kDa and two subunits of 44 kDa, which appear as two distinct bands on an SDS-PAGE gel (Burrows and Rastall 1998). Endoglycosidase H has a molecular weight of ~27 kDa when run on an SDS-PAGE gel (Tarentino and Maley 1974). There was no endoglycosidase H band visible, as the enzyme was at very low concentration and thus unable to be visualised on a gel. There was a faint band present at 55 kDa (Band d) which is inconsistent with any molecular weight of the proteins in solution, and thus may be an impurity in the enzyme preparation. This would be confirmed by running the enzymes α-mannosidase and endoglycosidase H on a gel; however, this was not feasible due to the high cost and limited supply of the endoglycosidase H enzyme. Upon addition of GA (Lane 2), the GOD bands remained unchanged.

There were no bands visible in the insulin amyloid fibrils or insulin amyloid fibrils and GA samples (Lane 3, 4), consistent with previous results in Section 4.3.1, Figure 4.2. When deglycosylated GOD was added to insulin amyloid fibrils, the bands seen for the deglycosylated GOD sample remained unchanged (Lane 5). This suggests that the non-covalent association seen between amyloid fibrils and GOD in Section 4.3.1 may involve the carbohydrate shell of the enzyme. Upon addition of GA (Lane 6), all deglycosylated GOD bands were diminished in intensity, confirmed by densitometry (data not included). This indicates that some of the deglycosylated GOD remained in the wells of the gel with the insulin amyloid fibrils, consistent with cross-linking. To assess the degree of cross-linking, samples were then spun in a sucrose gradient.

5.2.3 Centrifugation studies

Cross-linked deglycosylated samples and their associated controls were analysed by centrifugation through a sucrose gradient to separate free GOD from immobilised GOD, as described in Section 4.4. Fractions from the gradient were again tested for GOD activity using

the Amplex Red assay, the presence of amyloid fibrils using the ThT assay, and the protein concentration using the Bradford assay.

The sucrose gradient results for free deglycosylated GOD are shown in Figure 5.2. In the Amplex Red assay, there was a large amount of fluorescence seen in the mid-range densities of the sucrose gradient (Fractions 4 and 5). This was mirrored in the results of the Bradford assay. There was low fluorescence in the ThT assay for all fractions, consistent with previous results for free native GOD (Figure 4.16). Similar results were obtained for the sucrose gradient of deglycosylated GOD and GA (Figure 5.3). However, there was a small amount of fluorescence observed in the high sucrose density samples (Fractions 8 and 9). This is consistent with all other GOD and GA results, and is likely to be auto-fluorescent products of the GA reaction due to ageing of the GA, as discussed in Section 4.4.

The sucrose gradient results for insulin amyloid fibrils are given in Figure 5.4. These results are consistent with previous sucrose gradient results for insulin amyloid fibrils in Chapter Four, where there was a large amount of ThT fluorescence visible in the highest density sucrose sample (Fraction 9). There was no significant fluorescence seen in any of the fractions in the Amplex Red assay, or any significant absorbance seen in any of the fractions in the Bradford assay. This result was unchanged upon addition of GA, as shown in Figure 5.5.

The sucrose gradient results for GOD and insulin amyloid fibrils are given in Figure 5.6. These results were a combination of the sucrose gradient for deglycosylated GOD (Figure 5.2) and the gradient for insulin amyloid fibrils (Figure 5.4). There was a high Amplex Red fluorescence reading in the mid-density fractions (Fractions 3 and 4) and a high ThT fluorescence reading in the highest density fraction (Fraction 9). The Bradford assay has a high absorbance in both of these areas, reflecting the protein concentration of GOD in the mid-density fractions, and the protein concentration of the amyloid fibrils in the high density fraction. There was a small amount of GOD in the amyloid fibril pellet in the high density fraction (Fraction 9). This indicated that some of the GOD had been spun through the gradient with the amyloid fibrils, consistent with the effect seen in the native GOD and amyloid fibrils samples in Chapter Four.

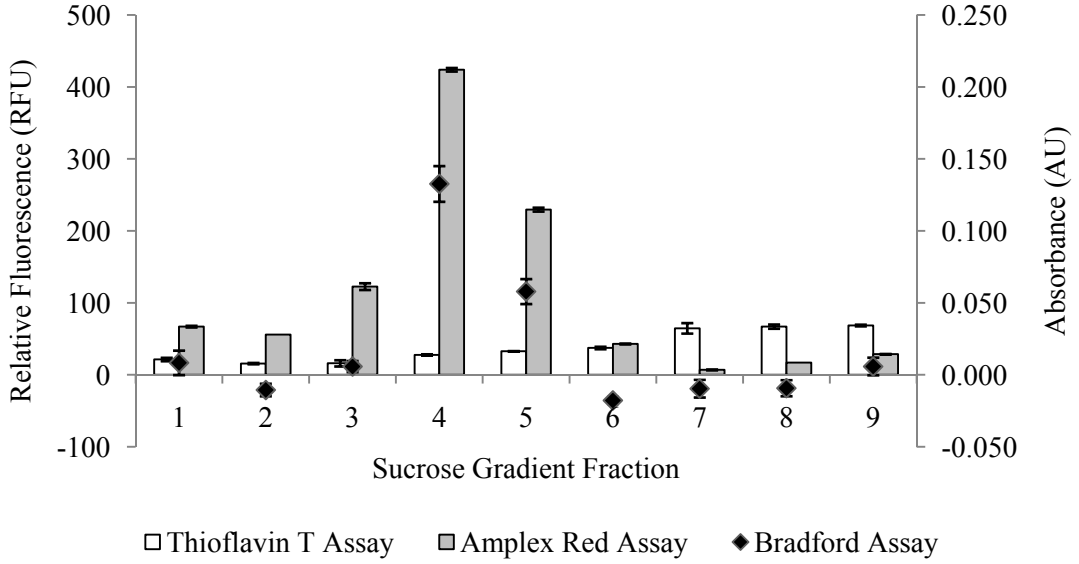

Figure 5.2

Sucrose gradient profile of deglycosylated GOD. *Thioflavin T assay results (white bars) and Amplex Red assay results (grey bars) are plotted on the left axis, and Bradford assay results (dark diamonds) are plotted on the right axis. Error bars indicate standard error of the mean of three replicates and are less than 5%. Values are corrected for fluorescence or absorbance of control.*

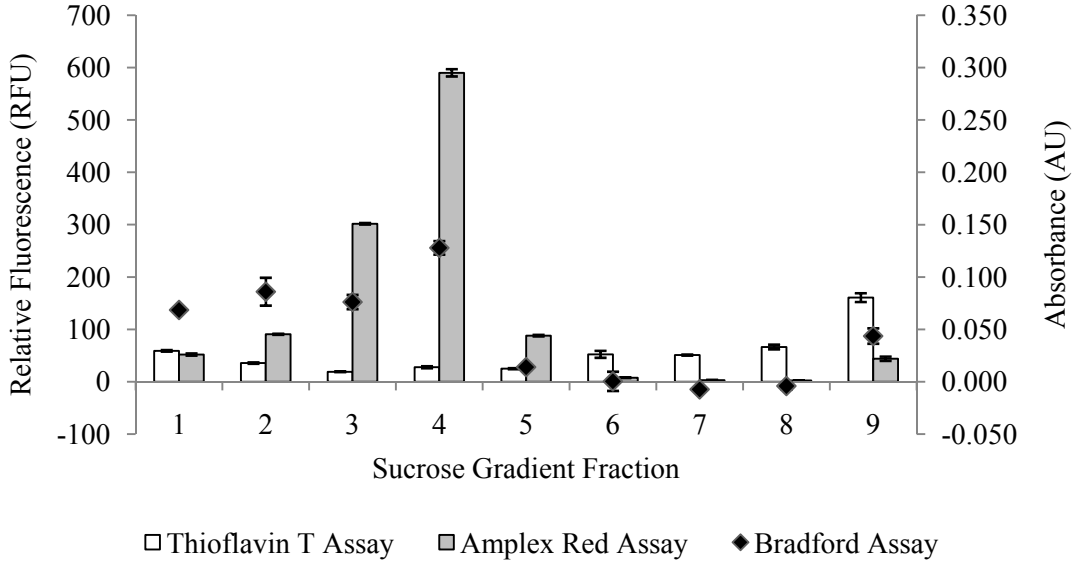

Figure 5.3

Sucrose gradient profile of deglycosylated GOD and GA. *Thioflavin T assay results (white bars) and Amplex Red assay results (grey bars) are plotted on the left axis, and Bradford assay results (dark diamonds) are plotted on the right axis. Error bars indicate standard error of the mean of three replicates and are less than 5%. Values are corrected for fluorescence or absorbance of control.*

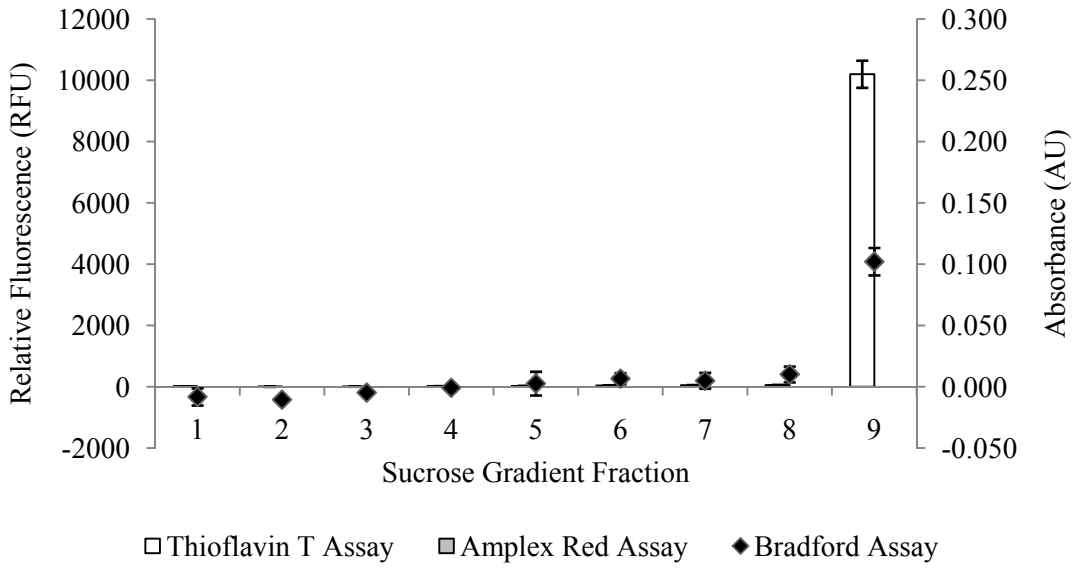

Figure 5.4

Sucrose gradient profile of insulin amyloid fibrils. *Thioflavin T assay results (white bars) and Amplex Red assay results (grey bars) are plotted on the left axis, and Bradford assay results (dark diamonds) are plotted on the right axis. Error bars indicate standard error of the mean of three replicates and are less than 5%. Values are corrected for fluorescence or absorbance of control.*

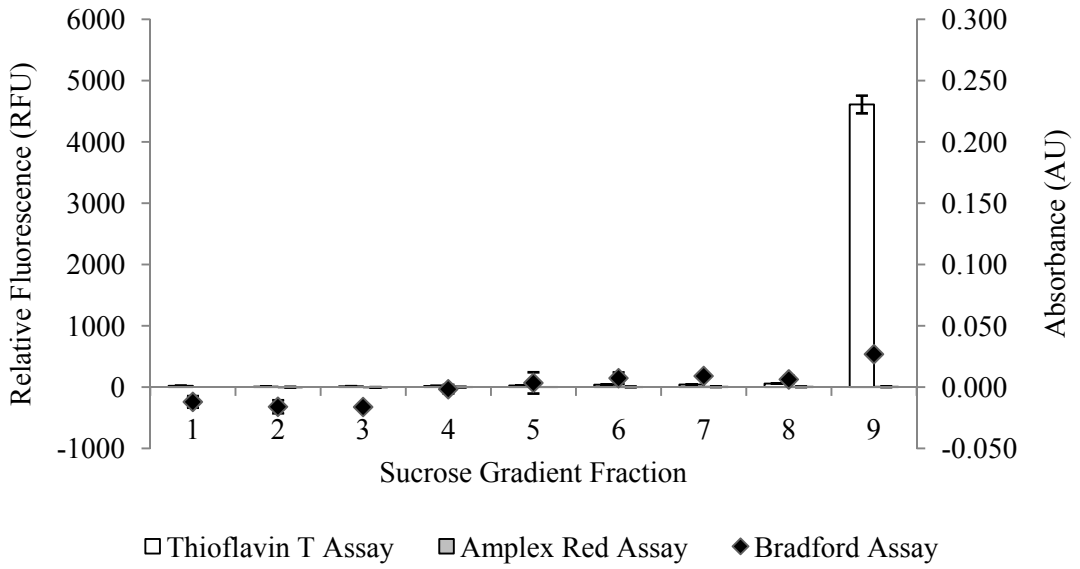

Figure 5.5

Sucrose gradient profile of insulin amyloid fibrils and GA. *Thioflavin T assay results (white bars) and Amplex Red assay results (grey bars) are plotted on the left axis, and Bradford assay results (dark diamonds) are plotted on the right axis. Error bars indicate standard error of the mean of three replicates and are less than 5%. Values are corrected for fluorescence or absorbance of control.*

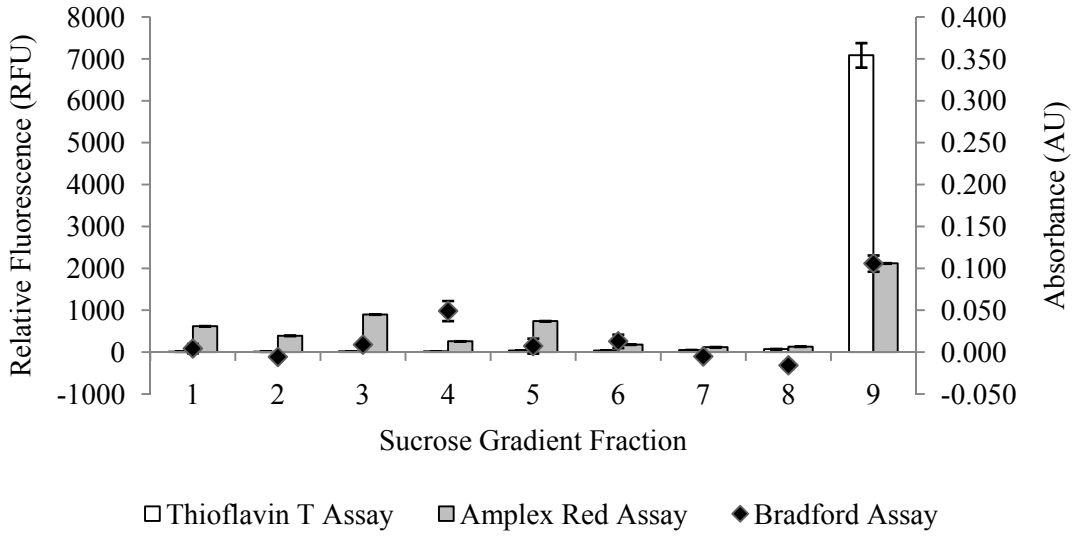

Figure 5.6

Sucrose gradient profile of insulin amyloid fibrils and deglycosylated GOD. *Thioflavin T assay results (white bars) and Amplex Red assay results (grey bars) are plotted on the left axis, and Bradford assay results (dark diamonds) are plotted on the right axis. Error bars indicate standard error of the mean of three replicates and are less than 5%. Values are corrected for fluorescence or absorbance of control.*

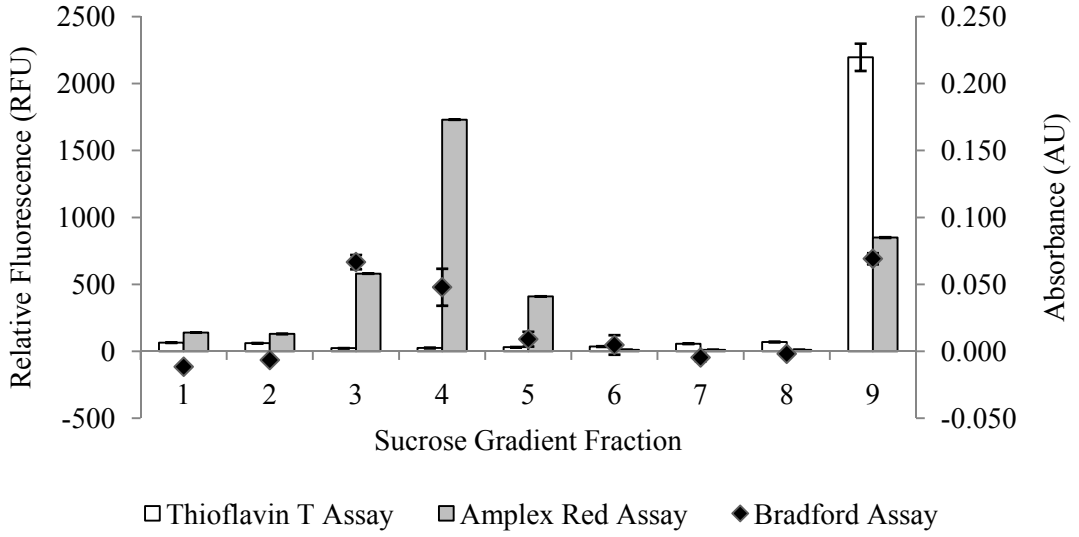

Figure 5.7

Sucrose gradient profile of insulin amyloid fibrils, deglycosylated GOD and GA. *Thioflavin T assay results (white bars) and Amplex Red assay results (grey bars) are plotted on the left axis, and Bradford assay results (dark diamonds) are plotted on the right axis. Error bars indicate standard error of the mean of three replicates and are less than 5%. Values are corrected for fluorescence or absorbance of control.*

The results for the sucrose gradient of GOD and insulin amyloid fibrils and GA (Figure 5.7) were very similar to the results for GOD and insulin amyloid fibrils. The absorbance readings for the Bradford assay were slightly lower, indicating that there may be cross-linking occurring between GOD and insulin amyloid fibrils, as the free amino groups are no longer available to react with the Bradford reagent. This is similar to the results obtained for native GOD and insulin amyloid fibrils and GA.

Deglycosylation is thus an effective method for removal of the glycoprotein shell of GOD, resulting in the increased availability of free amino groups for cross-linking, as shown by the ninhydrin test. However, the increased availability of free amino groups does not result in a significant increase in cross-linking. In previous research, deglycosylation was found to increase amount of enzyme loading, but not increase the specific activity of the enzyme (Volponi *et al.* 2008). This indicates that deglycosylated GOD may be cross-linking to amyloid fibrils with higher loading, but with no gain in activity. Deglycosylation was therefore not pursued further.

5.3 Oxidation of GOD by periodate

Another possible method of attachment of GOD to amyloid fibrils involves exploitation of the carbohydrate shell of GOD. Oxidation of the sugar molecules on the surface of the glycoprotein results in the formation of aldehyde groups, which can react with amines to produce an imine (Kozulic *et al.* 1987). In this way, the sugar residues could be used to cross-link GOD to the free amines on amyloid fibrils *via* reduction. The ability to cross-link GOD to amyloid fibrils *via* oxidation of the glycoprotein shell was investigated using the gel electrophoresis and centrifugation techniques used previously.

5.3.1 Electrophoretic studies

The use of sodium periodate to oxidise the hydroxyl groups of mannose residues on the surface of GOD to reactive aldehydes is an established method (Kozulic *et al.* 1987; Yoon *et al.* 2000). These aldehyde groups can then react with free amines, to form a Schiff base intermediate, which is in equilibrium with the starting materials (Zhang *et al.* 2004). This cross-linking experiment was designed to create reactive aldehydes on GOD that could form Schiff base intermediates with the free amino groups on amyloid fibrils. This Schiff base intermediate could

then be reduced to form an imine by reaction with sodium borohydride, thus capturing the Schiff base, and forming a permanent covalent bond between GOD and amyloid fibrils. This has previously been achieved using GOD and poly(allylamine), which has a number of free amine groups (Zhang *et al.* 2004).

Several concentrations of sodium periodate were used to oxidise GOD. The samples were run on an SDS-PAGE gel to establish the integrity of the protein following periodate oxidation (Figure 5.8).

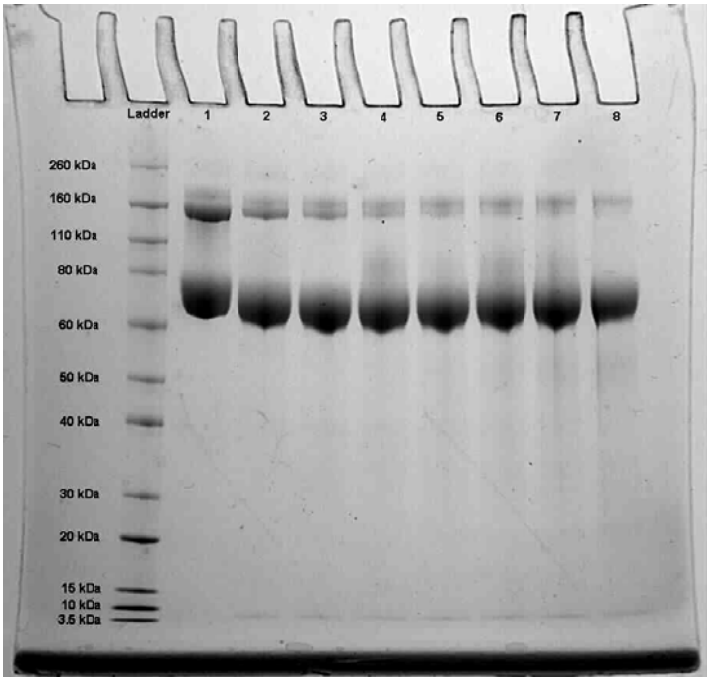

Figure 5.8

SDS-PAGE gel of sodium periodate oxidation of GOD. *Gel shows bands produced by 4 mg/ml native GOD (1) oxidised with increasing molar ratios of sodium periodate to mannose; 0.1:1 (2), 0.2:1 (3), 0.3:1 (4), 0.5:1 (5), 0.75:1 (6), 1:1 (7) and 2:1 (8).*

The untreated GOD sample (Lane 1) produced two bands at ~80 and 160 kDa, corresponding to the molecular weight of the monomer and dimer, respectively, consistent with Section 4.3.1 (Figure 4.2). A low concentration of periodate (Lane 2) produced a dimer band of decreased intensity, suggesting a decrease in stability of the dimeric state of the enzyme. As the concentration of periodate increased, the dimer band became less visible (Lanes 3 - 8), indicating that an increased concentration of periodate has an increased oxidising effect on the

glycoprotein shell of the enzyme that destabilised the dimer. The highest concentration of sodium periodate (Lane 8) was chosen for further experiments.

To determine the appropriate concentration of sodium borohydride to achieve optimal cross-linking to amyloid fibrils, several concentrations of sodium borohydride were used to reduce the reactive aldehyde groups on the GOD sample that had been oxidised with a molar ratio of sodium periodate of 2:1. As the concentration of sodium borohydride increased, there was increased reduction of aldehyde groups on GOD, so the highest sodium borohydride concentration was chosen for further experiments (data not shown).

The ability to attach GOD to amyloid fibrils using carbohydrate oxidation and subsequent Schiff base reduction was then investigated. Oxidised GOD was added to insulin amyloid fibrils and reduced using sodium borohydride, at a molar ratio of sodium borohydride to mannose of 100:1. The results of the cross-linking experiment using shell oxidation are given in Figure 5.9.

The oxidised GOD sample (Lane 1) produced one major band, consistent with the molecular weight of the GOD monomer at ~80 kDa. Upon addition of sodium borohydride (Lane 2), two bands are produced at ~80 and 160 kDa (indicated with arrow), consistent with the molecular weight of the GOD monomer and dimer, respectively. Insulin amyloid fibrils (Lane 3) did not produce any bands, consistent with previous results (Section 4.3.1, Figure 4.2). This remained unchanged upon addition of sodium borohydride.

The GOD and insulin amyloid fibrils sample produced a band with a molecular weight of ~80 kDa, consistent with the molecular weight of the monomer (Lane 5). Upon addition of sodium borohydride, only the monomer band was visible (Lane 6). This indicates that cross-linking is occurring, as the dimeric band seen in the GOD and sodium borohydride sample (Lane 2) is no longer visible, suggesting that GOD is attached to the amyloid fibrils. The monomer may also be binding; however, a difference in band density is not visible.

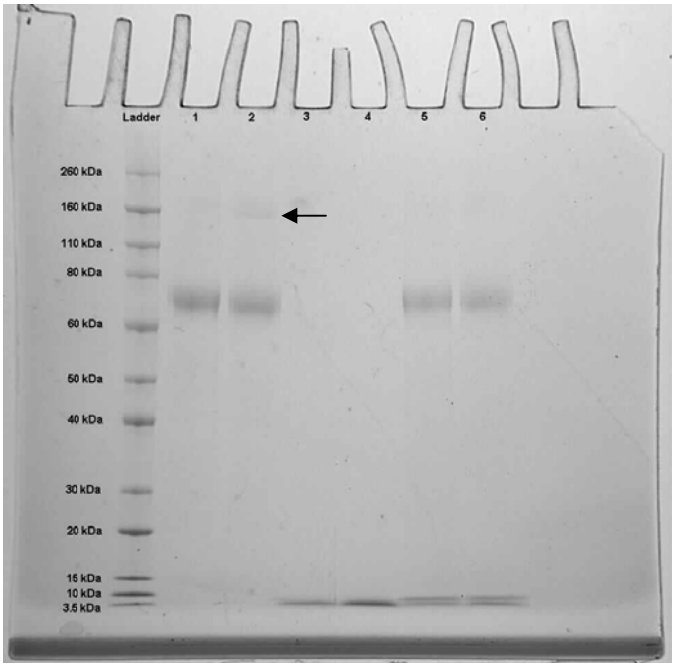

Figure 5.9

SDS-PAGE gel of cross-linking of oxidised GOD to insulin amyloid fibrils using sodium borohydride. *Gel shows bands produced by samples in lanes containing 0.6 mg/ml oxidised GOD (1) 0.6 mg/ml oxidised GOD and sodium borohydride (2), 1.9 mg/ml insulin amyloid fibrils (3), 1.9 mg/ml insulin amyloid fibrils and sodium borohydride (4), 1.9 mg/ml insulin amyloid fibrils and 0.6 mg/ml oxidised GOD (5) and 1.9 mg/ml insulin amyloid fibrils, 0.6 mg/ml oxidised GOD and sodium borohydride (6). For all samples, a molar ratio of sodium borohydride to mannose of 0.6 mg/ml GOD of 100:1 was used. GOD was oxidised with a molar ratio of sodium periodate to mannose of 2:1. A light band is indicated with an arrow.*

5.3.2 Centrifugation studies

The cross-linked samples and controls were then analysed by centrifugation through a sucrose gradient to separate free GOD from immobilised GOD, as described previously. Fractions from the gradient were tested for GOD activity using the Amplex Red assay, the presence of amyloid fibrils using the ThT assay, and protein concentration using the Bradford assay.

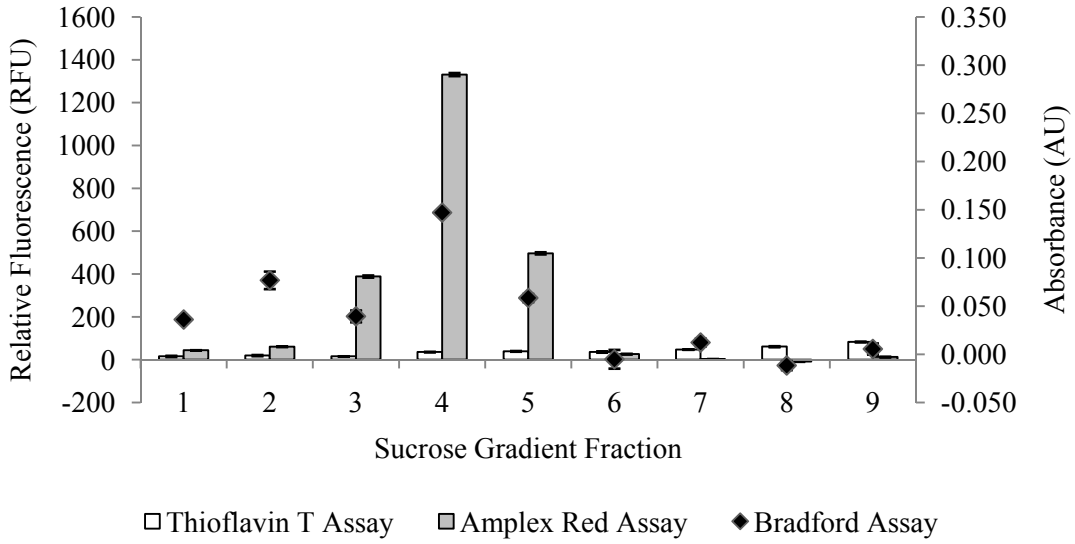

Figure 5.10

Sucrose gradient profile for oxidised GOD. *Thioflavin T assay results (clear bars) and Amplex Red assay results (grey bars) are plotted on the left axis, and Bradford assay results (dark diamonds) are plotted on the right axis. Error bars indicate standard error of the mean of three replicates and are less than 5%.*

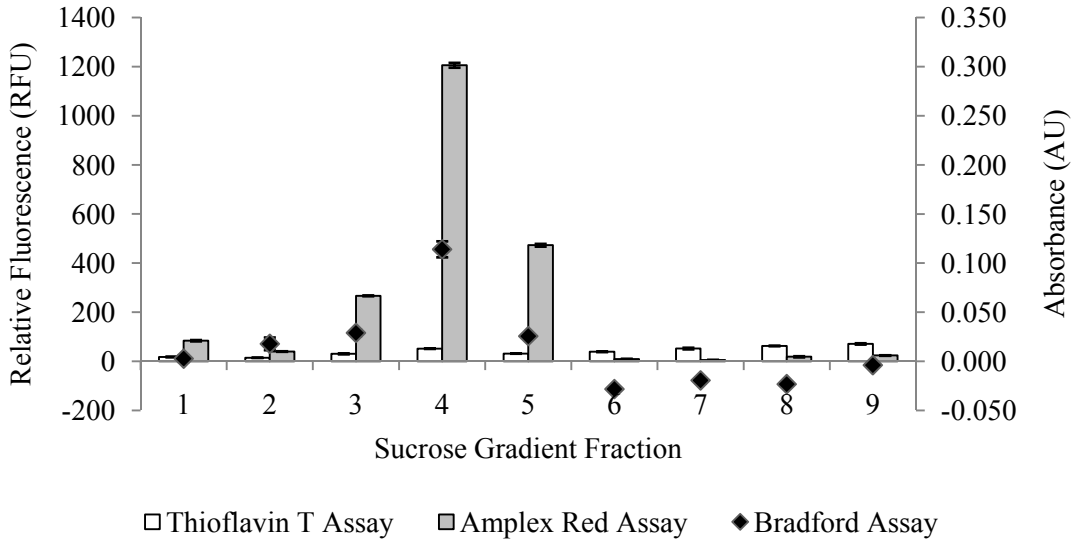

Figure 5.11

Sucrose gradient profile for cross-linked oxidised GOD. *Thioflavin T assay results (clear bars) and Amplex Red assay results (grey bars) are plotted on the left axis, and Bradford assay results (dark diamonds) are plotted on the right axis. Error bars indicate standard error of the mean of three replicates and are less than 5%.*

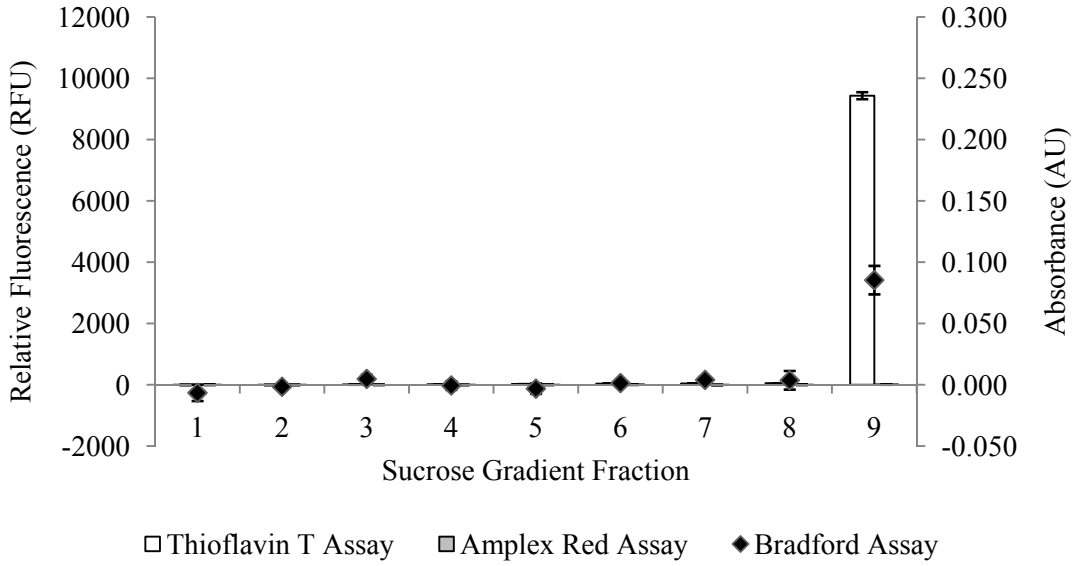

Figure 5.12

Sucrose gradient profile for insulin amyloid fibrils. *Thioflavin T assay results (clear bars) and Amplex Red assay results (grey bars) are plotted on the left axis, and Bradford assay results (dark diamonds) are plotted on the right axis. Error bars indicate standard error of the mean of three replicates and are less than 5%..*

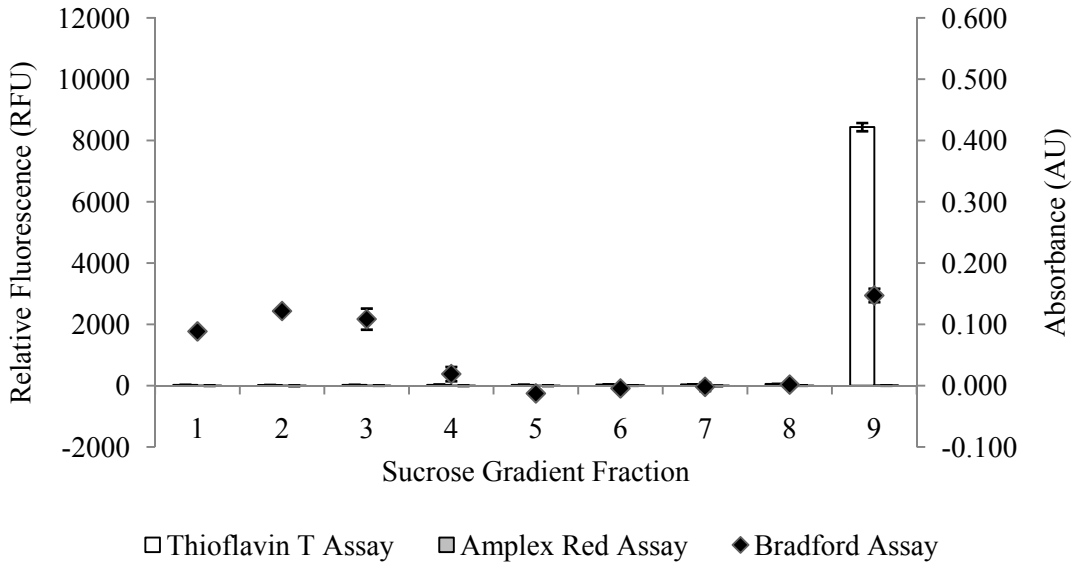

Figure 5.13

Sucrose gradient profile for insulin amyloid fibrils with sodium borohydride. *Thioflavin T assay results (clear bars) and Amplex Red assay results (grey bars) are plotted on the left axis, and Bradford assay results (dark diamonds) are plotted on the right axis. Error bars indicate standard error of the mean of three replicates and are less than 5%.*

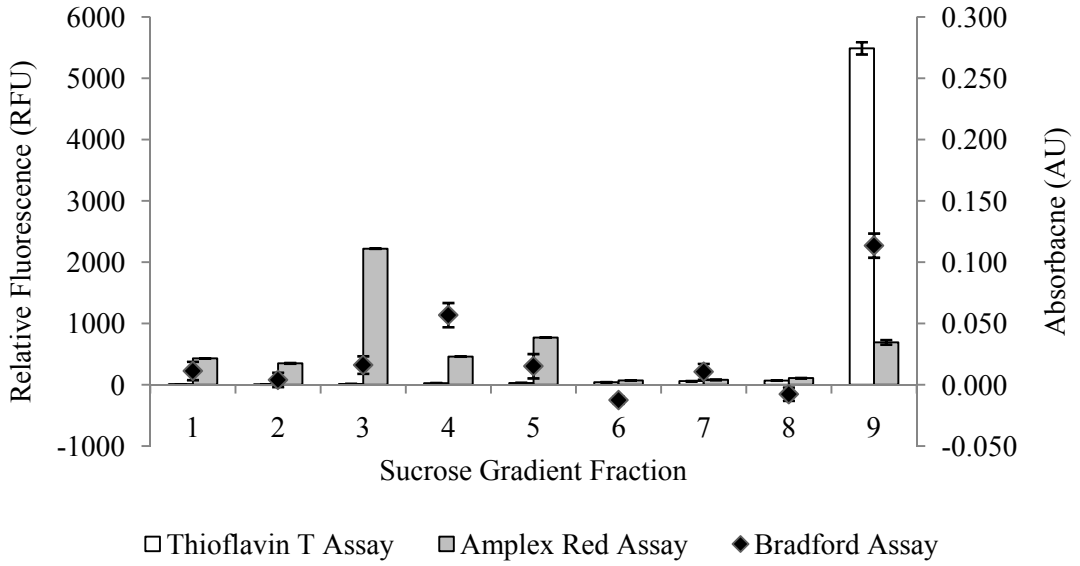

Figure 5.14

Sucrose gradient profile for insulin amyloid fibrils and oxidised GOD. *Thioflavin T assay results (clear bars) and Amplex Red assay results (grey bars) are plotted on the left axis, and Bradford assay results (dark diamonds) are plotted on the right axis. Error bars indicate standard error of the mean of three replicates and are less than 5%.*

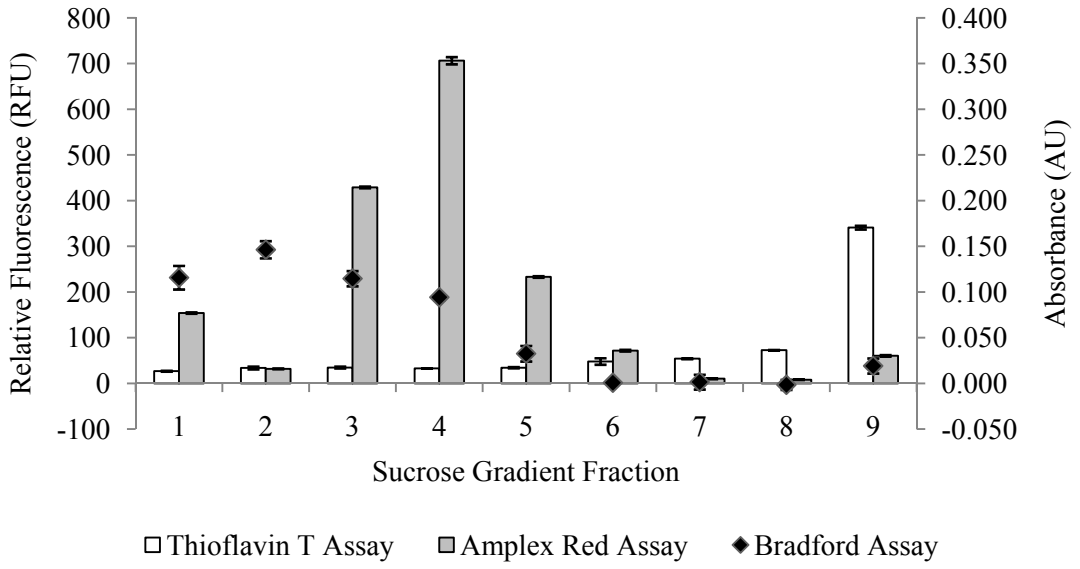

Figure 5.15

Sucrose gradient profile for insulin amyloid fibrils and oxidised GOD with sodium borohydride. *Thioflavin T assay results (clear bars) and Amplex Red assay results (grey bars) are plotted on the left axis, and Bradford assay results (dark diamonds) are plotted on the right axis. Error bars indicate standard error of the mean of three replicates and are less than 5%.*

The sucrose gradient results for oxidised GOD are shown in Figure 5.10. There was a large amount of fluorescence produced in the mid-density samples (Fractions 3 - 5) in the Amplex Red assay, consistent with previous results for native GOD. This is mirrored in the results of the Bradford assay, where there was a high absorbance in the mid-density samples. There was no significant fluorescence produced in any of the samples in the ThT assay. This result is unchanged upon addition of sodium borohydride (Figure 5.11).

The sucrose gradient results for insulin amyloid fibrils are given in Figure 5.12. There is a high amount of ThT fluorescence in the high density sucrose sample (Fraction 9). This is mirrored in the results of the Bradford assay, where there is a high absorbance in the high density sample. There is no significant absorbance in any of the fractions in the Amplex Red assay. This is consistent with previous results for unmodified insulin amyloid fibrils in Section 4.3.1 (Figure 4.2).

There is little change upon addition of sodium borohydride in the Amplex Red and ThT assays (Figure 5.13). However, in the Bradford assay, there is a small absorbance in the low density sucrose samples (Fractions 1-3). This may be low molecular weight protein due to reduction of the amyloid fibrils by sodium borohydride, causing destabilisation of the amyloid fibril structure.

The sucrose gradient results for oxidised GOD and insulin amyloid fibrils are shown in Figure 5.14. These results were a combination of the sucrose gradient for oxidised GOD (Figure 5.10) and insulin amyloid fibrils (Figure 5.12). There was a high Amplex Red fluorescence reading in the mid-density fractions (Fractions 3 - 5) and a high ThT fluorescence reading in the highest density fraction (Fraction 9). The Bradford assay has a high absorbance in both of these areas, reflecting the protein concentration of GOD in the mid-fractions, and the protein concentration of the amyloid fibrils in the high density fraction. There is a very small amount of GOD in the amyloid fibril pellet in the high density fraction (Fraction 9). This indicates that some of the GOD had been spun through the gradient with the amyloid fibrils, suggesting an association effect.

The sucrose gradient results for oxidised GOD and insulin amyloid fibrils treated with sodium borohydride are given in Figure 5.15. These results showed a high Amplex Red fluorescence reading in the mid-density fractions (Fractions 3 - 5) and a high ThT fluorescence reading in the highest density fraction (Fraction 9). The Bradford assay has a high absorbance in both of these

areas, reflecting the protein concentration of GOD in the mid-fractions, and the protein concentration of the amyloid fibrils in the high density fraction. There was a small absorbance in the Bradford assay in the low density sucrose fractions (Fractions 1 – 3), as previously seen in the reduced insulin amyloid fibrils sample (Figure 5.13). There was also a small absorbance reading in the highest density fraction (Fraction 9) in the Amplex Red assay. This indicated that some of the GOD had been spun through the gradient with the amyloid fibrils; however, this is a small effect compared to the effect seen in the native GOD and amyloid fibrils samples in Chapter Four.

Thus the use of sodium periodate is an effective method for oxidation of the glycoprotein shell of GOD. However, the use of sodium borohydride as a reducing agent may have a destabilising effect on the insulin amyloid fibrils, resulting in decreased attachment. The use of oxidation of the glycoprotein shell of GOD followed by reduction using sodium borohydride is therefore not as effective as the use of glutaraldehyde as a cross-linking agent.

5.4 Conclusions

Deglycosylation of GOD generates clean GOD bands and an increase in reactive lysine groups for use in GA cross-linking. However, the results of the sucrose gradient studies do not greatly differ from the results achieved with native GOD. The deglycosylation is both expensive and time consuming, and therefore is not the most effective method of cross-linking GOD to amyloid fibrils.

Oxidation of the carbohydrate shell of GOD results in reactive aldehyde groups which can, in turn, react with the amines of amyloid fibrils to form imine bonds. This technique was effective in cross-linking GOD to amyloid fibrils. However, due to the amount of time taken to achieve this result, and the loss of amyloid fibrils by reaction with sodium borohydride, further method development is needed. Thus, cross-linking GOD to amyloid fibrils *via* GA is the most effective method of cross-linking.

5.5 References

Baszkin, A., Boissonnade, M. M., Rosilio, V., Kamyshny, A. and Magdassi, S. (1997). Adsorption of hydrophobized glucose oxidase at solution/air interface. *Journal of Colloid and Interface Science* **190**: 313-317.

Burrows, H. M. and Rastall, R. A. (1998). Essential carboxyl and tryptophan residues in jack bean α-Mannosidase. *Phytochemistry* **48**: 257-260.

Frederick, K. R., Tung, J., Emerick, R. S., Masiarz, F. R., Chamberlain, S. H., Vasavada, A., Rosenberg, S., Chakraborty, S., Schopfer, L. M. and Schopter, L. M. (1990). Glucose oxidase from *Aspergillus niger*. Cloning, gene sequence, secretion from *Saccharomyces cerevisiae* and kinetic analysis of a yeast-derived enzyme. *Journal of Biological Chemistry* **265**: 3793-3802.

Friedman, M. and Williams, L. D. (1973). The reaction of ninhydrin with keratin proteins. *Analytical Biochemistry* **54**: 333-345.

Kalisz, H. M., Hecht, H. J., Schomburg, D. and Schmid, R. D. (1991). Effects of carbohydrate depletion on the structure, stability and activity of glucose oxidase from *Aspergillus niger*. *Biochimica et Biophysica Acta - Protein Structure and Molecular Enzymology* **1080**: 138-142.

Kozulic, B., Leustek, I., Pavlovic, B., Mildner, P. and Barbaric, S. (1987). Preparation of the stabilized glycoenzymes by cross-linking their carbohydrate chains. *Applied Biochemistry and Biotechnology* **15**: 265-278.

Leskovac, V., Trivic, S., Wohlfahrt, G., Kandrac, J. and Perićin, D. (2005). Glucose oxidase from *Aspergillus niger*: The mechanism of action with molecular oxygen, quinones, and one-electron acceptors. *International Journal of Biochemistry and Cell Biology* **37**: 731-750.

Sohail Akhtar, M. and Bhakuni, V. (2003). Alkaline treatment has contrasting effects on the structure of deglycosylated and glycosylated forms of glucose oxidase. *Archives of Biochemistry and Biophysics* **413**: 221-228.

Starcher, B. (2001). A ninhydrin-based assay to quantitate the total protein content of tissue samples. *Analytical Biochemistry* **292**: 125-129.

Tarentino, A. L. and Maley, F. (1974). Purification and properties of an endo-β-N-acetylglucosaminidase from *Streptomyces griseus*. *Journal of Biological Chemistry* **249**: 811-817.

Volponi, J. V., Miller, M. E. and Simmons, B. A. (2008). Efficient attachment of native & deglycosylated glucose oxidase to Amberzyme oxirane polymeric support. *Industrial Biotechnology* **4**: 288-293.

Wei, X., Cruz, J. and Gorski, W. (2002). Integration of enzymes and electrodes: Spectroscopic and electrochemical studies of chitosan-enzyme films. *Analytical Chemistry* **74**: 5039-5046.

Wilson, R. and Turner, A. P. F. (1992). Glucose oxidase: An ideal enzyme. *Biosensors and Bioelectronics* **7**: 165-185.

Wine, Y., Cohen-Hadar, N., Freeman, A. and Frolow, F. (2007). Elucidation of the mechanism and end products of glutaraldehyde crosslinking reaction by X-ray structure analysis. *Biotechnology and Bioengineering* **98**: 711-718.

Yoon, H. C., Hong, M.-Y. and Kim, H.-S. (2000). Functionalization of a poly(amidoamine) dendrimer with ferrocenyls and its application to the construction of a reagentless enzyme electrode. *Analytical Chemistry* **72**: 4420-4427.

Zhang, S., Yang, W., Niu, Y. and Sun, C. (2004). Multilayered construction of glucose oxidase on gold electrodes based on layer-by-layer covalent attachment. *Analytica Chimica Acta* **523**: 209-217.

6. CHAPTER SIX - INCORPORATING FUNCTIONALISED AMYLOID FIBRILS INTO A PVOH FILM SYSTEM

6.1 Introduction

Previous results described in Chapters Three and Four demonstrated the ability to use amyloid fibrils as a nanoscaffold for enzyme immobilisation. These functionalised amyloid fibrils have the potential to be incorporated into a film system for the creation of a new bionanomaterial.

The material used in the model film system in this chapter was poly(vinyl alcohol) (PVOH). As discussed in Section 1.12, PVOH is an ideal film system for investigating the ability to incorporate an enzyme scaffold, as it is inexpensive, readily available, and provides a favourable environment for the enzyme (Wong and Abdul-Aziz 2008). PVOH has been widely used in biomaterial research because of its elasticity, good film forming ability and water content similar to that of biological tissue (Wong and Abdul-Aziz 2008). This is important for limiting dehydration and denaturation of immobilised enzymes, which are common problems that can occur upon film drying, resulting in loss of enzyme structure and function (Kim *et al.* 2008). PVOH provides a stable environment for GOD by hydrogen bonding the H atoms of alcohol groups in the PVOH to the O atoms of glycoprotein shell carbohydrate groups in GOD, which inhibits unfavourable conformations of GOD (Wong and Abdul-Aziz 2008). The immobilisation of GOD and retention of its active conformation provides potential for the production of a film with antimicrobial activity, due to the hydrogen peroxide and gluconic acid produced in the GOD reaction, useful in the production of antimicrobial packaging (Vartiainen *et al.* 2005). Also, as previously described in Section 1.12, PVOH is known to have selective permeability for low molecular weight substances such as glucose, the substrate of the GOD-catalysed reaction (Wong and Abdul-Aziz 2008). This is an advantage for the production of antimicrobial films, as it allows preparation of the film without the addition of glucose, simplifying the film preparation method.

Despite the favourable properties of PVOH film for enzyme immobilisation, some properties of PVOH make the film less suitable for the production of a biomaterial, such as a high degree of crystallisation (Chang and Kim 2007). This causes PVOH film to be stiff and brittle; however, the addition of amyloid fibrils to PVOH films was predicted to change these properties. The addition of the immobilised enzyme scaffold may also provide useful properties such as prevention of desorption or leeching out of enzyme, which is a common problem with enzyme-film preparations (Gade *et al.* 2006).

In this chapter, the incorporation of the functionalised amyloid fibril scaffold into PVOH was investigated as a 'proof of concept' material to establish the potential use of amyloid fibrils as a nanoscaffold. Microscopy techniques were used to assess the spatial arrangement and mixing of film components, and the functionalised film was tested for antimicrobial activity.

6.2 Assessment of the contents of functionalised films

PVOH films were prepared using an established in-house solution casting method, as mentioned in Section 2.5 (Rao 2008). Cross-linked samples and controls were directly added to dissolved PVOH. Cross-linking was performed at a solution pH of 7.0. Upon addition of PVOH, the new solution pH was 5.0. This may have an effect on the distribution of amyloid fibrils throughout the film, due to increased clumping of fibrils at increasing pH (Chapter Three, Section 3.7). The solutions were mixed by inversion, taking care to reduce air bubbles, and cast in a rectangular gel casting tray (7 x 10 cm) to obtain equal sized films. The casting trays were measured with a spirit level to ensure the films were of even thickness. Films were also covered with paper to protect from dust contamination but allow evaporation. The water was then allowed to evaporate and resulting films were carefully removed from the trays. The distribution of film components was then assessed using SEM and confocal microscopy. SEM was used to visualise the surfaces of the films, and confocal microscopy was used to take visual sections through the films.

The enzyme-functionalised amyloid fibrils prepared during this research were highly heterogeneous, as shown in TEM images in Section 4.7. Before mechanical testing could be carried out on the functionalised films to test the effect of the addition of amyloid fibrils to the film properties, it was important to assess the degree of dispersion of the functionalised amyloid fibrils within the film. If its components are not evenly distributed, the film will contain points

of weakness, and the results of any mechanical testing will be affected (Mark Staiger, Personal Communication). Scanning electron microscopy (SEM) was used to view the surface of the film and confocal microscopy was used to view the distribution of constituents by taking image slices through the film. SEM is frequently used to investigate phase behaviour of blends of synthetic polymers and biopolymers, providing useful information on miscibility of polymers (Aoi *et al.* 2000a; Aoi *et al.* 2000b). Confocal microscopy has been used in a similar way for studying the phase-separated structures of polymer blends including PVOH hydrogel blends (Fergg *et al.* 2001; Jinnai *et al.* 2001).

6.2.1 Scanning electron microscopy of functionalised film

SEM was used to image the surface topography of the functionalised film. This technique has been used previously on PVOH/gelatin/chitosan blend films to visualise the surface morphology (Chen *et al.* 2008). Representative images from the SEM studies are given in Figure 6.1. Imaging the surface of the film is a useful tool for investigating the features of the film. These results show a variety of features, which may be influenced by the constituents of the film.

Without addition of other constituents, PVOH film had a relatively smooth surface at 1,000 x magnification, which remained unchanged upon addition of GA (Figure 6.1A, B). A small amount of dust and other contaminants were visible on the surface of the films. Upon addition of GOD to the PVOH films, there was the appearance of small voids, possibly due to bubbles in the film when casting (Figure 6.1C). These voids were accentuated upon addition of GA (Figure 6.1D). This effect could be due to increased phase separation of film constituents due to hydrophobicity introduced by cross-linking.

When insulin amyloid fibrils were added to PVOH film, there was a large amount of surface heterogeneity, with small bubble-like formations on the surface of the film (Figure 6.1E). These bubbles increased in size dramatically upon addition of GA (Figure 6.1F). The addition of GOD and insulin amyloid fibrils to the PVOH film produced a smoother film surface than amyloid fibrils alone, with rough patches of surface, and the addition of GA had little effect on the surface (Figure 6.1G, H). The addition of crystallin amyloid fibrils to PVOH produced an interesting surface, with long, thin indentations visible (Figure 6.1K). This effect was not seen in any of the other film samples (Figure 6.1I, K and L).

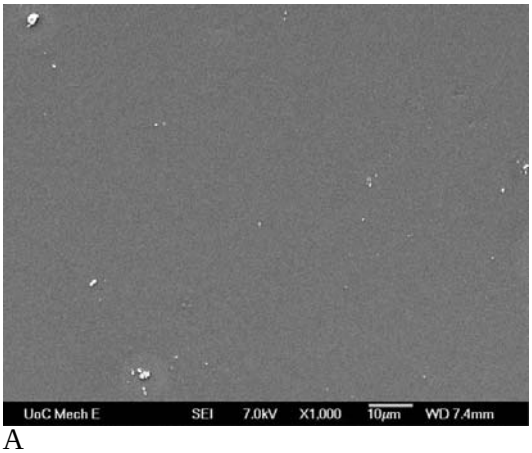
UoC Mech E SEI 7.0kV X1,000 10μm WD 7.4mm

A

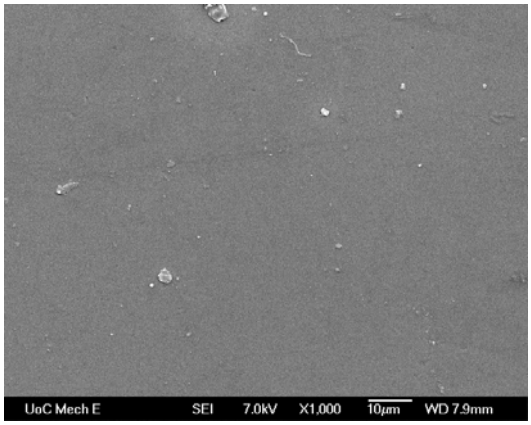
UoC Mech E SEI 7.0kV X1,000 10μm WD 7.9mm

B

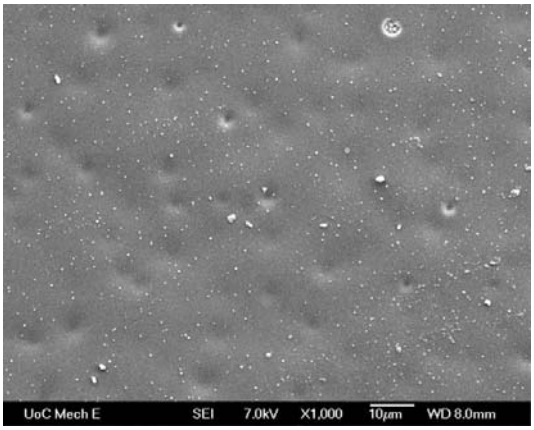
UoC Mech E SEI 7.0kV X1,000 10μm WD 8.0mm

C

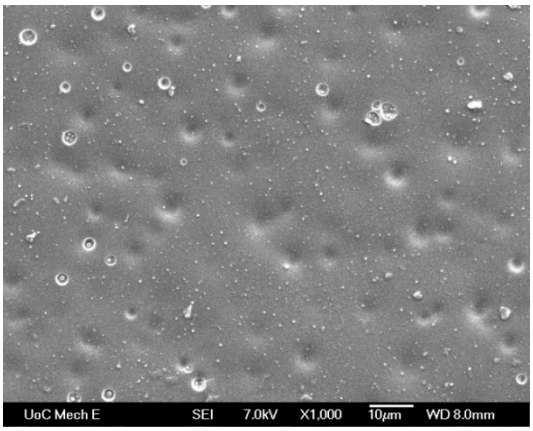
UoC Mech E SEI 7.0kV X1,000 10μm WD 8.0mm

D

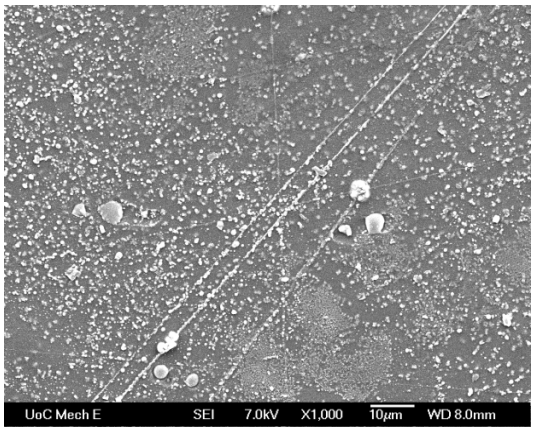
UoC Mech E SEI 7.0kV X1,000 10μm WD 8.0mm

E

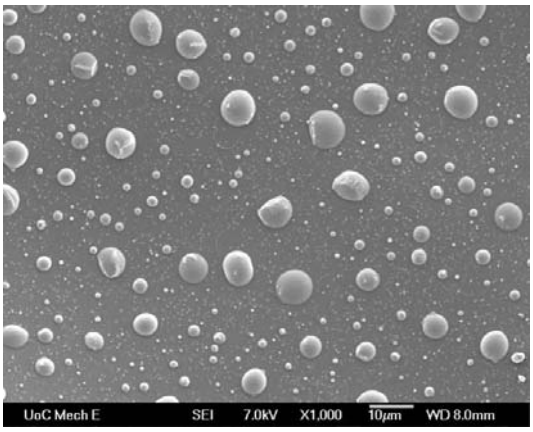
UoC Mech E SEI 7.0kV X1,000 10μm WD 8.0mm

F

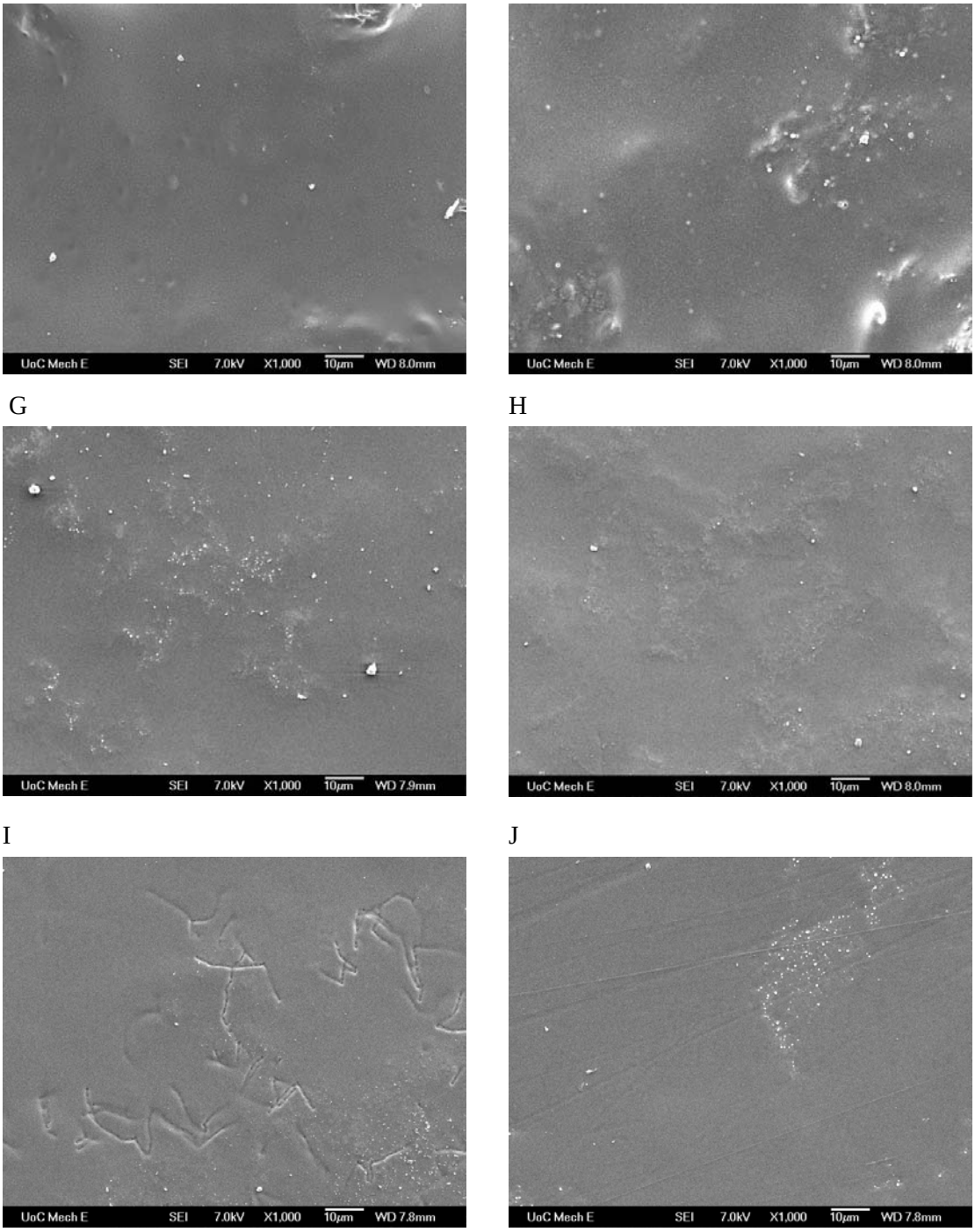

Figure 6.1

Representative SEM images of film surfaces. *Film surfaces were imaged at 1,000 x magnification in duplicate. 2.5% PVOH (A), 2.5% PVOH and 2 mM GA (B), 2.5% PVOH and 1.7 mg/ml GOD (C), 2.5% PVOH, 1.7 mg/ml GOD and 2 mM GA (D), 2.5% PVOH, and 1.5 mg/ml insulin amyloid fibrils (E), 2.5% PVOH, 1.5 mg/ml insulin amyloid fibrils and 2 mM GA (F), 2.5% PVOH, 1.5 mg/ml insulin amyloid fibrils and 1.7 mg/ml GOD (G), 2.5% PVOH, 1.5 mg/ml insulin amyloid fibrils, 1.7 mg/ml GOD and 2 mM GA (H), 2.5% PVOH and 1.5 mg/ml crystallin amyloid fibrils (I), 2.5% PVOH, 1.7 mg/ml crystallin*

amyloid fibrils and 2 mM GA (J), 2.5% PVOH, 1.5 mg/ml crystallin amyloid fibrils and 1.7 mg/ml GOD (K), and 2.5% PVOH, 1.5 mg/ml crystallin amyloid fibrils, 1.7 mg/ml GOD and 2 mM GA (L).

The surfaces of the crystallin amyloid fibrils, GA and PVOH film and the crystallin amyloid fibrils, GOD, GA and PVOH film (Figure 6.1J and L, respectively) were very similar, with a clustered rough surface, whereas the crystallin amyloid fibrils, GOD and PVOH film has a comparatively smooth surface.

The PVOH films have very different surfaces, where some features can be explained by the film constituents. The bubble-like formations could be phase-separation of constituents, caused by hydrophobic interactions between PVOH cross-linked by excess GA and water, or where hydrophobic amino acids cannot interact with hydrophilic PVOH (Mendieta-Taboada *et al.* 2008). The surfaces of these films are thus rough and highly variable. Therefore, more analysis of film composition and dispersal of constituents is needed before meaningful results can be obtained by mechanical testing methods.

6.3 Confocal microscopy

As discussed in Section 1.8, GOD contains one FAD cofactor per monomer (Wilson and Turner 1992). FAD has an intrinsic fluorescence with an emission at 530 nm (De Luca *et al.* 2007). This is useful when viewing the enzyme using confocal microscopy, as the FAD cofactor emits fluorescence, which has previously been used to assess GOD enzyme loading in immobilisation experiments (Park *et al.* 2004). Amyloid fibrils are reported to have some intrinsic fluorescence, which could be associated with constituent amino acid residues; however, the reason for this remains unknown (del Mercato *et al.* 2007).

The film samples and associated controls were mounted on slides and viewed using confocal microscopy as described in Section 2.5.2. Confocal microscopy was used to visualise fluorescence emitted by the FAD cofactor of the GOD enzyme and intrinsic fluorescence of the amyloid fibrils, in order to ascertain the spatial distribution of these constituents in the film.

The confocal images in Figure 6.2 show two types of fluorescence patterns, localised and diffuse fluorescence. The PVOH and PVOH and GA films (Figure 6.2A and B, respectively), did not exhibit any fluorescence. Upon addition of GOD, light spots of localised fluorescence

were visible (Figure 6.2C). Because individual GOD molecules are too small to be visualised at this magnification (Hecht *et al.* 1993), it is likely that the GOD was not homogeneously mixed throughout the PVOH film, resulting in pockets of GOD, where the combined fluorescence was large enough to be visible. The addition of GA produced more abundant localised fluorescence (Figure 6.2D). Glutaraldehyde has previously been used to increase auto-fluorescence of proteins upon cross-linking (Fester *et al.* 2008). This may be due to pyridinium links formed during the cross-linking reaction (Meade *et al.* 2003).

The PVOH and insulin amyloid fibrils film (Figure 6.2E) showed a more diffuse fluorescence pattern than the fluorescence of the PVOH and GOD film. This was mirrored in the PVOH and crystallin amyloid fibrils film image (Figure 6.2I). Similarly, the addition of GA increased the diffuse fluorescence pattern of both PVOH and insulin amyloid fibril and PVOH and crystallin amyloid fibril film samples (Figure 6.2F and J, respectively). The increase in fluorescence of both GOD and insulin amyloid fibrils upon addition of GA is consistent with an auto-fluorescent pyridinium reaction product of GA with amine residues on the enzyme and the amyloid fibrils, also seen in Chapter Four.

In the PVOH, insulin amyloid fibrils and GOD film sample (Figure 6.2G), there is a mixture of diffuse and localised fluorescence. This is consistent with a mixture of the PVOH and GOD film and the PVOH and insulin amyloid fibrils film, allowing the distribution of GOD and amyloid fibrils to be assessed together. The fluorescence of the sample was again greatly enhanced by addition of GA. The same trend was seen in the PVOH, crystallin amyloid fibrils and GOD and PVOH, crystallin amyloid fibrils, GOD and GA films (Figure 6.2K and L, respectively). However, the fluorescence produced by crystallin amyloid fibrils and GA was much more intense than the fluorescence produced by insulin amyloid fibrils and GA, which leads to oversaturation of the images. This could be because bovine crystallin has more free amine groups than bovine insulin, due to having a larger number of lysine residues in its amino acid sequence, which would be able to form more fluorescent adducts with the GA, consistent with the results seen in Chapter Four.

These confocal microscopy results indicated that in the prepared PVOH films, GOD produced a localised fluorescence pattern, and both insulin and crystallin amyloid fibrils produced a diffuse fluorescence pattern. Like the SEM, confocal microscopy also indicated heterogeneous mixtures and/or phase-separation in film samples.

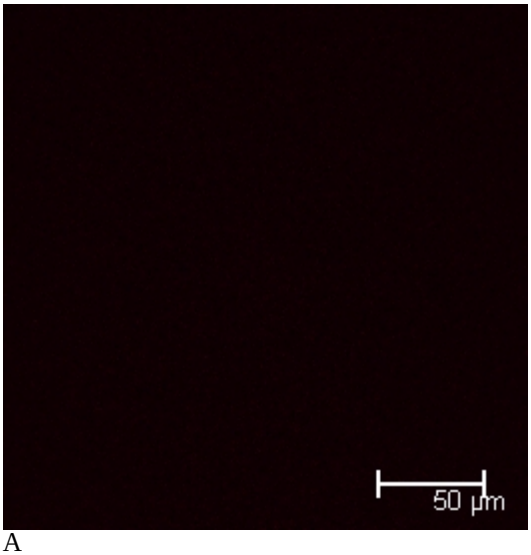

A

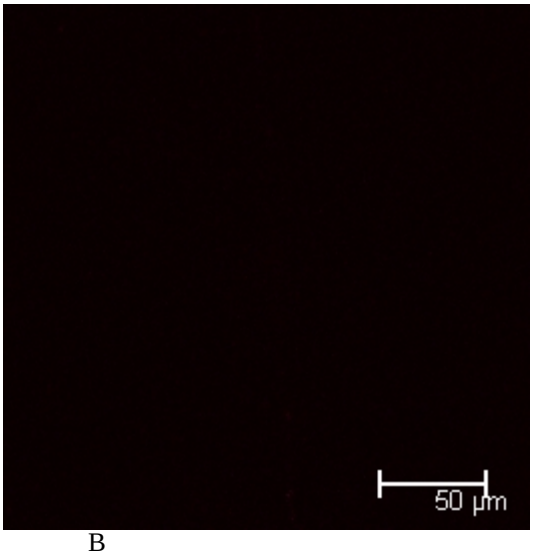

B

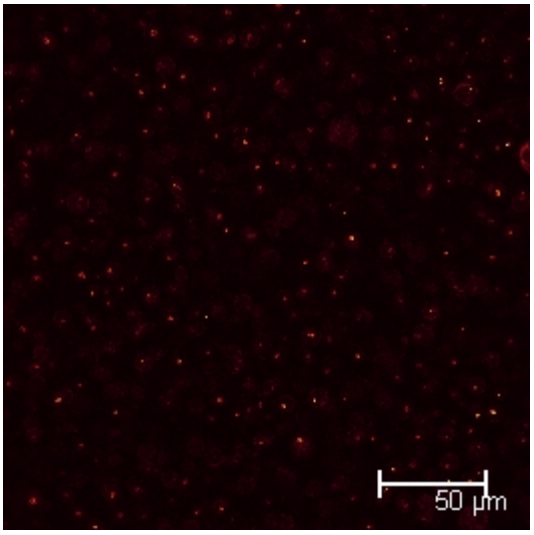

C

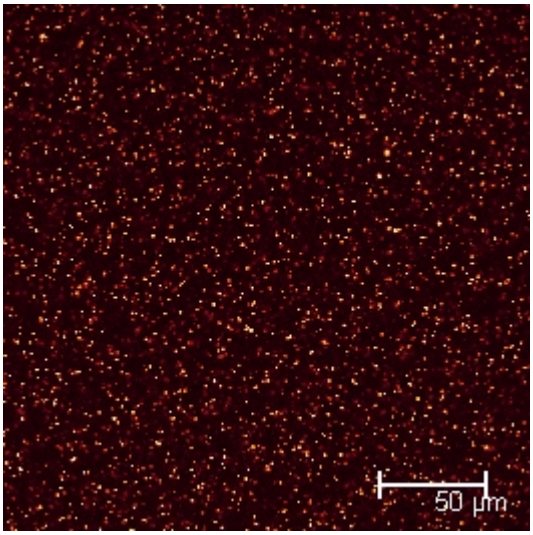

D

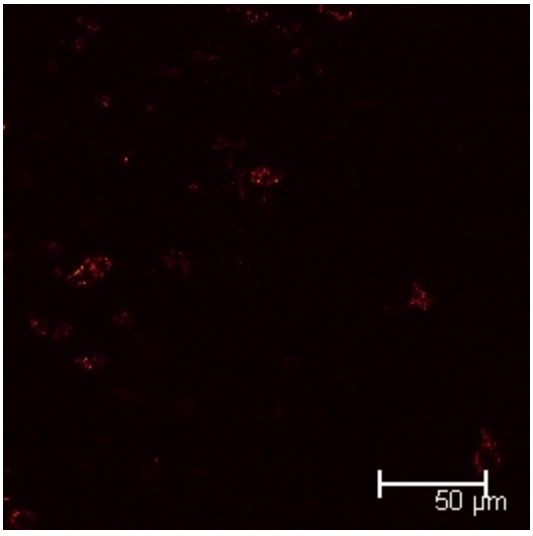

E

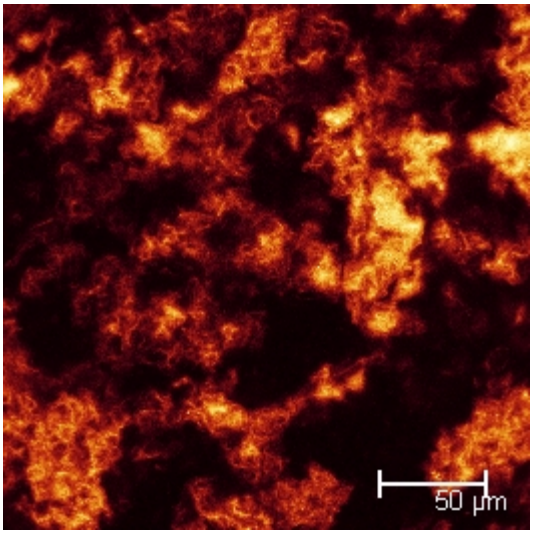

F

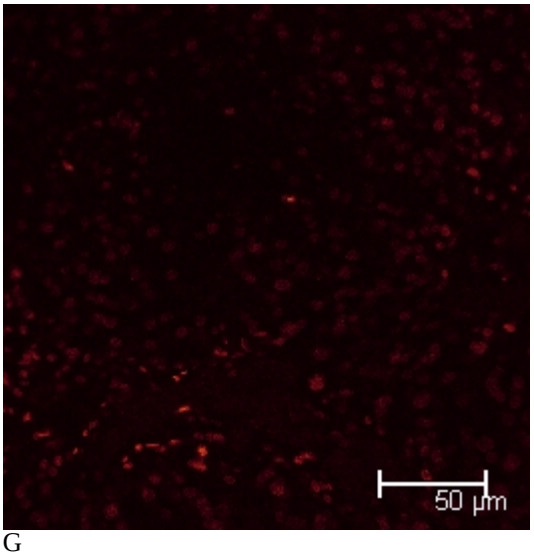

G

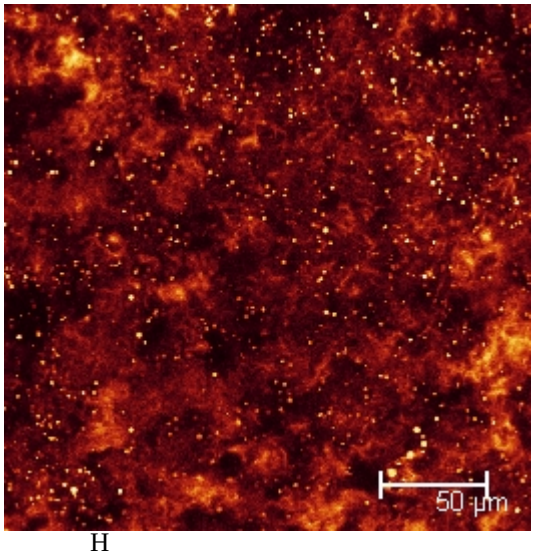

H

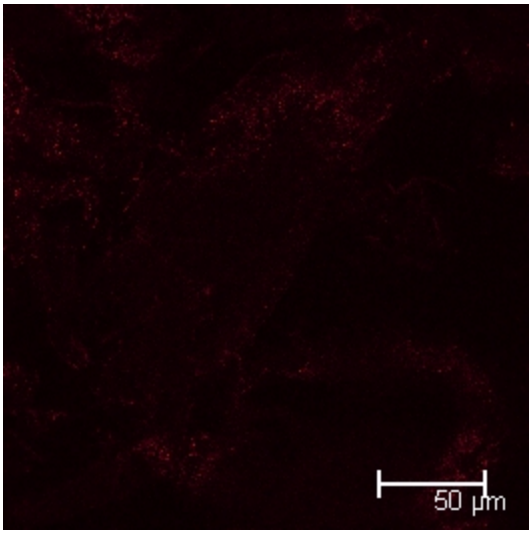

I

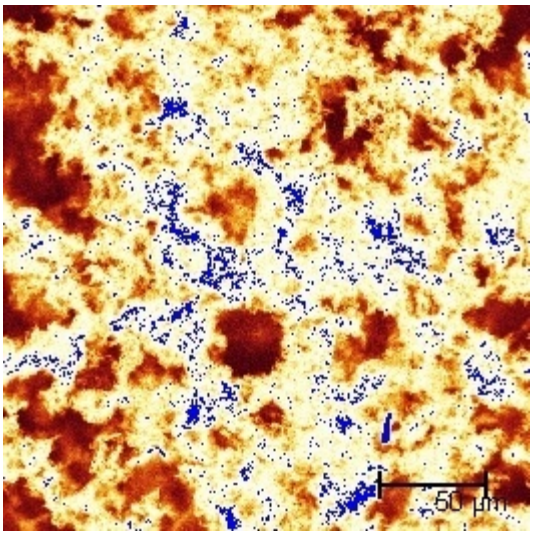

J

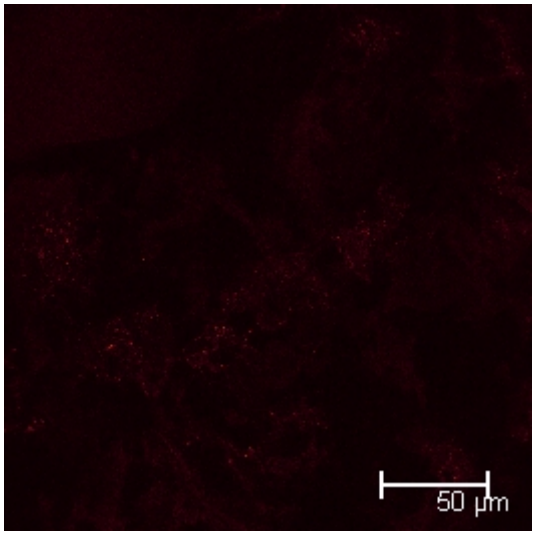

K

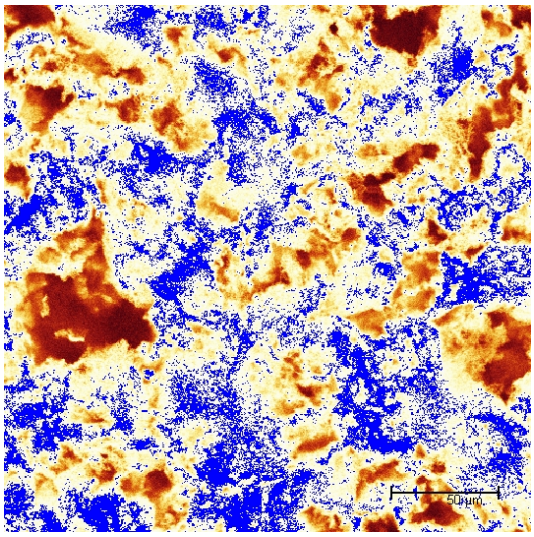

L

Figure 6.2

Confocal images of PVOH film samples. *Light emission images are representative of two film replicates and taken near the median focal plane of samples 2.5% PVOH (A), 2.5% PVOH and 2 mM GA (B), 2.5% PVOH and 1.7 mg/ml GOD (C), 2.5% PVOH, 1.7 mg/ml GOD and 2 mM GA (D), 2.5% PVOH, and 1.5 mg/ml insulin amyloid fibrils (E), 2.5% PVOH, 1.5 mg/ml insulin amyloid fibrils and 2 mM GA (F), 2.5% PVOH, 1.5 mg/ml insulin amyloid fibrils and 1.7 mg/ml GOD (G), 2.5% PVOH, 1.5 mg/ml insulin amyloid fibrils, 1.7 mg/ml GOD and 2 mM GA (H), 2.5% PVOH and 1.5 mg/ml crystallin amyloid fibrils (I), 2.5% PVOH, 1.7 mg/ml crystallin amyloid fibrils and 2 mM GA (J), 2.5% PVOH, 1.5 mg/ml crystallin amyloid fibrils and 1.7 mg/ml GOD (K), and 2.5% PVOH, 1.5 mg/ml crystallin amyloid fibrils, 1.7 mg/ml GOD and 2 mM GA (L).*

To establish whether the amyloid fibrils added to the PVOH film retained their fibrillar nature during film formation, ThT was added to the films prior to casting. PVOH films containing ThT also showed dark spots of no fluorescence (Figure 6.3A). This could be due to incomplete mixing or phase separation of ThT throughout the film, leaving pockets of unmixed PVOH. The pockets created by the addition of ThT make it difficult to visualise the fluorescence from individual constituents, such as GOD.

Despite the low magnification of confocal microscopy in comparison to TEM (630 x and 89,000 x respectively) used to visualise amyloid fibrils, long, thin fibrillar structures were visible in the PVOH, ThT and insulin amyloid fibrils film samples. These fibrillar structures are larger in size than the amyloid fibrils viewed in the TEM images, which had a width of 6 nm (Section 3.2 (Figure 2) and Section 3.5 (Figure 6A)). This is consistent with previous reports of ThT binding in channels along the length of the fibril (Krebs *et al.* 2005). This is an interesting result as it implies that amyloid fibrils are still intact in the PVOH film, and shows the clustered distribution of fibrils throughout the film. The background fluorescence of the film (Figure 6.3A) is higher than in images without ThT (Figure 6.2A), due to the fluorescence spectrum of unbound ThT. Unbound ThT gives a fluorescence spectrum with an excitation/emission maximum of 385/445 nm, whereas bound ThT undergoes a spectral shift with an excitation/emission maxima at 450/482 nm (LeVine III 1993). Therefore, when excited at 405 nm, fluorescence from both bound and unbound ThT is visible at the wavelengths detected by the confocal microscope (430 - 520 nm).

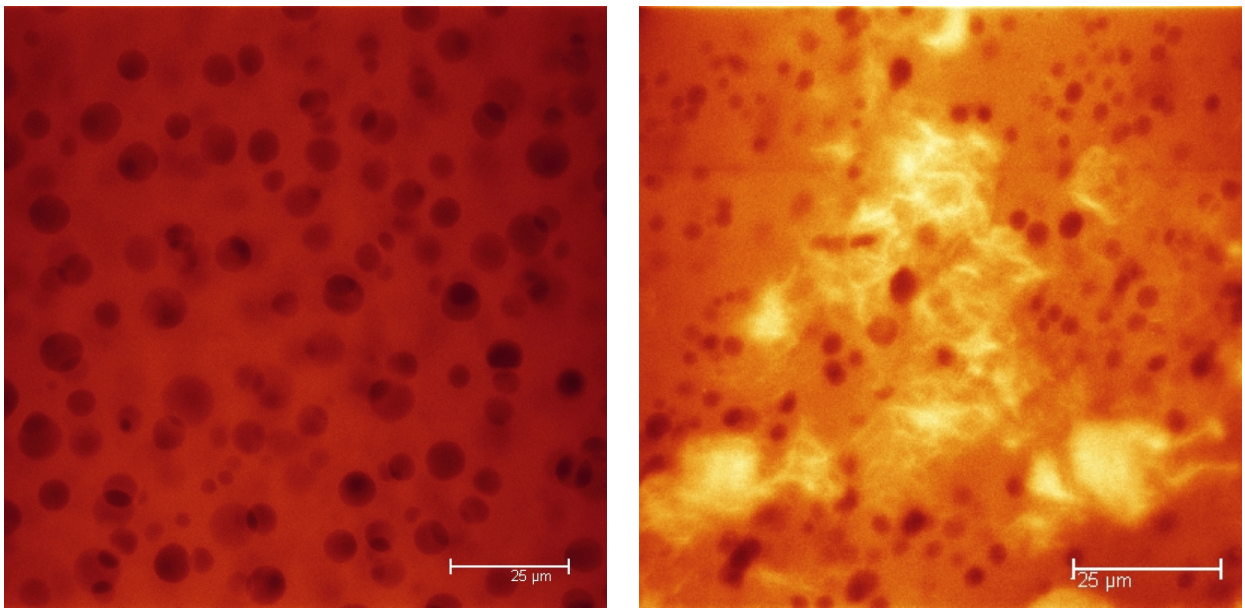

A B

Figure 6.3

Confocal microscopy of PVOH film samples containing ThT. *Light emission images are representative of two film replicates and taken near the median focal plane of samples 2.5% PVOH and ThT (A) and 2.5% PVOH, ThT, and 1.5 mg/ml insulin amyloid fibrils (B).*

Before mechanical testing can be carried out on the films, methods must be developed to ensure homogeneous mixing, removing weaknesses in the film and producing meaningful mechanical testing results in tests such as dynamic mechanical analysis (DMA). DMA is the application of oscillating force to a film sample in order to measure the response of the material. DMA testing can then determine the mechanical properties and detect molecular motion, so that morphology relationships such as crystallinity can be developed (Aoi *et al.* 2000a; Park *et al.* 2001). This knowledge is important for use in film applications, and is thus important for future studies (Mendieta-Taboada *et al.* 2008). A possible method to improve dispersion could involve mechanically stirring films before casting or heat pressing films, which are methods commonly used to facilitate even dispersal of film components (Yang *et al.* 2004; Ljungberg and Wesslén 2005; Mendieta-Taboada *et al.* 2008). However, a heat pressing method would need development, as a disadvantage of heat pressing films is the high temperatures reached in the hot press of around 200°C, which would denature the GOD enzyme (Yang *et al.* 2004; Ljungberg and Wesslén 2005).

6.4 Activity assay

Before the functionalised film can be developed for any applications, the retention of enzyme activity in the film system must be established. The Amplex Red assay was used to qualify GOD activity, as described in Section 2.3. The exact activity of GOD in the PVOH film is difficult to quantify, due to uneven dispersion throughout the film; however, the visual colour change (Section 1.9) gave a qualitative measure. At the time of publication, GOD was still active in the film after storage at room temperature for 6 months, as qualitatively indicated by a pink colour change in the presence of Amplex Red reaction mixture.

6.5 Antibacterial effect of film

Hydrogen peroxide produced by GOD is known to have a natural antibacterial and antifungal action when produced by some insect and fungal species (Taormina *et al.* 2001; Wong *et al.* 2008). Thus, if GOD is active when attached to amyloid fibrils and incorporated into a PVOH film, it would be expected to retain antimicrobial activity. GOD has been encapsulated in PVOH using glutaraldehyde in previous research and has retained antimicrobial activity (Wong and Abdul-Aziz 2008). Thus, because GOD was still active when attached to amyloid fibrils using glutaraldehyde, it would be expected to retain antimicrobial activity when incorporated into a PVOH film system. Functionalised film samples and controls were tested for antimicrobial activity against the bacterium *E. coli.* *E. coli* normally colonises the human gastrointestinal tract; however, pathogenic strains are able to cause a broad spectrum of diseases, and even non-pathogenic *E. coli* can cause infection in immunocompromised hosts (Nataro and Kaper 1998). Thus an effective antibacterial agent is invaluable for use in food packaging, providing protection from *E. coli* infection. *E. coli* is also a good model for demonstrating antibacterial activity, as much is known about the bacterium. Once the antibacterial activity of the film against *E. coli* is demonstrated, the antibacterial effect of the film on other bacteria can be investigated.

Film samples were cut and placed on LB agar plates inoculated with a lawn of *E. coli*, as described in Section 2.6.1. This allowed assessment of the effect of the functionalised film on the growth of the bacterium, where areas of restricted growth are seen as a halo around the film sample. The permeability of the functionalised film to glucose can was also assessed by using media with and without glucose, as PVOH film containing GOD and GA has been shown to be

permeable to low molecular weight substances such as glucose (Wong and Abdul-Aziz 2008). Representative photographs of the effect of film samples on *E. coli* growth are shown in Figure 6.4. The halo effect is only seen in the film samples on plates containing glucose. This shows that the addition of amyloid fibrils does not affect the permeability of the functionalised PVOH films to glucose.

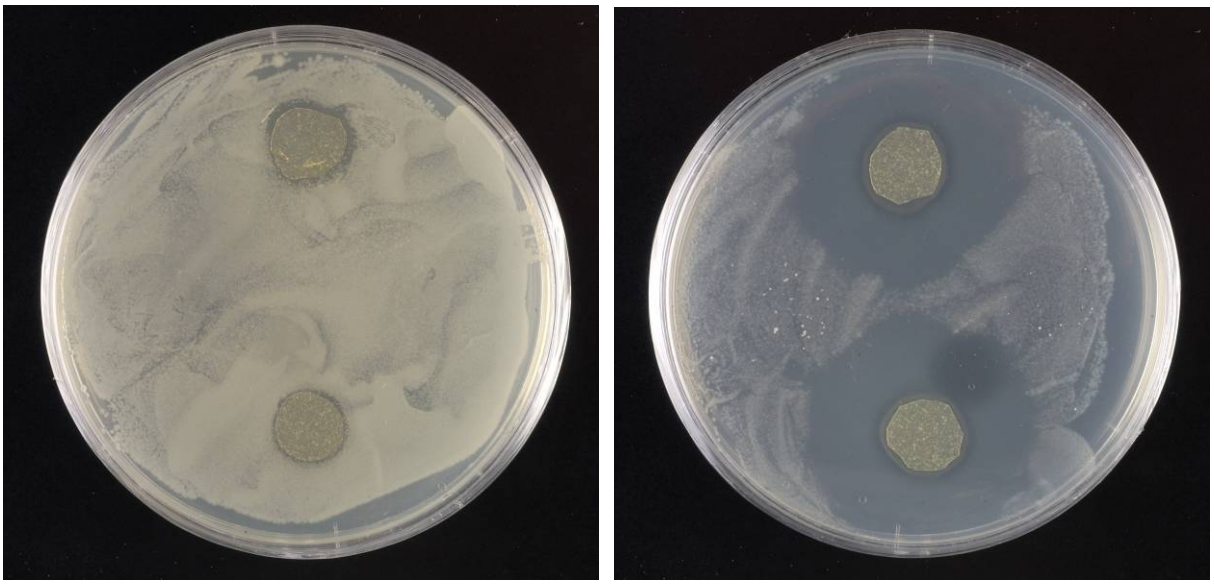

Figure 6.4

Effect of film samples on* E. coli *growth. *PVOH film samples containing GOD and amyloid fibrils are located at the top and bottom of the plate, and PVOH samples are located at the left and right of each plate.* E. coli *was inoculated on LB medium (left) and LB medium containing 10 g/l glucose (right).*

The results of the functionalised amyloid fibril film samples and the associated controls are presented in Table 6.1, showing the film sample and whether the halo effect was produced with *E. coli*. The halo effect was produced in all film samples containing the GOD enzyme. This indicates that GOD has antibacterial activity in the PVOH film, including when attached to amyloid fibrils.

Table 6.1

***Effect of film samples on growth of* E. coli.** *The film samples and their effect on* E. coli *growth are shown.*

Film	Halo Effect Produced
PVOH	No
PVOH and GA	No
PVOH and GOD	Yes
PVOH, GOD and GA	Yes
PVOH and insulin amyloid fibrils	No
PVOH, insulin amyloid fibrils and GA	No
PVOH, insulin amyloid fibrils and GOD	Yes
PVOH, insulin amyloid fibrils, GOD and GA	Yes
PVOH and crystallin amyloid fibrils	No
PVOH, crystallin amyloid fibrils and GA	No
PVOH, crystallin amyloid fibrils and GOD	Yes
PVOH, crystallin amyloid fibrils, GOD and GA	Yes

6.6 Antimicrobial effect of film

This film was tested for antifungal activity against the fungi *Fusarium*, *Penicillium* and *Rhizopus*. *Penicillium* and *Rhizopus* are both commonly found fungi involved in food spoilage. *Fusarium* is a plant fungus that is known to cause rot in roots and shoots of crops such as rye and wheat (Miedaner 1997). Thus these fungal species are known to be the main contaminants of bread (Gerez *et al.* 2009). The antifungal experiments were conducted in a similar way to the antibacterial experiments, where film samples were placed on an agar plate inoculated with a fungal species. A halo of restricted growth of the fungus was expected if an antifungal activity was present.

Table 6.2

Effect of film samples on fungal growth. *Film samples are listed, with their inhibitory effect on the fungi Fusarium, Penicillium and Rhizopus given (yes/no).*

Film	Halo Effect Produced		
	Fusarium	*Penicillium*	*Rhizopus*
PVOH	No	No	No
PVOH and GA	No	No	No
PVOH and GOD	No	No	No
PVOH, GOD and GA	No	No	No
PVOH and insulin amyloid fibrils	No	No	No
PVOH, insulin amyloid fibrils and GA	No	No	No
PVOH, insulin amyloid fibrils and GOD	No	No	No
PVOH, insulin amyloid fibrils, GOD and GA	No	No	No
PVOH and crystallin amyloid fibrils	No	No	No
PVOH, crystallin amyloid fibrils and GA	No	No	No
PVOH, crystallin amyloid fibrils and GOD	No	No	No
PVOH, crystallin amyloid fibrils, GOD and GA	No	No	No

None of the film samples inhibited growth of the fungi. This could be due to the production of catalase by the fungi. Catalase uses hydrogen peroxide as a substrate, thus removing it before an inhibitory effect on growth of the fungi can occur (Wu *et al.* 1995). This effect could be reduced by co-immobilising another enzyme such as lactoperoxidase, which uses hydrogen peroxide in the generation of other products with antimicrobial properties (Vartiainen *et al.* 2005).

A common issue encountered during antimicrobial film experiments was the growth of contaminants, specifically the growth of a pink species, identified as a yeast (Craig Galilee, Personal Communication). Reduction in contaminants can be achieved by sterilising the film. Methods of sterilisation include moist heat, dry heat, gases, filtration and radiation. A major problem for sterilisation using moist heat is the high solubility of the PVOH film in water, due to the high affinity of the hydroxyl groups in PVOH for water. This could be altered by creating strong hydrogen bonding between intramolecular and intermolecular hydroxyl groups, greatly inhibiting the solubility of PVOH in water (Kim *et al.* 2007). Dry heat cannot be used for the

PVOH film samples due to the loss of enzymatic activity of GOD at temperatures above 60 °C, and filtration cannot be used to sterilise the PVOH before addition of other film constituents due to the high viscosity of the liquid. UV radiation is very effective at removing the pink yeast; however, the impact of UV radiation on the activity of the GOD enzyme is unknown. A gas such as ethylene oxide would be ideal for sterilising the PVOH films in further experiments, provided that the effect of exposure on GOD activity is investigated prior to film sterilisation.

Another interesting factor encountered during the antimicrobial experiments was the curling of film pieces, most notably in the insulin amyloid fibrils and GA film samples. When placed on the agar plate, these film samples would curl up away from the agar, as opposed to other film samples which would remain in place on the agar plate. This suggests that excess GA in the film has a cross-linking effect on the PVOH. This would cause the PVOH to become more hydrophobic, resulting in film curling away from the hydrophilic agar plate. This could also be a drying effect. A solution to this problem could be to quench GA cross-linking before addition to the PVOH film.

6.7 Conclusion

The incorporation of immobilised GOD into a PVOH film system yielded a novel bionanomaterial, with well characterised dispersal of constituents and retention of GOD activity and thus antimicrobial activity. Further work on the dispersion of the nanoscaffold into the film matrix is required in order to move this research closer to materials of commercial utility. Despite this, the addition of a GOD functionalised amyloid fibril scaffold to a PVOH film provides a good ‘proof of concept’ bionanomaterial, based on enzyme immobilisation onto amyloid fibrils.

6.8 References

Aoi, K., Nakamura, R. and Okada, M. (2000a). Polypeptide-synthetic polymer hybrids, 2. Miscibility of poly(vinyl alcohol) with polysarcosine. *Macromolecular Chemistry and Physics* **201**: 1059-1066.

Aoi, K., Takasu, A. and Okada, M. (2000b). DNA-based polymer hybrids. Part 1. Compatibility and physical properties of poly(vinyl alcohol)/DNA sodium salt blend. *Polymer* **41**: 2847-2853.

Chang, M. H. and Kim, B. C. (2007). Rheological investigation of the effects of introducing diethylene glycol on the physical properties of PVA solutions and PVA films. *Macromolecular Symposia* **249-250**: 591-600.

Chen, C.-H., Wang, F.-Y., Mao, C.-F., Liao, W.-T. and Hsieh, C.-D. (2008). Studies of chitosan: II. Preparation and characterization of chitosan/poly(vinyl alcohol)/gelatin ternary blend films. *International Journal of Biological Macromolecules* **43**: 37-42.

De Luca, P., Lepore, M., Portaccio, M., Esposito, R., Rossi, S., Bencivenga, U. and Mita, D. G. (2007). Glucose determination by means of steady-state and time-course UV fluorescence in free or immobilized glucose oxidase. *Sensors* **7**: 2612-2625.

del Mercato, L. L., Pompa, P. P., Maruccio, G., Torre, A. D., Sabella, S., Tamburro, A. M., Cingolani, R. and Rinaldi, R. (2007). Charge transport and intrinsic fluorescence in amyloid-like fibrils. *Proceedings of the National Academy of Science of the United States of America* **104**: 18019-18024.

Fergg, F., Keil, F. J. and Quader, H. (2001). Investigations of the microscopic structure of poly(vinyl alcohol) hydrogels by confocal laser scanning microscopy. *Colloid & Polymer Science* **279**: 61-67.

Fester, T., Berg, R. H. and Taylor, C. G. (2008). An easy method using glutaraldehyde-introduced fluorescence for the microscopic analysis of plant biotrophic interactions. *Journal of Microscopy* **231**: 342-348.

Gade, V. K., Shirale, D. J., Gaikwad, P. D., Savale, P. A., Kakde, K. P., Kharat, H. J. and Shirsat, M. D. (2006). Immobilization of GOD on electrochemically synthesized Ppy-PVS composite film by cross-linking via glutaraldehyde for determination of glucose. *Reactive and Functional Polymers* **66**: 1420-1426.

Gerez, C. L., Torino, M. I., Rollán, G. and Font de Valdez, G. (2009). Prevention of bread mould spoilage by using lactic acid bacteria with antifungal properties. *Food Control* **20**: 144-148.

Hecht, H. J., Kalisz, H. M., Hendle, J., Schmid, R. D. and Schomburg, D. (1993). Crystal structure of glucose oxidase from *Aspergillus niger* refined at 2.3 Å resolution. *Journal of Molecular Biology* **229**: 153-172.

Jinnai, H., Yoshida, H., Kimishima, K., Funaki, Y., Hirokawa, Y., Ribbe, A. E. and Hashimoto, T. (2001). Observation of fine structure in bicontinuous phase-separated domains of a polymer blend by laser scanning confocal microscopy. *Macromolecules* **34**: 5186-5191.

Kim, D.-N., Lee, W. and Koh, W.-G. (2008). Micropatterning of proteins on the surface of three-dimensional poly(ethylene glycol) hydrogel microstructures. *Analytica Chimica Acta* **609**: 59-65.

Kim, E. M., Han, M. H., Lee, Y. J., Song, D. H., Lee, H. K., Kwon, O. W., Shin, D. S., Han, S. S., Noh, S. K., Shin, J. K., Gal, Y. S. and Lyoo, W. S. (2007). Characterization of poly(vinyl alcohol) films with various molecular parameters. *Journal of Applied Polymer Science* **106**: 3259-3267.

Krebs, M. R. H., Bromley, E. H. C. and Donald, A. M. (2005). The binding of thioflavin-T to amyloid fibrils: localisation and implications. *Journal of Structural Biology* **149**: 30-37.

LeVine III, H. (1993). Thioflavine T interaction with synthetic Alzheimer's disease β-amyloid peptides: Detection of amyloid aggregation in solution. *Protein Science* **2**: 404-410.

Ljungberg, N. and Wesslén, B. (2005). Preparation and properties of plasticized poly(lactic acid) films. *Biomacromolecules* **6**: 1789-1796.

Meade, S. J., Miller, A. G. and Gerrard, J. A. (2003). The role of dicarbonyl compounds in non-enzymatic crosslinking: a structure-activity study. *Bioorganic & Medicinal Chemistry* **11**: 853-862.

Mendieta-Taboada, O., Sobral, P. J. d. A., Carvalho, R. A. and Habitante, A. M. B. Q. (2008). Thermomechanical properties of biodegradable films based on blends of gelatin and poly(vinyl alcohol). *Food Hydrocolloids* **22**: 1485-1492.

Miedaner, T. (1997). Breeding wheat and rye for resistance to *Fusarium* diseases. *Plant Breeding* **116**: 201-220.

Nataro, J. P. and Kaper, J. B. (1998). Diarrheagenic *Escherichia coli*. *Clinical Microbiology Reviews* **11**: 142-201.

Park, J. S., Park, J. W. and Ruckenstein, E. (2001). Thermal and dynamic mechanical analysis of PVA/MC blend hydrogels. *Polymer* **42**: 4271-4280.

Park, T., Choo, J., Lee, M., Kim, Y. S., Lee, E. K. and Lee, H. S. (2004). Enhancement of the protein loading density by a pre-cleaning process of a gold substrate: Confocal laser scanning microscopic study. *Analytical Sciences* **20**: 1255-1258.

Rao, S. P. (2008). PhD Thesis. Amyloid fibrils in bionanomaterials. *School of Biological Sciences, University of Canterbury, Christchurch.*

Taormina, P. J., Niemira, B. A. and Beuchat, L. R. (2001). Inhibitory activity of honey against foodborne pathogens as influenced by the presence of hydrogen peroxide and level of antioxidant power. *International Journal of Food Microbiology* **69**: 217-225.

Vartiainen, J., Rátto, M. and Paulussen, S. (2005). Antimicrobial activity of glucose oxidase-immobilized plasma-activated polypropylene films. *Packaging Technology and Science* **18**: 243-251.

Wilson, R. and Turner, A. P. F. (1992). Glucose oxidase: An ideal enzyme. *Biosensors and Bioelectronics* **7**: 165-185.

Wong, C. M., Wong, K. H. and Chen, X. D. (2008). Glucose oxidase: natural occurrence, function, properties and industrial applications. *Applied Microbiology and Biotechnology* **78**: 927-938.

Wong, F.-L. and Abdul-Aziz, A. (2008). Comparative study of poly(vinyl alcohol)-based support materials for the immobilization of glucose oxidase. *Journal of Chemical Technology & Biotechnology* **83**: 41-46.

Wu, G., Shortt, B. J., Lawrence, E. B., Levine, E. B., Fitzsimmons, K. C. and Shah, D. M. (1995). Disease resistance conferred by expression of a gene encoding H_2O_2-generating glucose oxidase in transgenic potato plants. *Plant Cell* **7**: 1357-1368.

Yang, J. M., Su, W. Y., Leu, T. L. and Yang, M. C. (2004). Evaluation of chitosan/PVA blended hydrogel membranes. *Journal of Membrane Science* **236**: 39-51.

7. CHAPTER SEVEN - SUMMARY AND CONCLUSIONS

Amyloid fibrils have considerable potential for use in the creation of bionanomaterials. To ensure feasibility for the use of amyloid fibrils in the production of new materials in bionanotechnology, the amyloidogenic protein must be readily available and inexpensively sourced (Waterhouse and Gerrard 2004). This thesis aimed to investigate whether amyloid fibrils could be prepared from a crude agricultural waste protein, bovine lens crystallin, and functionalised *via* attachment of GOD. It also explored the incorporation of this functionalised enzyme scaffold into a film system in the creation of a novel bionanomaterial. Using PVOH as a model film, the ability to incorporate an amyloid fibril scaffold with GOD activity was assessed.

Initially, the ability to form amyloid fibrils from a crude mixture of bovine lens crystallins was investigated, building on previous work by Garvey *et al*. crystallin proteins were purified using size exclusion chromatography and the ability of the purified fractions to form amyloid fibrils was assessed by TEM (Garvey *et al.* 2009). Long, thin structures characteristic of amyloid fibrils were visible in only the α- and β_H-crystallins fractions. The method of crude crystallin extraction was modified to give a higher crude protein yield. This method produced a higher proportion of long, straight fibrils in a scaffold formation ideal for enzyme immobilisation directly from a crude extract, without purification, and was thus used for further experiments.

The effect of proteolytic digestion and increase in pH on crude crystallin samples was also investigated. Proteolytic digestion removed the short, curly structures, leaving a scaffold of long, straight fibrils. An increase in environmental pH caused the amyloid fibrils to clump together, and individual fibrils became difficult to visualise. This effect could have been due to either increase of pH or addition of salt. However, this is useful information when incorporating amyloid fibrils into bionanomaterials.

Three different methods of attaching GOD to amyloid fibrils were then assessed. The first method of attaching GOD to amyloid fibrils using GA was established, and the effect of this immobilisation on the integrity of the amyloid fibrils was assessed by TEM. Results showed no

change of amyloid fibril morphology upon cross-linking, with both amyloid fibrils and enzyme aggregate visible. GOD retained activity upon immobilisation to both insulin and crystallin amyloid fibrils, and separation techniques such as electrophoresis and centrifugation were then used to assess the degree of cross-linking. Electrophoresis of cross-linked samples indicated that cross-linking was occurring and this result was corroborated with centrifugation data. Centrifugation was a more efficient method of separating cross-linked material, and showed a non-covalent interaction between amyloid fibrils and GOD.

Two other methods of enzyme attachment were then investigated; deglycosylation of GOD and attachment *via* glutaraldehyde cross-linking and attachment *via* periodate oxidation of the carbohydrate shell. The efficacy of these attachment methods were tested by electrophoresis and centrifugation. Both of these methods were successful in attaching GOD to amyloid fibrils; however, no additional attachment effect was seen, and thus glutaraldehyde cross-linking to native GOD was chosen for further experiments.

PVOH films were manufactured with the addition of functionalised insulin amyloid fibrils or functionalised crystallin amyloid fibrils using a solution casting method (Rao 2008). SEM and confocal microscopy studies revealed an uneven distribution of film components. ThT was then added to the casting solutions to confirm the integrity of amyloid fibrils in the films, viewed using confocal microscopy. Immobilised GOD retained activity when incorporated into the PVOH film, as determined by antibacterial experiments, where growth of *E. coli* was inhibited by film samples containing GOD-functionalised amyloid fibrils. No growth inhibition of *Fusarium*, *Rhizopus* or *Penicillium* was observed in antifungal experiments.

Following this established proof of concept, future work on the addition of functionalised enzyme scaffolds to film systems should include the development of methods to evenly disperse film components, test the effect of the addition of amyloid fibrils on the mechanical properties of the film and optimise a commercially viable film system (Ljungberg and Wesslén 2005; Mendieta-Taboada *et al.* 2008). The model of GOD immobilisation to amyloid fibrils also has the potential to be applied to other enzymes. Functionalised amyloid fibril polymer blends have the potential to create novel bionanomaterials with a wide range of enzymatic activities and thus a large number of potential applications.

7.1 References

Garvey, M., Gras, S. L., Meehan, S., Meade, S. J., Carver, J. A. and Gerrard, J. A. (2009). Protein nanofibres of defined morphology prepared from mixtures of crude crystallins. *International Journal of Nanotechnology* **6**: 258-273.

Ljungberg, N. and Wesslén, B. (2005). Preparation and properties of plasticized poly(lactic acid) films. *Biomacromolecules* **6**: 1789-1796.

Mendieta-Taboada, O., Sobral, P. J. d. A., Carvalho, R. A. and Habitante, A. M. B. Q. (2008). Thermomechanical properties of biodegradable films based on blends of gelatin and poly(vinyl alcohol). *Food Hydrocolloids* **22**: 1485-1492.

Rao, S. P. (2008). PhD Thesis. Amyloid fibrils in bionanomaterials. *School of Biological Sciences, University of Canterbury, Christchurch*.

Waterhouse, S. H. and Gerrard, J. A. (2004). Amyloid fibrils in bionanotechnology. *Australian Journal of Chemistry* **57**: 519-523.